MÖSSBAUER EFFECT: INVESTIGATIONS OF CERTAIN IRON BEARING MINERALS AND ROCKS

INAAM Y. ELADAS

A Thesis
in
The Department
of
Physis

Presented in Partial Fulfillment of the Requirments
for the Degree of Master of Science at
Concordia University
Montreal, Quebec, Canada

AUGUST 1981

ABSTRACT

MÖSSBAUER EFFECT: INVESTIGATIONS OF

CERTAIN IRON BEARING MINEARALS AND ROCKS

Inaam Y. Eladas

The Mössbauer spectra of three bulk rocks, four orthopyroxenes, six clinopyroxenes, two pyrites and six samples taken from a calcareous formation adjacent to the Copper mountain plug of the Gaspe Copper mines (Quebec), have been recorded at room temperature. The spectra were computer fitted to Lorentzian line shapes and the component peaks of each spectrum were assigned to particular positions of Fe^{2+} and Fe^{3+} in the various minerals.

Andradite and hedenbergite were identified as the main Fe containing minerals in the samples taken from the Gaspé Copper mines. It was found that the percentages of andradite and hedenbergite, vary linearly with the iron contents of the samples. An attempt was made to relate the variation in iron contents to the distance from the Copper mountain plug; no unique conclusion could be drawn. In ortho and clinopyroxenes, the variation in the quadrupole splitting was related to the variation of the ratio Fe/(Fe+Mg).

It is concluded that the Mössbauer effect can be used as a finger print technique in mineral studies.

ACKNOWLEDGEMENTS

The author would like to thank Dr. S.K. Misra for suggesting this work and for his continued interest and advice.

He is also grateful to Dr. S. Kumarapeli, Professor J.T. Jenkins and Professor E. Procyshyn of the Geology Department, for the supply of samples and for many helpful discussions.

Special thanks are due to Dr. N. Eddy for assistance and help during the whole experimental work, and to Pawel Mikolajczak for the encouragement and help during the early stages of this work.

Financial assistance came from Dr. Misra's NSERC Grant Number A4485.

This thesis was typed by Marie Berryman.

TABLE OF CONTENTS

		PAGE
	ABSTRACT	i
	ACKNOWLEDGEMENTS	ii
	LIST OF TABLES	v
	LIST OF FIGURES	vi
CHAPTER I	INTRODUCTION	1
CHAPTER II	THEORY	3
2.1	Resonance - Recoil Free Emission	3
2.2	Hyperfine Structure	5
2.2.a	Isomer Shift	6
2.2.b	Quadrupole Splitting	9
2.2.c	Magnetic Splitting	13
CHAPTER III	EXPERIMENTAL	15
3.1	Method	15
3.2.	Source	17
3.3	Driving Unit	20
3.4	Multichannel Analyzer	22
3.5	Detector - Amplification System	23
3.6	Calibration	23
3.7	Data Transfer	24
CHAPTER IV	IRON IN MINERALS	29
4.1	Characterization of the Oxidation State of Iron - Coordination Number	29
4.2	Correlation of the Quadrupole Splitting with Structural Variation	32

		PAGE
CHAPTER V	ANALYSIS OF SPECTRA	36
5.1	Computer Analysis - Method	36
5.2	Line Shapes - Mineral Spectra	37
5.3	Estimation of Percentage Composition	39
CHAPTER VI	RESULTS AND INTERPRETATIONS - PART I	42
6.1	Estimation of Iron Sites in Bulk Samples	42
6.2	Pyroxene Structure	47
6.3	Orthopyroxenes	50
6.4	Clinopyroxenes	59
6.5	Pyrites	69
CHAPTER VII	RESULTS AND INTERPRETATIONS - PART II	72
7.1	Introduction	72
7.2	The Formation and the Samples	73
7.3	Absorbers Preparation Results	74
7.4	Interpretation of Results	84
7.5	Discussion of Results	88
CHAPTER VIII	CONCLUSION	89
APPENDIX A	Description of Samples	91
APPENDIX B	Programme MOSSBR	93
APPENDIX C	Data Transfer - Programmes and Steps	108
APPENDIX D	Published Data on Orthopyroxenes, Clinopyroxenes, and Pyrites	120
LIST OF REFERENCES	.....	124

LIST OF TABLES

		PAGES
1.	Electron Densities at the Iron Nucleus for Different Configurations	8
2.	Properties and Parameters of the 14.4kev Gamma Rays	19
3.	Isomer Shift Scales	19
4.	Isomer Shifts for High Spin Iron	30
5.	δ Values for Various Electronic States and Coordination Numbers	32
6.	Parameters of Bulk Samples	46
7.	Calculated Parameters of Orthopyroxenes	51
8.	Calculated Parameters of Clinopyroxenes	67
9.	Calculated Parameters of Pyrite	69
10.	Calculated Parameters of Gaspé Copper Mines Samples	83

LIST OF FIGURES

		PAGES
1.	Classical Emmission of Gamma Rays	3
2.	Nuclear Energy Levels and the Isomer Shift	7
3.	Quadrupole Splitting and the Resultant Mössbauer Spectrum	12
4.	Magnetic Splitting in ^{57}Fe	14
5.	Block Diagram of the Mössbauer Experiment	16
6.	Decay Scheme of ^{57}Co	18
7.	Drive Velocity Waveform, the Corresponding Channel Advance and Absorption Spectrum	21
8.	Positions and Splitting in an Iron Foil Spectrum	24
9.	Iron Foil Spectrum at a Velocity of 10mm/sec	25
10.	Iron Foil Spectrum at a Velocity of 4mm/sec	26
11.	Schematic of Data Transfer Arrangement (6809)	27
12.	Schematic of Data Transfer Arrangement (6800)	28
13	^{57}Fe Isomer Shift Data in Various States	29
14.	Variation in Quadrupole Splitting versus Coordination Number	33
15.	Qualitative Relative Distortion from Octahedral Symmetry versus Δ in Silicates	34
16.	Absorption Spectrum of Sample E288.c	43
17.	Absorption Spectrum of Sample E282.b	44
18.	Absorption Spectrum of Sample E294	45
19.	Pyroxenes in the System (Ca-Fe-Mg)	47
20.	Idealized Illustration of a Single Pyroxene Chain	48
21.	Crystal Structure of Diopside	49
22.	Absorption Spectrum of CGW1	52

		PAGES
23.	Absorption Spectrum of CG3	53
24.	Absorption Spectrum of CG5	54
25.	Absorption Spectrum of CG12	55
26.	Quadrupole Splitting versus the Ratio Fe/(Fe+Mg) in Orthopyroxenes	57
27.	Fe^{2+} site Occupancy at M_1 against M_2 of Natural Orthopyroxenes	59
28.	Absorption Spectrum of CG1	60
29.	Absorption Spectrum of CG6	61
30.	Absorption Spectrum of CG8	62
31.	Absorption Spectrum of CG11	63
32.	Absorption Spectrum of CG14	64
33.	Absorption Spectrum of CGW3	65
34.	Variation of ΔM_1 against Fe/(Fe+Mg) in Diopside-Hedenbergite	68
35.	Absorption Spectrum of Pyrite SS7P	70
36.	Absorption Spectrum of Pyrite SS8P	71
37.	Geological Map of the Gaspé Copper Mines Area	73
38.	Cross Section Through the Copper Mountain Plug	75
39.	Drill Holes and Variation of Thickness in the Cap Bon Ami Formation	76
40.	Absorption Spectrum of Sample A (S675-2612)	77
41.	Absorption Spectrum of Sample B (S678-2761)	78
42.	Absorption Spectrum of Sample C (S258-2027)	79
43.	Absorption Spectrum of Sample D (U3587-1552.5)	80
44.	Absorption Spectrum of Sample E (U1467-240)	81
45.	Absorption Spectrum of Sample F (S674-2313)	82

PAGES

46. The Copper Mountain Plug and Metamorphic Zones 84

47. Variation of Fe^{3+} Against Absorption 85

48. Fe^{3+} versus Distance from Center of Plug 86

49. Fe^{3+} versus Distance from Plug Boundary 87

CHAPTER I

INTRODUCTION

The first studies of geologically important minerals using gamma ray resonant absorption were performed shortly after the discovery of the Mössbauer effect. They were concerned with the quadrupole perturbed magnetic hyperfine interaction of ^{57}Fe in hematite ($\alpha - Fe_2O_3$) by Kistner and Sunyar[1] in 1960, and the effect of the Verwey transition ($Fe^{2+} \leftrightarrow Fe^{3+}$) on the internal magnetic fields in magnetite (Fe_3O_4) by Bauminger et.al.[2] in 1961. The aims in the early period were primarily directed towards the properties of nuclear states (low energy nuclear physics). General interest in its applications to mineralogy, geology and crystallography developed a few years later, where attention was focused on ^{57}Fe resonance in minerals, while little work has been performed on other Mössbauer nuclei.

Former applications in mineralogy and geology, cover mainly the following areas, (i) the analysis of the oxidation states of iron at different crystal sites (ii) The assignment of distinct hyperfine patterns to non equivalent lattice positions which leads to the determination of the Fe^{2+}, Fe^{3+} site preference. (iii) The study of area ratios of distinct hyperfine patterns, which leads to the determination of certain thermodynamical parameters, like the exchange energies of chemical reactions between non-equivalent lattice sites, activation energies, order-disorder phemomena, etc... (iv) The identification of iron minerals using the finger print technique[3] (comparing observed parameters, with previously published data on refined minerals). This technique is followed mainly in the analysis of bulk rock, meteorites and lunar soils.

The main objectives behind this work are:

A - To investigate the possible use of Mossbauer spectroscopy as a geochemical prospecting technique: firstly, in rapid semiquantitative analysis of fine grained rocks (e.g. alteration products around certain ore deposits), and secondly, for the detection of very small amounts of iron minerals formed at a considerable distance from an actual ore body but which are by products of the same ore forming process. The possible use of Mossbauer spectroscopy in geochemical prospecting, was suggested by Bancroft[3] in 1973. Our investigation is carried on the Gaspé Copper mines in the Gaspé Peninsula of Quebec by studying samples belonging to specific formations of the area and others which are picked randomly.

B - To reinvestigate previously proposed relations concerning the variation of the quadrupole splitting of iron in certain minerals with the variation of iron contents or the iron ratio in pyroxenes (Bancroft 1967)[13].

The theory of the Mössbauer effect is presented in Chapter 2, while the Mössbauer experimental technique is presented in Chapter 3. Chapter 4 constitutes the background on iron minerals. The method of analysis and description of the Computer programme used, are given in Chapter 5. A brief presentation on the pyroxene crystal structure is followed by the results and interpretations in the study of the bulk samples, the orthopyroxenes and the clinopyroxenes, in Chapter 6. The potential use of Mossbauer spectroscopy in studying alteration patterns related to ore forming processes is illustrated by the results of six samples taken from a formation adjacent to the Copper Mountain plug at Gaspe Copper mines in the Gaspé peninsula of Québec, in Chapter 7. Chapter 8 is a conclusion.

CHAPTER II

THEORY

2.1 RESONANCE-RECOIL FREE EMISSION.

According to the laws of conservation of energy and momentum, the emission of a gamma ray by a nucleus of a free atom (moving in the X-direction with a velocity V) due to its transition from an excited state Ee to a ground state Eg; subjects the nucleus to have a total momentum MV before and after emission, i.e. the momentum of the emitted gamma ray (E/c) is balanced by a change in the velocity of the nucleus, Figure 1. The difference between the nuclear transition Energy E_0 and the gamma ray energy $E\gamma$ is given by equation 1.

$$\delta E = E_o - E\gamma = E_R + E_D \qquad (1)$$

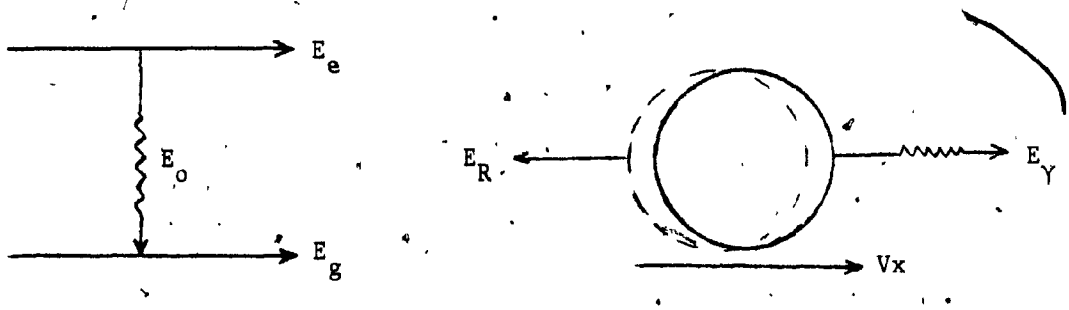

Figure 1

CLASSICAL EMISSION OF GAMMA RAYS

δE is the sum of two factors: a) the recoil energy $E_R = \frac{1}{2}Mv_R^2$ where v_R is the recoil velocity and M the mass of the nucleus, b) a Doppler term $E_D = Mv_R V_X$ because the energy of a gamma ray emitted by a nucleus

moving with a velocity V along the gamma ray propagation is shifted by a first order Doppler term. δE is very small compared to $E\gamma$ but it is significant if we consider the line width Γ of the gamma ray[4]. This is an aspect of Heisenberg's uncertainty principle which for energy and time is given by equation 2.

$$\Delta E.\ \Delta t \geq \hbar \qquad (2)$$

h is Planck's constant; ΔE is associated with the line width Γ of a gamma ray and Δt with the mean life τ of the excited state. The least uncertainty in such a case is $\tau\Gamma = \hbar$ or $\Delta E = \Gamma = \hbar/\tau$.

The natural line width Γ is defined as the full width at half maximum of an emission curve, and is very small when compared to the recoil energy of the nucleus, i.e. δE is greater than the line width. Absorption of gamma quanta could not be observed in systems of similar transition energies because emission and absorption profiles do not overlap[4].

Mössbauer discovered while studying the scattering of gamma rays of ^{191}Ir by Ir and Pt that for some low energy gamme rays δE is negligible, and that emission and absorption profiles overlap[5]. Mössbauer interpreted the situation by postulating that a fraction of the gamma rays emitted by solid sources are without recoil. His interpretation viewed a crystal lattice as a quantized system (electrons and nuclei) where it cannot be excited in any fashion but as a simple Einstein model of a solid, it needs an energy of $\pm h\nu$; $\pm 2h\nu$.... to be excited; i.e. the recoil energy E_R of a nucleus must be

equal to or greater than $\hbar\nu$ to excite the lattice to its lowest states. If E_R is less than $h\nu$, the lattice is not excited and the emitting atom does not recoil but the whole crystal lattice mass takes up the recoil energy. In such a case E_R and E_D are small compared to E_γ, and resonance or overlapping of emission and absorption profiles takes place.

Due to the comparable magnitudes of the recoil energy and the lattice excitation energy, only a fraction of the gamma rays is emitted without recoil. This fraction is known as Mössbauer fraction and is given by equation 3[3].

$$f = \exp\left[\frac{-4\pi^2 \langle X^2 \rangle}{\lambda^2}\right] \qquad (3)$$

λ stands for the wave length of the gamma quanta and $\langle X^2 \rangle$ is the component of the mean square vibrational amplitude of the emitting nucleus in the direction of the gamma ray.

2.2 HYPERFINE STRUCTURE

Prior to Mössbauer discovery, the ability to resolve hyperfine interactions by observing the transitions of gamma rays was discounted, although a less direct measure of quadrupole and magnetic splitting could be obtained from gamma-gamma directional correlation[1]. These interactions are attributed to the nuclear charge distribution and the extra-nuclear electric and magnetic fields. There are three main hyperfine interactions corresponding to the nuclear moments determining the nuclear levels:

A. Electric Monopole Interaction (E_o) - Isomer Shift

B. Electric Quadrupole Interaction (E_2) - Quadrupole Splitting

C. Magnetic Dipole Interaction (M_1) - Nuclear Zeeman Effect

2.2.a ISOMER SHIFT

A nucleus occupies a finite volume. The s-electrons have the ability to penetrate the nucleus and spend a fraction of time inside the nuclear region. The p, d, and f electrons do not possess this ability except in the case of relativistic effects where $p_{\frac{1}{2}}$ electrons can spend a very small fraction of time inside the nucleus[6]. Due to the electrostatic interaction between the nuclear charge and the s-electron charge, the nuclear energy levels are shifted by a small amount δ. This shift δ (known as the Isomer, chemical or central shift), was computed classically by Wertheim[4], assuming that the nucleus is a uniformly charged sphere of radius R, where the electron cloud is uniformly distributed over the nuclear range. δ then represents the energy difference between the electrostatic interaction of a point nucleus and one with radius R, having the same charge Ze. The derived expression of δ is given by equation 4 where $-e|\psi_{(o)}|^2$ is the electronic charge density.

$$\delta = \frac{2\pi}{5} Ze^2R^2|\psi_{(o)}|^2 \qquad (4)$$

The energy difference between the ground state g and an excited state e of the nucleus is given by equation 5:

$$\delta = (\delta E)_e - (\delta E)_g = \frac{2\pi}{5} Ze^2(R_e^2 - R_g^2)|\psi_{(o)}|^2 \qquad (5)$$

In a Mössbauer experiment, we actually observe the difference of the electrostatic shift between a source and an absorber of different electrostatic environments, where the electron density is different from source to abosrber. Equation 6:

$$\delta = \frac{4\pi}{5} Ze^2R^2 \left(\frac{\delta R}{R}\right) \left[|\psi_{(o)}|^2_A - |\psi_{(o)}|^2_S \right] \qquad (6)$$

δR stands for the difference between the radii of the excited and ground states. The corresponding resonant Doppler velocity in an experiment is given by equation 7:

$$V = \left(\frac{4\pi c}{5E_\gamma}\right) Ze^2R^2 \frac{\delta R}{R} \left[|\psi_{(o)}|^2_A - |\psi_{(o)}|^2_S \right] \qquad (7)$$

δ then is the distance of the center of gravity of the absorption peak or peaks from the zero Doppler velocity Figure 2.

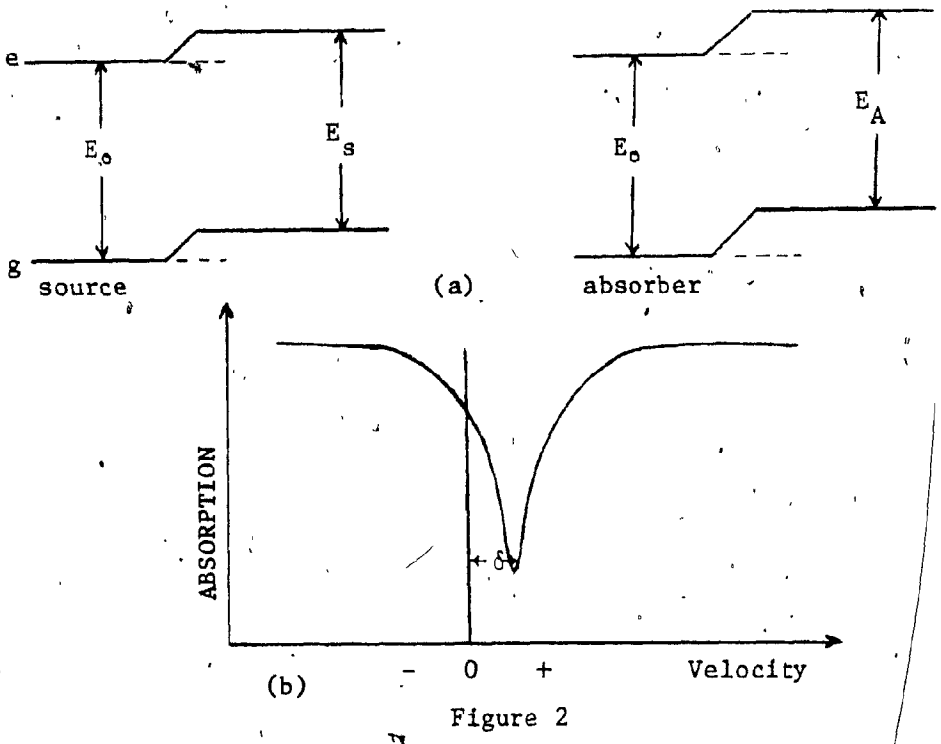

Figure 2

(a) SOURCE AND ABSORBER NUCLEAR ENERGY LEVELS

(b) RESULTANT ISOMER SHIFT

From the previous expression of the Isomer shift, it is noticed that δ is dependent mainly on two factors, $|\psi_{(o)}|^2$ and R. The ratio $\frac{\delta R}{R}$ is known but not to a great accuracy[7] while the electron density is dominated by the s-electrons which can be assumed as being composed of two contributions. The direct s-density contributions and the indirect s-changes caused by the shielding of the outer s-electrons from the nucleus by the charge densities of the p, d, and f electrons. Changes in the valence shell structure influence the s-electron density directly by altering the s-electron population where increasing s-density will increase $|\psi_{(o)}|^2$ and shielding s-electrons by p, d, and f electrons, i.e. increasing the density of p, d, and f respectively will cause s-electrons cloud to expand[2,4] and thus decrease $|\psi_{(o)}|^2$. The Isomer shift between $Fe^{2+}(3d^6)$ and $Fe^{3+}(3d^5)$ is a direct illustration of the facts mentioned above. 3d has no charge density at the nucleus and this suggests no shifts, however, the behaviour of the 3s and 4s electrons in iron depends on the number of 3d electrons where an added 3d electron partially screens the nuclear potential seen by the 3s electrons leading to a larger average radius and a lower $|\psi_{(o)}|^2$. Table 1 shows electron densities at the iron nucleus for different configurations.

TABLE 1

ELECTRON DENSITIES AT THE IRON NUCLEUS FOR DIFFERENT CONFIGURATIONS[8]

	$3d^8$	$3d^7$	$3d^6$	$3d^5$	$3d^6\ 4s^2$
From 1 electron in 1S	5378.005	5377.973	5377.840	5377.625	5377.873
From 1 electron in 2S	493.953	493.873	493.796	493.793	493.968
From 1 electron in 3S	67.524	67.764	68.274	69.433	68.028
From 1 electron in 4S	-	-	-	-	-
$\|\psi_{(o)}\|^2$	11878.9	11870.2	11879.8	11881.7	11885.8

(in atomic units: electrons per cubic Bohr radius)

Other expressions for the Isomer shift have been derived taking into account relativistic self consistent fields of electrons. One of these expressions is equation 8. Its derivation assumes that the difference in electron density for two different states can be expressed as a change in the electron density alone and that the radial coefficients a_2 and a_4 depend only on the nuclear charge[7].

$$\delta = \frac{2}{3}\pi Ze^2\ \Delta\rho_e(o)[\Delta\langle r^2\rangle - b^4\ \langle r^4\rangle + b^6\ \langle r^6\rangle \ldots] \quad (8)$$

where $\Delta\rho(r) = \Delta\rho(o)\ [1 - a_2(Z)r^2 + a_4(Z)r^4 \ldots]$

$b^4 = 3/10\ a_2\ ;\ b_6 = 1/2\ a_4$

2.2.b QUADRUPOLE SPLITTING

The derivation of the Isomer shift expression by Wertheim assumes the nucleus to be uniformly charged and spherically symmetrical. However, in reality a nucleus is more or less charged ellipsoidal. This deviation is given by the electric quadrupole moment eQ which is a tensor. A nuclear state with $I > 1/2$ has a non-zero quadrupole moment that interacts with the electric field gradient EFG at the nucleus. This interaction results in a splitting of the nuclear energy levels and is known as the electric quadrupole interaction expressed in the general form by the Hamiltonian of equation 9.

$$H = \hat{Q}\ .\ (\hat{\nabla}\hat{E}) \quad (9)$$

$\hat{Q}$ denotes the operator of the nuclear electric quadrupole moment and $(\hat{\nabla}\hat{E})$ the EFG tensor operator. Q is a constant for a given Mossbauer

nuclide in different compounds, and the changes in quadrupole interaction arises only from changes of the EFG expressed as equation (10).

$$EFG = \nabla E = -\nabla\nabla V = -\begin{vmatrix} V_{xx} & V_{xy} & V_{xz} \\ V_{yx} & V_{yy} & V_{yz} \\ V_{zx} & V_{zy} & V_{zz} \end{vmatrix} \qquad (10)$$

where

$$V_{ij} = \frac{\partial^2 V}{\partial_i \partial_j} \; ; \; (V_i, V_j = x,y,z)$$

The EFG, which is a 3x3 tensor, can be reduced to diagonal form in the proper coordinate system so that it could be specified by the three diagonal components only. These components obey Laplace's equation in a region where the charge density vanishes.

$$V_{xx} + V_{yy} + V_{zz} = 0 \qquad (11)$$

In such a case, there remains only two independent parameters normally chosen to be V_{zz} and η the assymmetry parameter defined as equation 12.

$$\eta = \frac{V_{xx} - V_{yy}}{V_{zz}} \qquad (12)$$

The EFG axis are chosen such that; the off-diagonal components are zero and $|V_{zz}| \geq |V_{yy}| \geq |V_{xx}|$[3]. This constrains η to have values between zero and one. If the off-diagonal elements are non-zero, then the tensor must be diagonalized before the diagonal elements are chosen as above. Further more, two mutually perpendicular axis of three fold or

higher symmetry give rise to a vanishing EFG[9].

In general there are two fundamental sources which can contribute to the total EFG[3]. a - charges on distant atoms or ions surrounding the Mössbauer atom in non-cubic symmetry, usually called the ligand-lattice contributions. b - non-cubic electron distribution in partially filled valence orbitals of the Mössbauer atom usually denoted as the valence electron contribution. In the simple case where η is zero Q is expressed as equation (13).

$$Q = (1 - \gamma_\infty)\, Q_{lattice} + (1 - R)\, Q_{valence} \qquad (13)$$

R and γ_∞ are respectively the Sternheimer anti shielding factors, $Q_{lattice}$ is the contribution from external Ligand Charges, whereas $Q_{valence}$ is the Contribution from the valence electrons.

The Hamiltonian representing the interaction between the nuclear quadrupole moment and the electric field gradient with its eigenvalues are given below by equations (14) and (15) respectively. Where I is the nuclear spin, $\hat{I}$ the nuclear spin operator, $\hat{I}_+$ and $\hat{I}_-$ the raising and lowering operators respectively. M_I is the nuclear magnetic spin quantum number.

$$\mathcal{H} = \frac{e^2 Q V_{zz}}{4I(2I-1)} \left[3\hat{I}_z^2 - \hat{I}^2 + \frac{\eta}{2}(\hat{I}_+^2 + \hat{I}_-^2)\right] \qquad (14)$$

$$F_Q = \frac{eQV_{zz}}{4I(2I-1)} \left[3M_I^2 - I(I+1)\right]\left(1 + \frac{\eta^2}{3}\right)^{\frac{1}{2}} \qquad (15)$$

The splitting of the nuclear energy levels by the electric quadrupole interaction are illustrated by the ^{57}Fe case where the excited state

has $I = \frac{3}{2}$ and the ground state has $I = \frac{1}{2}$. The excited state splits into two $(M_I = \pm\frac{3}{2}; \pm\frac{1}{2})$ while the ground state is not split because its quadrupole moment vanishes. Both transitions are allowed and the spectrum observed is a two line spectrum. In Figure 3, the seperation of the peaks is the quadrupole splitting Δ and the center of the two peaks relative to the source is the isomer shift(δ).

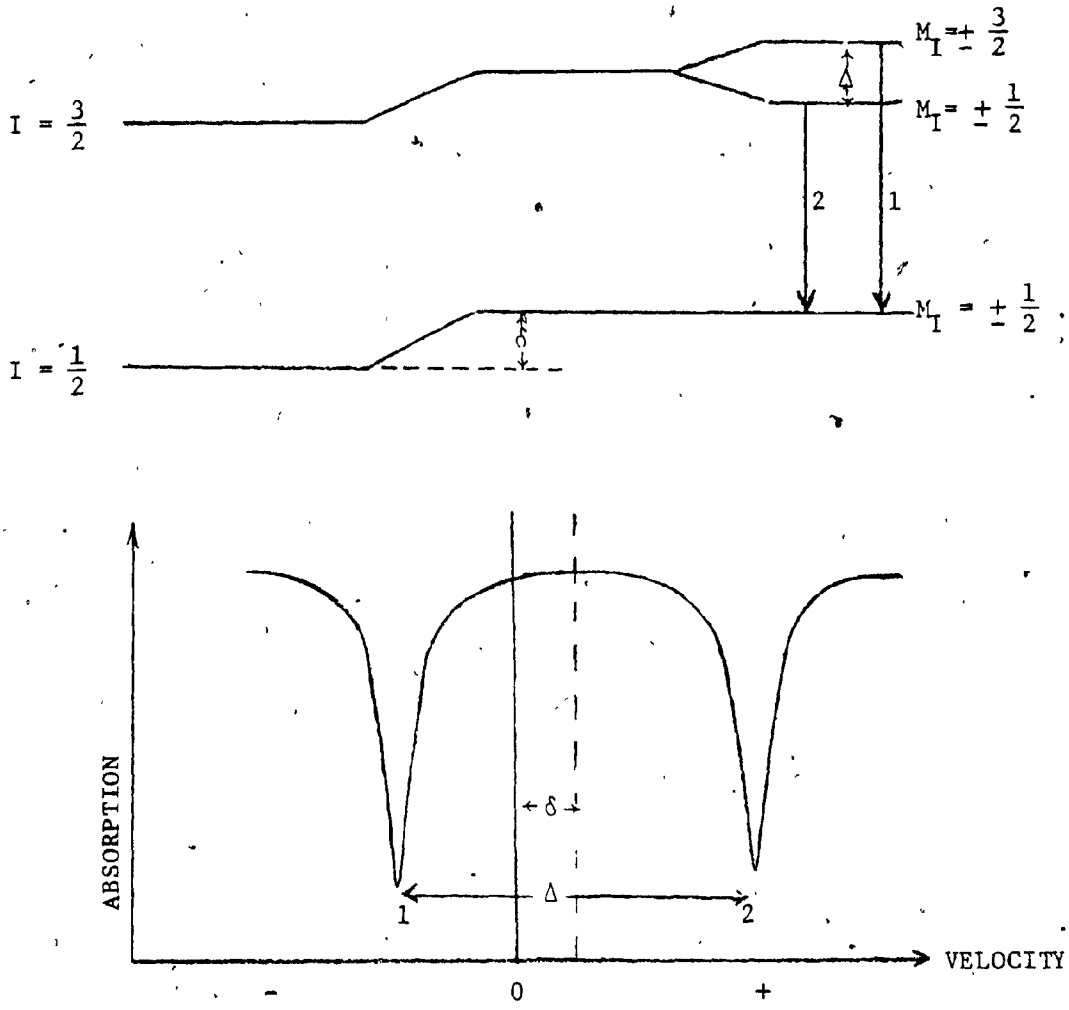

Figure 3

(a) Quadrupole Splitting (b) Resultant Mössbauer spectrum

2.2.c MAGNETIC SPLITTING

A nucleus with a non-zero spin has a magnetic dipole moment μ which can interact with local or applied magnetic fields at the nucleus. The Hamiltonian of the interaction is given by equation 16 where g_n is the gyromagnetic ratio (nuclear g-factor) and $\beta_n = e\hbar/2mc$ is the nuclear Bohr magneton.

$$\mathcal{H}(M_I) = -\vec{\mu} \cdot \vec{H} = -g_n \beta_n \vec{I} \cdot \vec{H} \qquad (16)$$

The eigenvalues of $\mathcal{H}$ that are obtained using the first order perturbation theory[6] are given by equation 17.

$$E_m (M_I) = -\mu H M_I/I = -g_n \beta_n H M_I \qquad (17)$$

Due to the magnetic interaction, a nuclear level with a spin I is split into $2I + 1$ equally spaced sublevels. These sublevels are characterized by the nuclear magnetic spin quantum number M_I, $M_I = I, I-1, \ldots, -I$. For ^{57}Fe, the excited and ground states have $I_e = \frac{3}{2}$ and $I_g = \frac{1}{2}$ respectively. Both states have magnetic dipole moments and are split by magnetic interaction. The Selection rule $\Delta I = 1$; $\Delta M = 0, \pm 1$ gives rise to a symmetric six lines spectrum as shown in Figures 4 and 10. The isomer shift δ is given by the center of gravity of the six lines; these have in general equal line widths but different intensities[3], the intensities are given as:

$$I_1 = I_6 = 3(1 + \cos^2 \Theta)$$
$$I_2 = I_5 = 4 \sin^2 \Theta$$

$$I_3 = I_4 = 1 + \cos^2\theta$$

θ is the angle between the direction of radiation and the effective magnetic field H.

Except for mettalic iron, pure nuclear magnetic dipole interactions are not encountered, but frequently the nucleus experiences both magnetic and quadrupole interactions. As a result, for the case of ^{57}Fe the sublevels of $I = \frac{3}{2}$ state are no longer equal and the spectrum is not symmetric. Many cases arise. One case is when the EFG tensor is axially symmetric and its principle axis make an angle β with the axis of the magnetic field. First order perturbation theory yields equation 18 as the general expression for the eigenvalues[6].

$$E = -g_n \beta_n H M_I + (-1)^{|M_I|+\frac{1}{2}} eQ \frac{V_{zz}}{8} (3\cos^2\beta - 1) \quad (18)$$

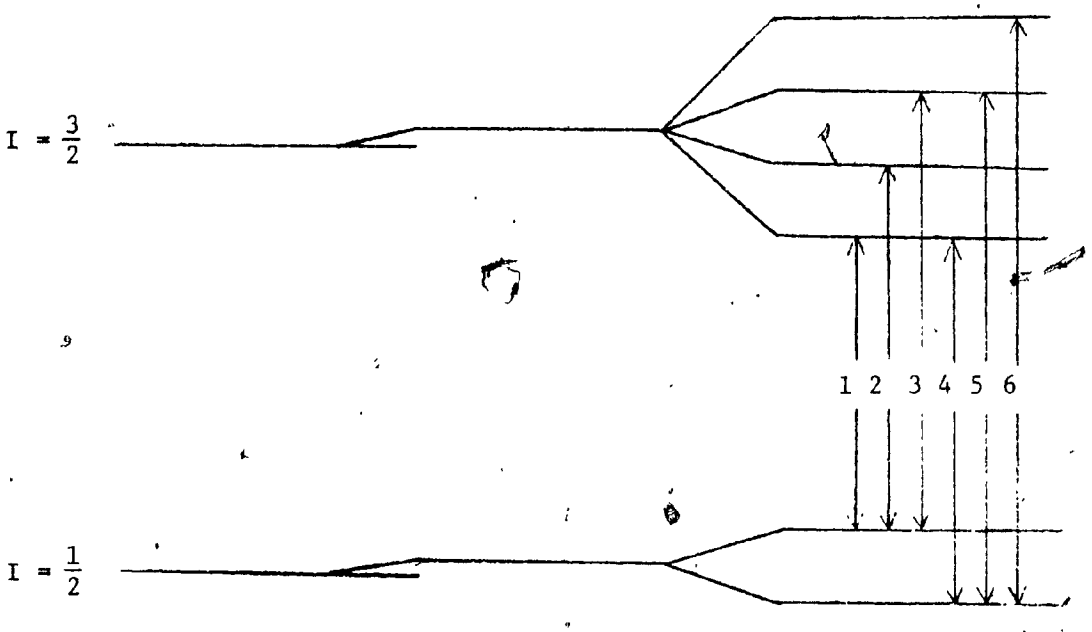

Figure 4

MAGNETIC SPLITTING IN ^{57}Fe

CHAPTER III

EXPERIMENTAL

3.1 METHOD

A Doppler Velocity V is applied to a source (Section 3.2) mounted on a transducer driven by a Velocity driver (Section 3.3). The applied velocity shifts the initial energy E_0 of the emitted gamma rays by a value dE (the Doppler Velocity is considered positive when the Source moves towards the absorber and negative when it moves away). Some gamma rays are resonantly absorped by an absorber placed in between the Source and the detector (whenever the energy of the emitted gamma rays equals the excitation energy of the nuclei of the absorber). The gamma rays which are transmitted through the absorber are transformed into pulses proportional to their energies by a detector and an amplification system consisting of a pre-amplifier and an amplifier. A single channel analyzer (Section 3.5) selects the 14.4 kev gamma rays only. The resulting pulses are fed into a 512 multi-channel analyzer (Section 3.4). A time-base generator opens one channel after the other with constant intervals of time; each channel corresponds to a certain velocity of the source. The acquired spectrum, stored by the memory of the MCA, as displayed on a cathode ray oscilloscope, consists of two parts, one being the mirror image of the other. This is because of the particular driving signal used. Figure 5 represents a block diagram of the experiment.

The spectra so obtained, may consist of one or more absorption peaks, these peaks are defined by their heights, halfwidths, positions and areas. A good spectrum is characterized by having minimal errors

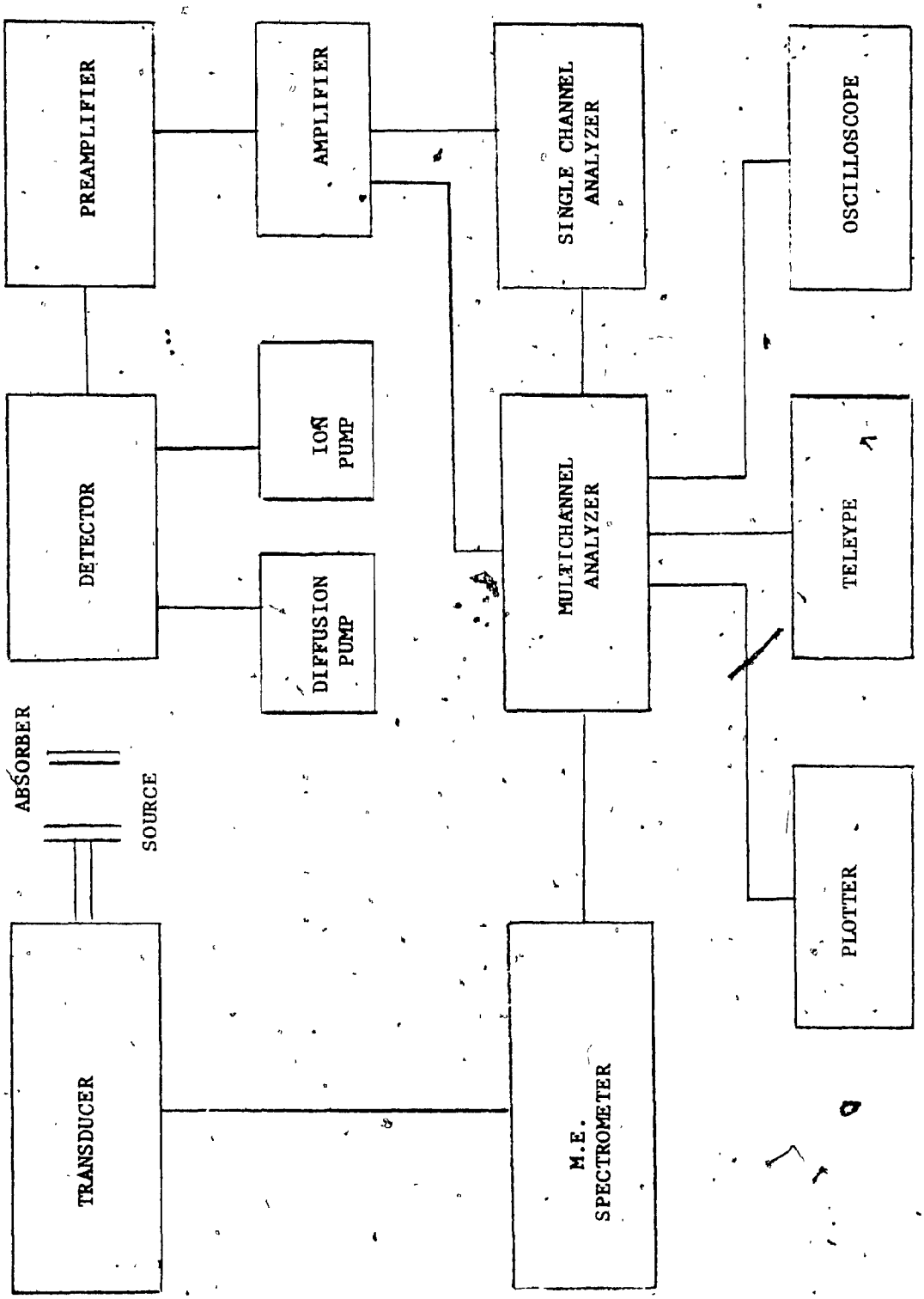

FIGURE 5

BLOCK DIAGRAM OF THE MÖSSBAUER EXPERIMENT

in the calculated and observed spectrum. Errors in position of the peaks mainly arise from the non-linearity of the waveform that drives the source. Several methods have been described in different texts to eliminate this error.. The well known positions of the six peaks of an iron foil are used for Velocity Calibration (Section 2.6).

The data stored by the memory unit of the MCA is transferred to the main CDC computer where it is analyzed. The transfer procedure and the system carrying the operation is described in Section 2.7. While description of the Computer Programme and analysis is dicussed in Chapter 4.

3.2 SOURCE

The most commonly used isotope in Mössbauer experiments is ^{57}Fe. Besides the great abundance of systems containing iron, the ^{57}Fe nuclear parameters are very favorable. It has relatively low energy gamma transitions, a large recoilless fraction at room temperature. A long lived parent nucleus, little interference from other gamma rays and x-rays, and a relatively narrow line.

The source used is ^{57}Co in a Pd matrix of few millicurie strength. The decay scheme of ^{57}Co is shown in Figure 6 and the parameters of the 14.4 Kev gamma transition are given in Table 2. The source lattice should have a high Debye temperature and a symmetric structure so that the gamma rays are not modified by either electric quadrupole or magnetic dipole interactions. The effective temperature of a Mössbauer nucleus introduced as an impurity in a host lattice is given by equation 19[9] where M_{host} and M_{imp} are the masses of the host and impurity atoms respectively, and θ_D the Debye temperature of the lattice.

$$\theta_{eff} = \theta_D \left[\frac{M_{host}}{M_{imp}}\right]^{\frac{1}{2}} \qquad (19)$$

Because of the host matrix, the 14.4 Kev gamma ray undergoes an isomer shift. Isomer shifts for ^{57}Fe 14.4 kev relative to sodium nitro puris-side at room temperature are given in Table 3. (All isomer shift values reported in this thesis are expressed relative to sodium nitro purrisside).

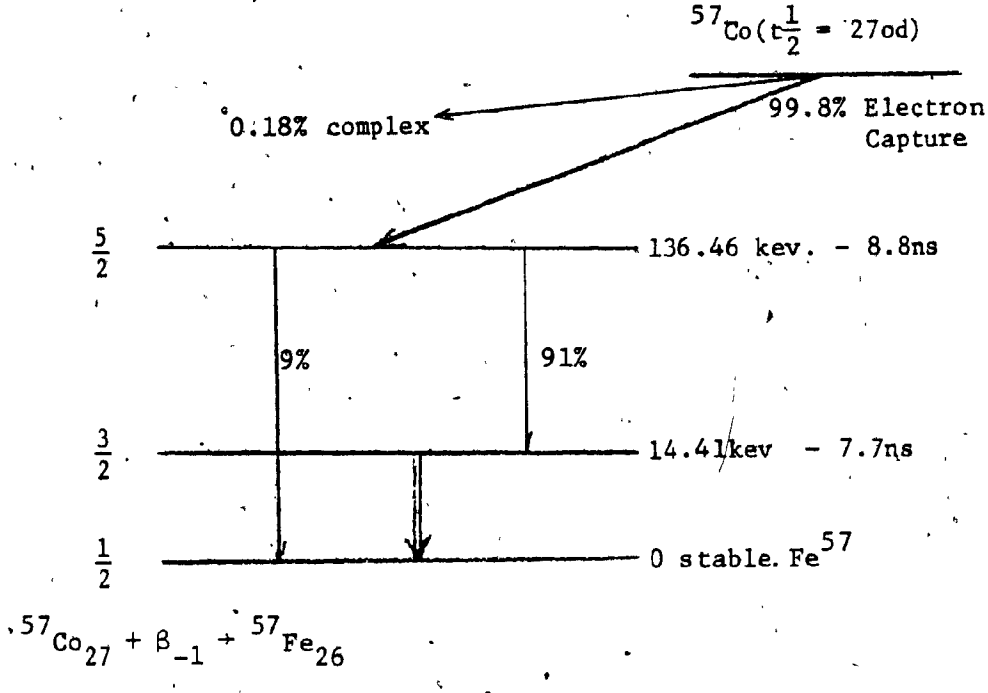

Figure 6

DECAY SCHEME OF ^{57}Co

TABLE 2

PRACTICAL PROPERTIES AND PARAMETERS[10]

• $E\gamma$	:14.41125±0.0006kev
• half life time $t\frac{1}{2}(\gamma_m)$	:97.7±0.2x10^{-19}sec
• Total internal conversion coefficient $\alpha_T(\gamma_m)$	:8.18±0.16
• Natural isotopic abundance	:2.19%
• Magnetic moment of the ground state	:+0.0904206±0.00000012nm
• Magnetic moment of the first excited state	:-0.15463±0.0002nm
• Quadrupole moment of the first excited state	:+0.196±0.008b
• Cross Section σ_0	:2.569x10^{-18}cm^2
• Natural line witdth Γ	:4.670x10^{-9}eV
• Observable line width W_0	:0.1943 mm/sec
• Free atom recoil energy	:1.958x10^{-3}ev

TABLE 3

ISOMER SHIFT SCALE[7]

Material	δ(mmsec^{-1})
$Na_2Fe(CN)_5No\ H_2O$	0
Cr	0.106±0.009
Stainless Steel	0.17±0.02
α-Iron	0.260±0.002
Pd	0.437±0.002
Cu	0.485±0.002
Pt	0.609±0.006

δ- RELATIVE TO SODIUM NITRO PURRISSIDE AT 300°K

3.3 DRIVING UNIT

The Mössbauer effect Spectrometer is an apparatus which imparts a Doppler Velocity or motion to the source. It also coordinates the counting rate at the detector so that the spectrum channel number will be a function of the Source Velocity.

The spectrometer used is the model AM-1, manufactured by Nuclear Science and Engineering Corporation. It consists of three parts:

i - The Base Plate - a solid aluminium plate on which the transducer, the source and the absorber holder are mounted.

ii - The Transducer - a precision electromechanical unit which provides a forward and retrograde motion to the source with constant acceleration. The operating frequency range is 15 - 50 cps and the velocity range is 0 - 60 cm/sec. The linearity precision of the triangular waveform is about 1% over 95% of the half period of the velocity waveform.

iii - The Control Unit - a solid state electronic unit which accepts a square wave signal from the address register of a multi channel analyzer. It contains input signal idealizing circuitry, triangular function generating circuitry and the necessary servo and D.C. power amplifier required to drive the transducer. In Figure 7, the drive velocity waveform, the corresponding channel advance, and an absorption spectrum for a single line source and absorber, are displayed.

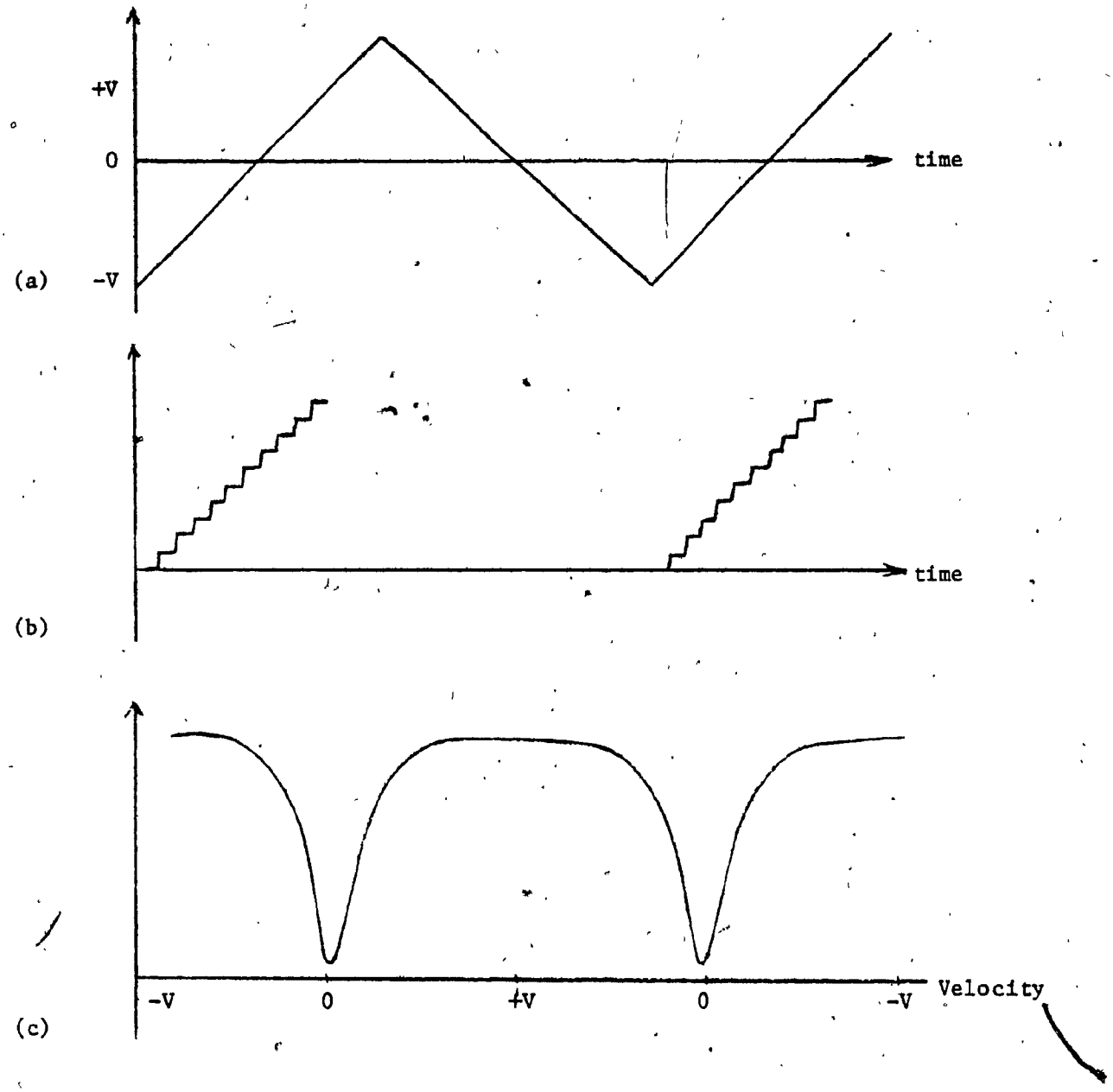

FIGURE 7

(a) DRIVE VELOCITY WAVE FORM,

(b) CORRESPONDING CHANNEL ADVANCE

(c) ABSORPTION SPECTRUM FOR A SINGLE LINE SOURCE AND ABSORBER

3.4 MULTICHANNEL ANALYZER (MCA)

The MCA used is the Series 2200 - NUCLEAR DATA System Analyzer. It consists of four units.

i - ADC - Analog to digital Converter: Is designed primarily for the processing of amplitude modulated signal pulses such as encountered in pulse height analysis. Data acquisition efficiency is enhanced by a 50 megahertz digitizing rate.

ii - Master Control - it contains facilities for establishing the primary operating modes (data acquisition, display, read in, read out) and all the data handling functions of the system. Analysis data may be added to or subtracted from data previously stored in the system memory. After data has been acquired it can be subjected to operations such as transfer from one selected memory group to another. Front panel controls enable digital selection of memory groups for data storage, display, processing and read out.

iii - Read in/out Display - it incorporates those features necessary for selection of a particular read out (print, plot, type) or control of the appropriate device. This unit is capable of driving high speed digital printers and x-y plotters.

iv - System Memory - it is divided into three modules: the memory scalar module, the memory drivers module and the memory array module. The memory scalar module contains the memory address scalar and register which allows the content of a single channel to be transferred back into the identical channel location of the memory. The memory Drivers module consists of all the driving and sensing circuits for the memory array module which permits proper handling of the data being stored. The memory array

module is designed in a manner that allows expansion up to the maximum of 24-bit, 4096 channels where each channel can store up to 1 million counts.

3.5 DETECTOR - AMPLIFICATION SYSTEM

The detector used is a Si (Li) drift solid state detector, manufactured by Simtec Ltd. model K-036 used with a Simtec P-11 HR/CN pre amplifier and a Simtec M-31 linear amplifier. The detector area is 50 mm^2 and the window is Beryllium oxide of 250μ thickness. The Simtec model P-11 HR/CN pre-amplifier is a cooled N-channel FET optimized for Simtec ultra high resolution silicon and germanium photon spectrometer elements with capacity less than 10 picofarads. The detector and the FET preamplifier are kept at temperature of liquid nitrogen. This requires low pressure in the cryostat, which is attained by a mechanical diffusion pump and monitored by an ion appendage pump control. The 14.4 kev gamma rays are selected by a Hewlett-Packard 5583A - Single channel analyzer.

3.6 CALIBRATION

The well known positions of the six lines of a natural iron foil were used to calibrate the velocity scan of the Mossbauer spectrometer. This is needed to eliminate any error in the position of the absorption peaks of the different absorbers studied. Figure 8 shows the splitting between the three doublets of an iron foil spectrum and the corresponding velocities for a ^{57}Co source in a Pd matrix[10].

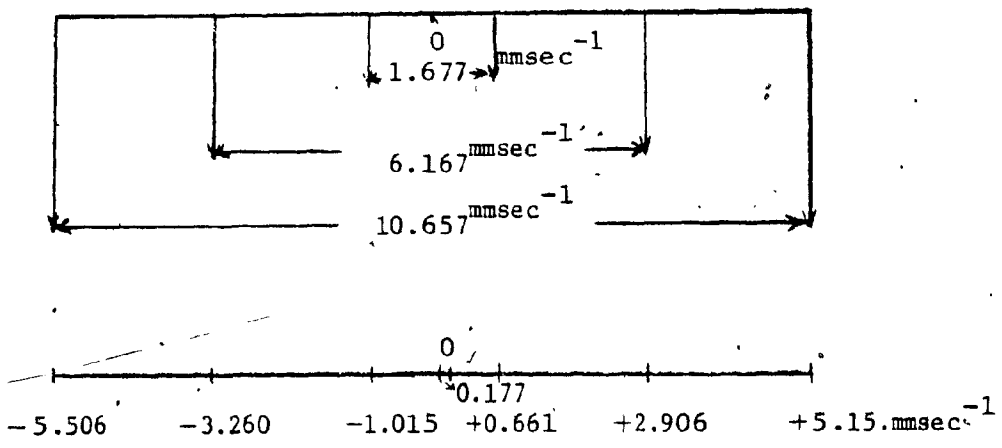

Figure 8

SPECTRUM OF AN IRON FOIL

The use of an iron foil for calibration is justified by the velocity ranges during the experiment (4 → 10 mm/sec) and the assignment of the above velocities for the peaks obtained in our experiment insures the elimination of any error in position and the parameters derived, such as the isomer shift and the quadrupole splitting. Figures 9 and 10 show the iron spectra obtained at 10 and 4 mm respectively.

3.7 DATA TRANSFER

Analysis of the absorption spectra by programme MOSSBR and the University Computer facilities, is outlined in Chapter 5. Transfer of the data stored by the memory unit of the multi channel analyzer to the university main computer (CYBER), was carried through two Computer Systems via the two main steps as outlined below.

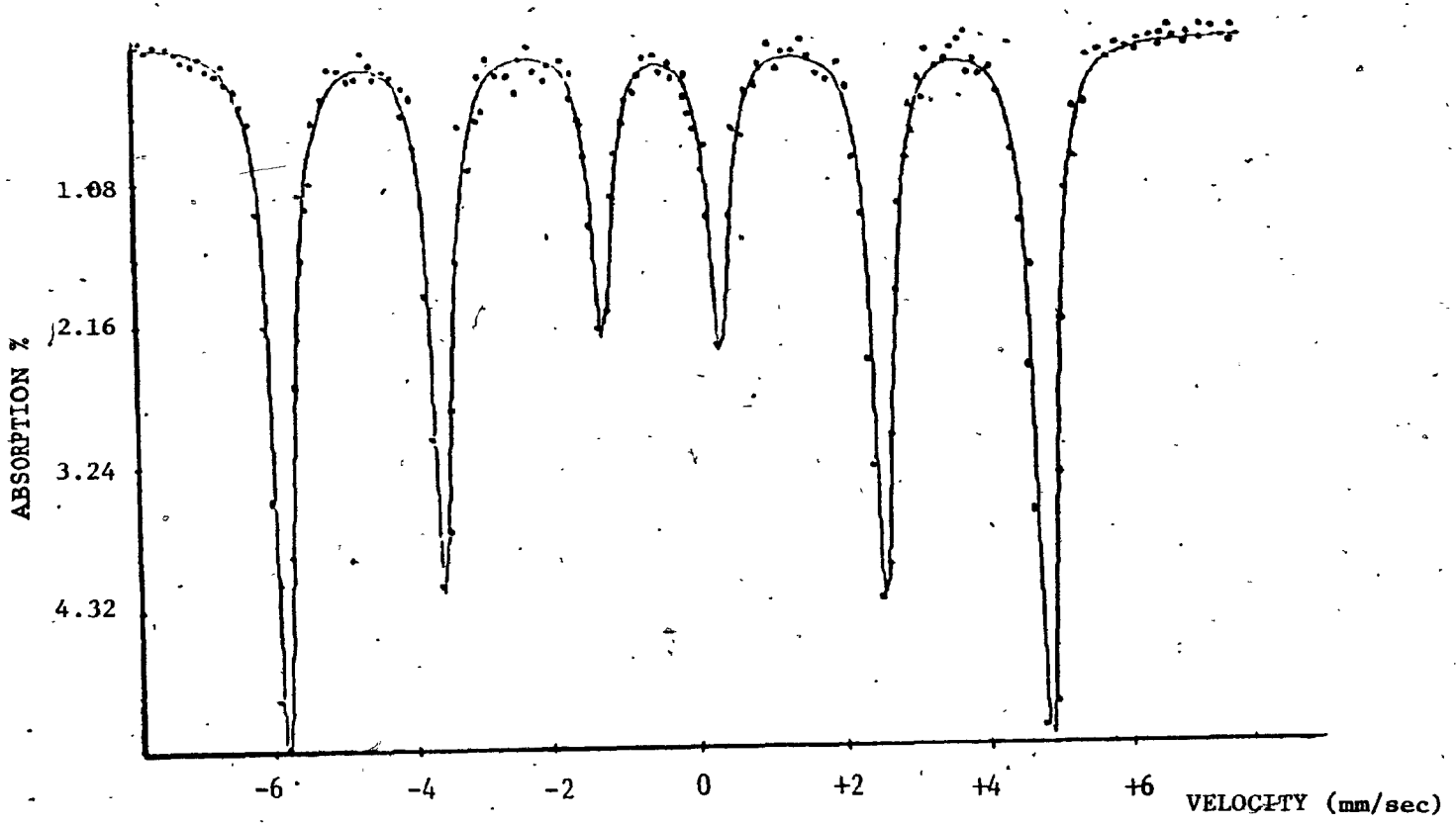

FIGURE 9

MÖSSBAUER SPECTRUM OF AN IRON FOIL (10mm/sec)

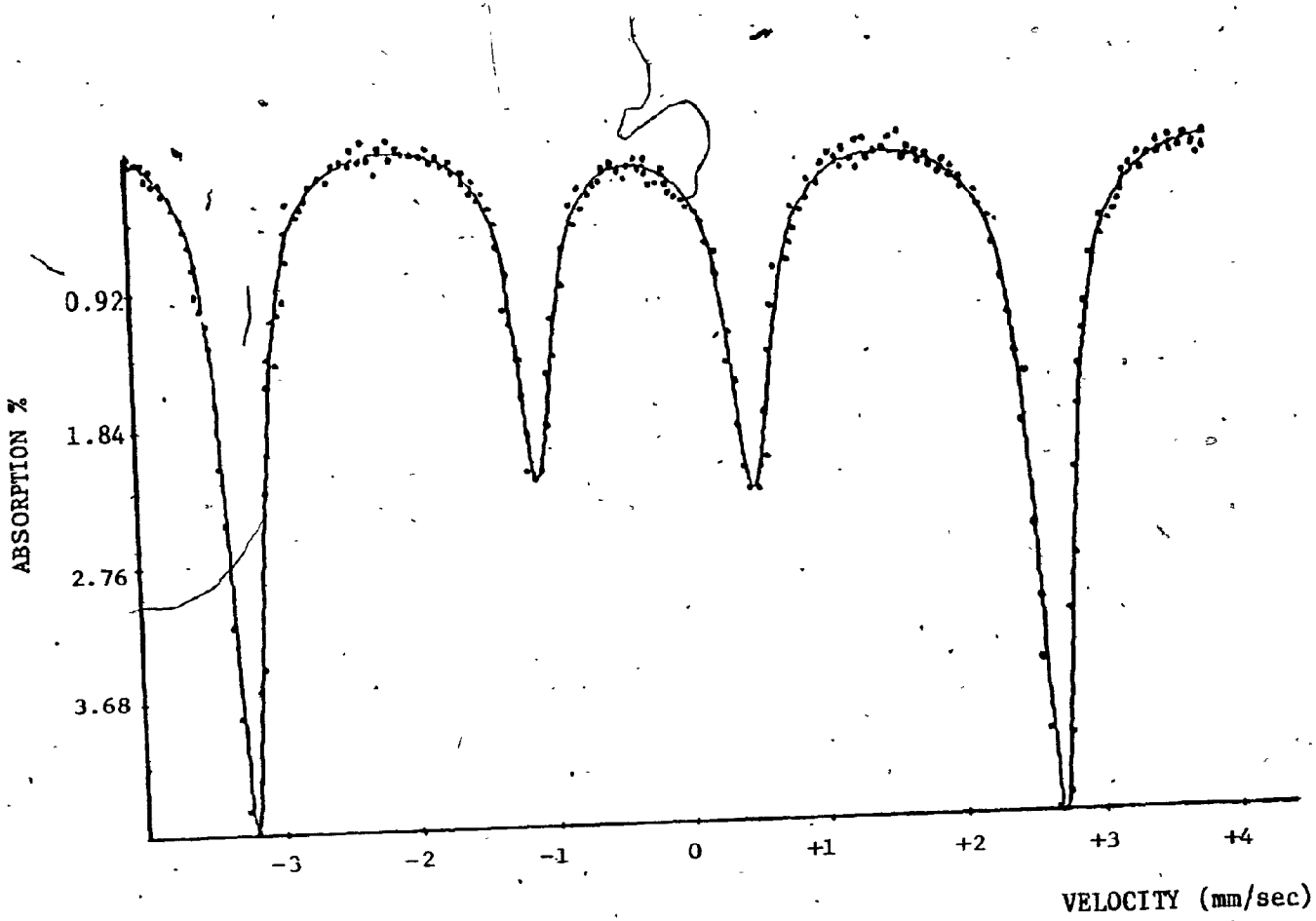

FIGURE 10.

MÖSSBAUER SPECTRUM OF AN IRON FOIL (4mm/sec).

A. LOADING OF DATA ON MAGNETIC TAPES

The ability of the "read in/out - display" unit of the multi channel analyzer to drive plotters and fast printers, has been explained in Section 3.4. Figure 11 shows the set up for the 6809 Computer System (Southwest Technical Prod. Corp.) which was assembled and programmed with the aid of the expertize available in the Physics department of Concordia University.

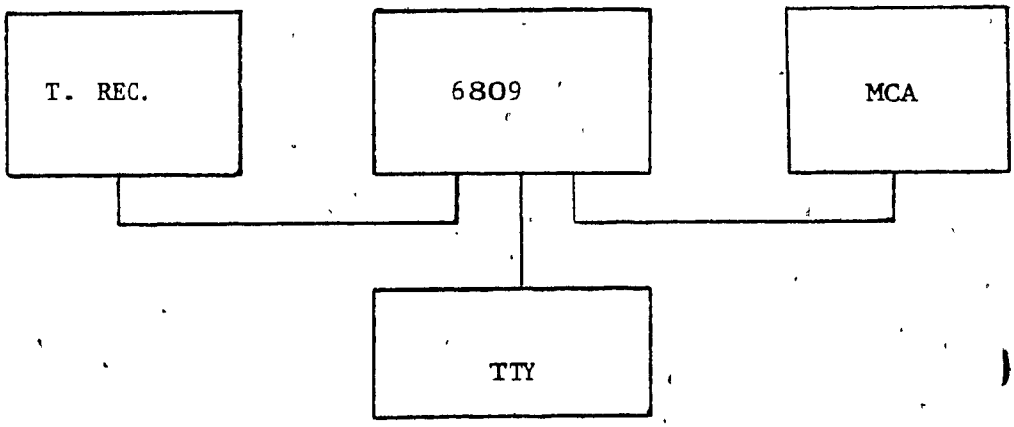

FIGURE 11

SCHEMATIC OF DATA-TRANSFER ARRANGEMENT (6809)

The 6809 is linked to the MCA, Teletype and tape recorder by an MP-LA parallel interface board and two MP-S Serial interface boards respectively. The Commands that drive the System are given through the teletype. The data is read to the memory of the 6809 from the MCA, and then recorded on magnetic tapes by a tape recorder (relevant programmes and steps are listed in Appendix C).

B. LOADING OF DATA ON CYBER

The procedure followed is similar to that of the previous step A. The data is read from a magnetic tape to the memory of the MSI 6800 Computer System (Midwest Scientific Instruments) and then from the 6800 to the Concordia CYBER. The set up is illustrated in Figure 12, the Commands are given through a teletype or a video, while the Programmes that drive the system and perform various operations are stored on discs; the disc drives are shown in Figure 12 also (Programmes and steps are listed in Appendix C).

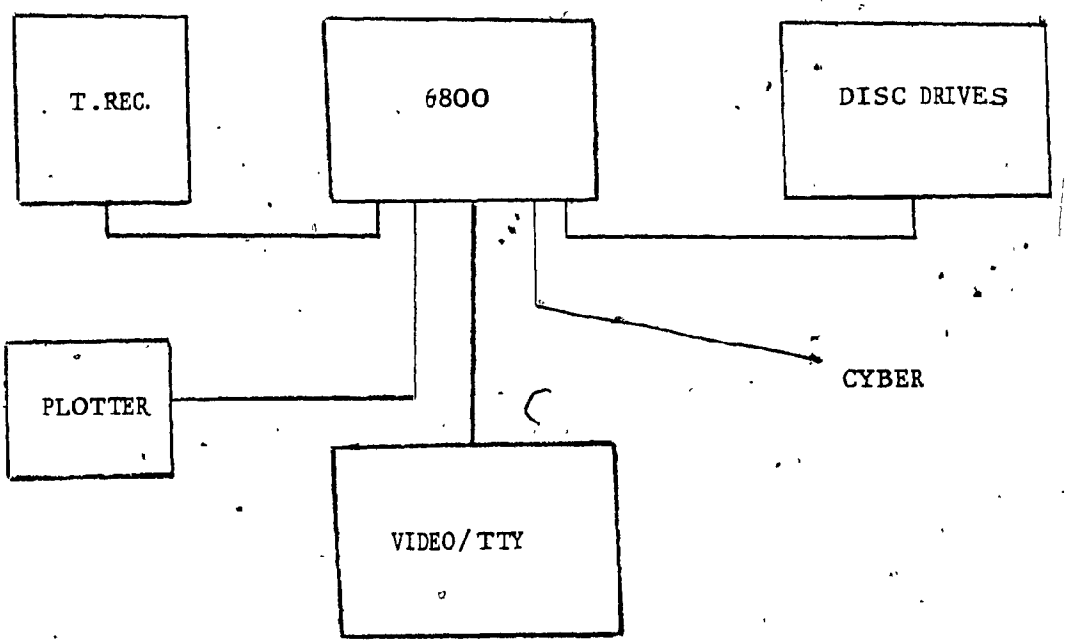

FIGURE 12

SCHEMATIC OF DATA-TRANSFER ARRANGEMENT (6800)

CHAPTER IV

IRON IN MINERALS

4.1 CHARACTERIZATION OF THE OXIDATION STATE OF IRON-COORDINATION NUMBER

Since the early investigations of iron compounds, a correlation of the isomer shift δ with the formal oxidation state of iron was established. The isomer shift is sensitive to the spin state of iron in a complex compound. As a result, the δ-values of high spin iron ($S = 2$) appear in a region well seperated from the δ-values of low spin iron ($S = 0$). Where S is the spin quantum number. Figure 13.

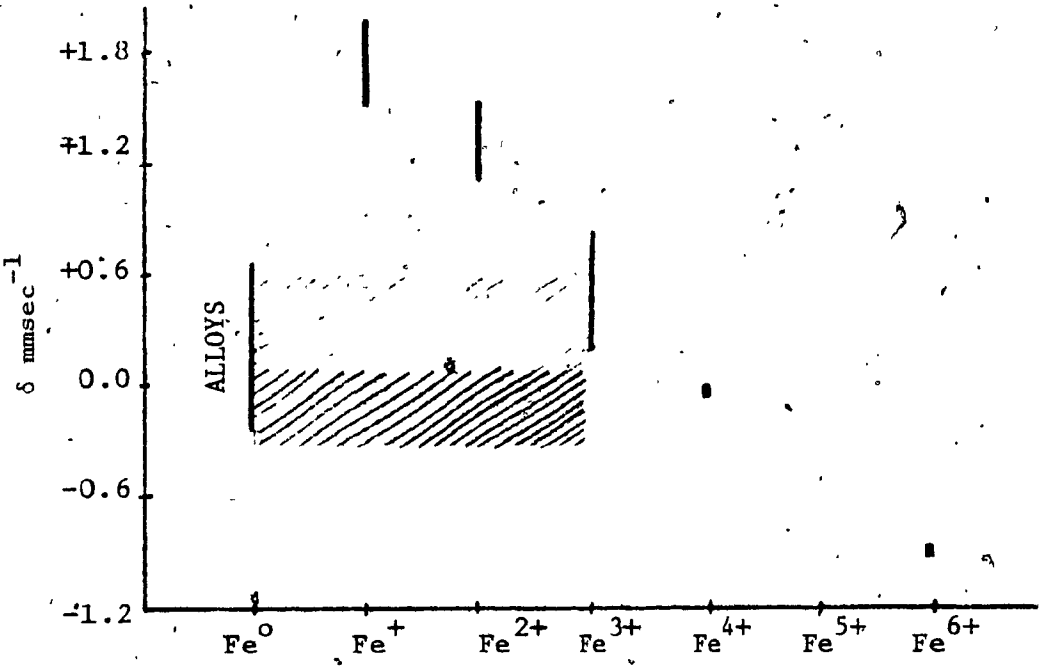

Figure 13

^{57}Fe ISOMER SHIFT DATA. IN VARIOUS IONIZATION STATES INDICATED BY BARS, AND IN HIGHLY COVALENT MATERIALS INDICATED BY SHADED AREAS[6].

Table 4 below shows that for ionic iron (high spin) the δ-values become more positive with decreasing oxidation states, and the δ-ranges for different oxidation states of high spin iron hardly overlap.

TABLE 4

ISOMER SHIFT (δ) - FOR HIGH SPIN IRON

Oxidation state:	+1	+2	+3	+4	+6
Isomer shift (mm sec^{-1}):	∿+2.2	∿+1.4	∿+0.7	∿+0.2	∿-0.6

For low spin iron II and iron III the δ-values do overlap and it is very difficult to distinguish compounds using δ-values only. However, in this case the quadrupole splitting Δ-values which range from 0 to +0.8 mm/sec for low spin iron II and from +0.7 to +1.7 mm/sec for low spin iron III can be very useful.

The dependence of the isomer shift on the electron configuration was discussed before in Section 2.2a. Table 1 showed that the s-orbitals are the main contributors and that the difference in densities originates from changes in the 3s shell. The removal of 3d electrons leads to an increase in the electron density at the nucleus due to the shielding of the 3s electrons from the nuclear charge by 3d electrons. While adding 4s electrons increases the electron density at the nucleus and causes the isomer shift to become more negative ($\frac{\delta R}{R}$ is negative for Fe^{57}). The widespread ranges of the δ-values for each oxidation state is a direct consequence of the nature of the chemical bond and the capabilities of the ligands to donate or accept electrons from the iron metal via

σ-bonding or π-bonding respectively.

In minerals, iron is conclusively ferrous and ferric. The δ-values for these two high spin states vary around the mean values 1.4 mm/sec and 0.7 mm/sec respectively. The variation depends on the coordination number, site symmetry and type of ligand. In Mossbauer analysis the determination of the oxidation state is valuable because of the certainity it provides over other techniques such as x-ray or chemical analysis[3]. However, in few minerals the oxidation state cannot be assigned readily. e.g. pentlandite $(Ni, Fe_9) S_8$ which has two quadrupole doublets of isomer shifts 0.83 and 0.62 mm/sec. These values have been attributed to electron exchange where the oxidation state is in between Fe^{2+} and Fe^{3+}. Table 5 shows how the isomer shift is correlated to the coordination number in minerals. The fact that the δ-values generally increase with increasing coordination number is very useful in assigning the structure of iron in a certain species, but the limited variation of δ and the anomalous behaviour in some minerals makes it necessary to use extra information available from Mössbauer analysis and from other techniques.

TABLE 5

MÖSSBAUER δ-VALUES FOR VARIOUS ELECTRONIC STATES AND COORDINATION NUMBER[3]

Mineral or Species	Type of Iron	δ mmsec^{-1}
Almandine garnet	8 coordinate Fe^{2+}	1.56
Silicates	6 coordinate Fe^{2+}	1.30 - 1.43
Staurdite	4 coordinate Fe^{2+}	1.22
Spinels	4 coordinate Fe^{2+}	1.07
Gillespite	4 coordinate Fe^{2+} (square planar)	1.01
Epidote	6 coordinate Fe^{3+}	0.61
Amphiboles	6 coordinate Fe^{3+}	~0.65
Iron orthoclase	4 coordinate Fe^{3+}	0.72

4.2 CORRELATION OF THE QUADRUPOLE SPLITTING WITH STRUCTURAL VARIATIONS

Figure 14 shows the variation in the quadrupole splitting Δ against coordination number. Variations in Δ-values are related to structural effects by consideration of the field gradient expressed earlier by equation 13 of Chapter 2.

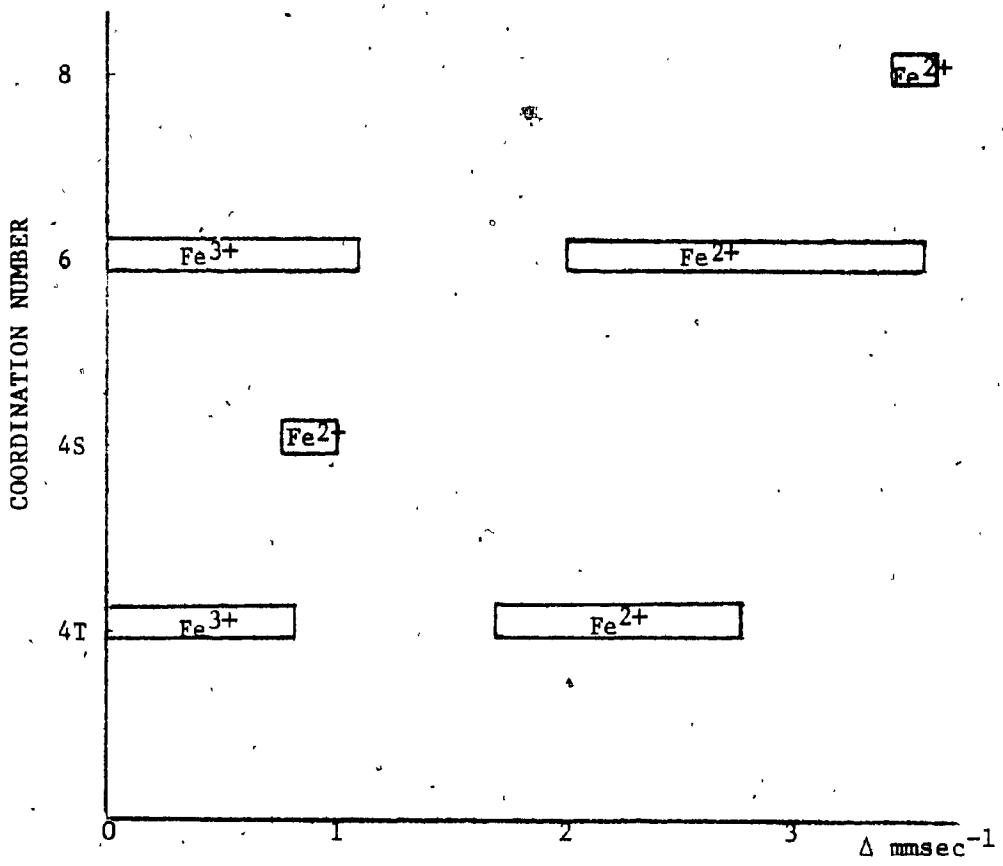

Figure 14

VARIATION IN QUADRUPOLE SPLITTING
(Δ) VERSUS COORDINATION NUMBER[3].

For ferric iron in minerals, we suppose $Q_{valence}$ is zero and the quadrupole splitting observed is due to $Q_{lattice}$ only. The ferric quadrupole splitting is expected to increase as the distortion from octahedral symmetry about Fe^{3+} increases[3]. Ferrous iron gives rise to a large $Q_{valence}$ term, the distortion from octahedral symmetry being small, a very large Δ results. Broadly the Δ-values decrease as the distortion increases, Figure 15.

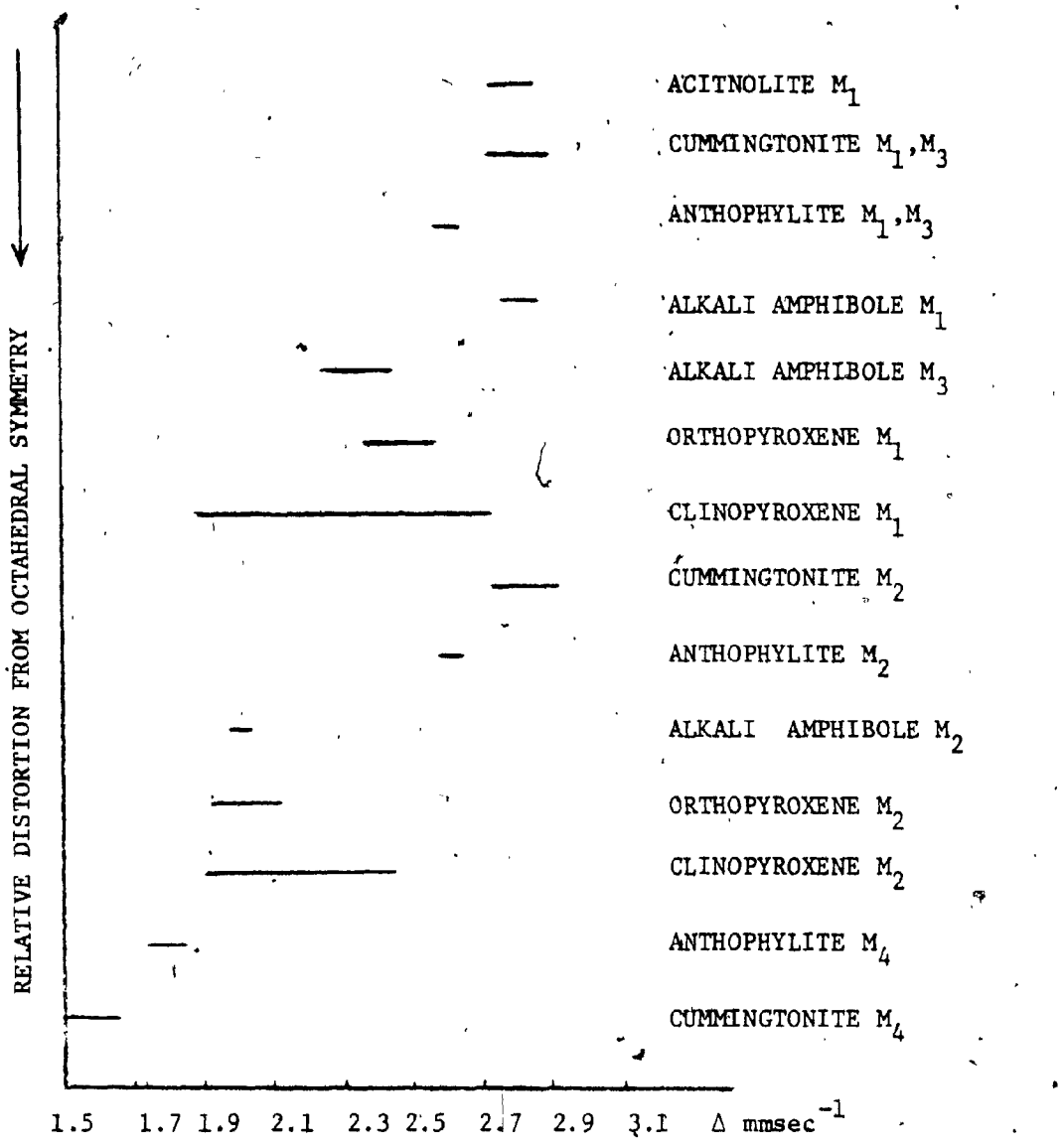

FIGURE 15

QUALITATIVE RELATIVE DISTORTION FROM OCTAHEDRAL SYMMETRY VS Δ IN SILICATES[3]

The above distortion theory is very useful for the assignment of ferrous positions in silicates for instance, the ferrous iron of the pyroxene M2 and the amphibole M_4 Crystal sites give a smaller Δ than the Pyroxene M_1 and Amphibole M_{123} less distorted sites respectively as expected. However, the distortion treatment cannot be applied conclusively because of many deviations such as, the Pyroxene M_1 and

the Amphibole M_2 Crystal sites. Where the variation in distortion is weak but Δ may vary up to 1mm/sec and 0.4 mm/sec in the above sites respectively.

The large variations are attributed to the contribution to the $Q_{lattice}$ by the other factors such as the effective charges on the oxygen atoms, the symmetry and charge on the neighbouring cations, silicons and oxygens as in the substitution of Ca^{2+} for Fe^{2+} in the orthopyroxene M_2 and the cummingtonite M_4 which influences Δ markedly. Contributions by other factors are usually difficult to estimate and the distortion criteria is useful which applied with caution.

CHAPTER V

ANALYSIS OF SPECTRA

5.1 COMPUTER ANALYSIS - METHOD

The absorption line shapes of minerals using sources with narrow lines, such as ^{57}Co embedded in Pd matrix, have been found to be ideal Lorentzians[3]. The intensity of a Lorentzian-shape transmitted gamma beam, as a function of its energy, has the form of equation 20

$$I(v) = b - \frac{I(0)}{1 + \left(\frac{V - V(0)}{\Gamma/2}\right)^2} \qquad (20)$$

$I(0)$ is the intensity at the resonance velocity $V(0)$, Γ the full width at half height of the absorption line, and b is the background or base-line intensity.

For n lines, the above function is represented by equation 21.

$$I(v) = b - \Sigma_i \frac{I(0)_i}{1 + \left(\frac{V - V(0)_i}{\Gamma/2}\right)} \qquad (21)$$

The n line spectrum is a function of $3n+2$ parameters; position, width, and intensity of each line, plus the background and slope of the background. The best fit ideally should correspond to the minimum weighted sum of squares X^2, as given by equation 22.

$$X^2 = \sum_{c=1}^{n} Wc \left[Ic - I(Vc/q_i)\right]^2 \qquad (22)$$

where n is the number of channels fit; Ic the observed count at channel C; $I(Vc/q_i)$ is the transmission function; q_i denotes the 3n+2 parameters, and W_c is the inverse of the variance for Channel C.

Initial estimates are chosen for the 3n+2 parameters, and using $\frac{dX^2}{dq_i} = 0$ for each q_i, corrections are determined for each q_i such that X^2 is minimized. The procedure is repeated using the corrected estimates from the previous iteration, until X^2 reaches a minimum.

The fitting mentioned above is carried through the programme MOSSBR (Appendix B). MOSSBR consists of a main block and several subroutines. The main block reads in the data, applies corrections to it and prints the results. Subroutine FUNC calculates the function derivatives; subroutine CURFIT carries the least square fitting; subroutine MATINEV is for matrix inversion and accompanying solution of linear equations; Subroutine JACOBI is for matrix diagonalization through successive rotations, subroutine EXAM applies corrections to the eigenvalues if any is zero or negative otherwise the fitting will diverge, while subroutine PLOTB plots the raw and calculated spectra.

5.2 LINE SHAPES - MINERAL SPECTRA

The spectral shape of an emission line centered at an energy E_s with a natural width Γ_0, when a Doppler velocity V is applied; is given by the distribution of equation 23, known as Breit-Wigner, or Lorentzian distribution[6].

$$I(E,V) = \frac{\Gamma_0}{2\pi} \left[\frac{1}{E-E_s-E\gamma\left(\frac{V}{c}\right)^2 + \left(\frac{1}{2}\Gamma_0\right)^2} \right] \qquad (23)$$

If the emission line is broadened; it is sufficient to replace Γ_0 in equation 23 by an effective line width Γ_s[3,6]. The experimentally determined full width at half height Γ_{ex} is usually expressed as equation 24[3].

$$\Gamma_{ex} = \Gamma_a + \Gamma_s + 0.27\ \Gamma_n X \qquad (24)$$

Γ_n is the natural line width as determined by the lifetime of the excited state, while X is given by equation 25.

$$X = n\ f_a \sigma_o \qquad (25)$$

n is the number of atoms of the Mossbauer isotope per cm^2; f_a the recoil free fraction of the absorber, and σ_o is the maximum cross section as given by equation 26[7].

$$\sigma_o = \frac{\lambda^2}{2\pi} \cdot \frac{2I_e + 1}{2I_g + 1}\ \frac{1}{\alpha_t + 1} \qquad (26)$$

I_e and I_g are the nuclear spins of the excited and ground states respectively; α_t is the total internal conversion coefficient.

In order to get Symmetrical Lorentzian lines; very thin absorbers must be used (not exceeding 10 mg per cm^2 in the case of iron). If this is obeyed, the last term in equation 24 is minimal when compared to Γ_a and Γ_s[3]. Otherwise the shoulders of a line may deviate from the Lorentzian shape. A line can also be broadened by the cosine angle effect, when the source is too close to the detector. This depends on the areas of the source, the detector and the distance seperating them from the absorber. However, this effect is easily minimized by applying corrections to the

spectra or by collimation of the gamma beam.

Mineral spectra are often characterized by the presence of two or more quadrupole doublets with close absorption peaks; i.e. an absorption envelope may consist of several lines, non-resolved visually, and a fit may diverge if the initial guess of the number of lines, or the values of the parameters are far from their true values. To overcome the fitting difficulties, the use of constraints (such as assigning the intensities or the widths of a doublet to be the same) was justified, and the weighted sum of squares (X^2) value was regarded as an indicator to the goodness of a fit[3,11,12]. An acceptable X^2 value should lie within a 5% difference from the total number of degrees of freedom of a certain fit where the number of degrees of freedom is the number of fitted channels and parameters. However, the X^2 value is sometimes misleading, since it may drop when the number of fitted lines is increased, and the best fit does not always correspond to a minimum of X^2 [11]. In such a case the parameter values are taken as a guide; for instance, the line width and the intensities of a doublet are expected to be very close when the resolution of a spectrum is satisfactory and the base line is linear.

The use of constraints is helpful when the number of absorption peaks in a certain envelope is high, or when a certain quadrupole doublet, overlapping another doublet, accounts to less than ten percent of the total absorption. It should be mentioned also that it is very difficult to resolve peaks contributing to less than 5 percent of the total intensity[13].

5.3 ESTIMATION OF PERCENTAGE COMPOSITION

For non-overlapping Lorentzians, area ratios for thin absorbers can be expressed as equation 27[1,14]

$$\frac{A_A}{A_B} = C \frac{N_A}{N_B} \qquad (27)$$

where A_A and A_B are the areas of lines A and B respectively; C a constant given by equation 28; N_A and N_B are the numbers of Iron atoms at sites A and B respectively.

$$C = \frac{\Gamma_A}{\Gamma_B} \frac{G(X_A)}{G(X_B)} \frac{f_a}{f_b} \qquad (28)$$

In equation 28; Γ is the line width, $G(x)$ represents saturation corrections depending on the thickness of absorbers; where for very thin absorbers $G(x)$ approaches unity. f_a and f_b are the recoil free fractions for A and B.

For silicates C is almost unity or very close to it[3], implying equal line widths, no isotope fractionation between sites and that the f-factors are identical for each iron atom in every mineral. However, the usual overlap of lines in silicates (Pyroxenes) makes it difficult to apply the method quantitatively.

An alternative method derives the fractions from intensity ratios directly. As is the case in estimating fractions of iron of the M_1 and M_2 sites in orthopyroxenes, where the widths are in general equal[15]. The standard error $\frac{\Delta\Gamma}{\Gamma}$ of the line width is about 10-15 times larger than the standard error $\frac{\Delta I}{I}$ of the corresponding peak heights. The areas of Lorentzians, being proportional to the product $I \times \Gamma$; the relative line errors in widths and areas are due to the strong overlap of Lorentzian tails, even when the peaks are well seperated[16]. The relations given by equation 29 are for a two doublets fit, where I refers to the intensity,

A and B are the two doublets, where the subscripts 1 and 2 refer to the low and high velocity peaks respectively; $T(M_1)$ and $T(M_2)$ are the fractions of iron at sites M_1 and M_2 respectively.

$$T(M_1) = [I(A_1) + I(B_1)]/[I(A_1) + I(B_1) + I(A_2) + I(B_2)]$$

$$T(M_2) = [I(A_2) + I(B_2)]/[I(A_1) + I(B_1) + I(A_2) + I(B_2)] \quad (29)$$

In Chapter 6, explanations are provided, as to which method is used for the estimation of iron sites.

CHAPTER VI

RESULTS AND INTERPRETATIONS - PART I

6.1 ESTIMATION OF IRON SITES IN BULK SAMPLES

The samples studied are E288.C; E282.b and E294 (for samples description see Appendix A). Each sample was crushed and then powdered. Absorbers were prepared by enclosing an amount of powder (100mg) between two circular plastic sections of diameter close to an inch. The absorption spectra for the above three samples are shown in Figures 16, 17 and 18 respectively. The results obtained by computer analysis are listed in Table 6.

Initial spectra of these samples revealed the presence of magnetite in small amounts; the magnetite lines were very weak to analyze. For later runs, the magnetite was removed by means of a hand magnet. No absorption lines due to any magnetite left appeared.

Sample E282.b gave a single doublet spectrum. The quadrupole splitting and the isomer shift of this doublet are characteristic of ferrous iron in pyroxenes. The width of the lines is more than expected from a single mineral (using ^{57}Co in a Pd matrix, silicates line widths are up to 0.35 mm/sec)[7], especially the low velocity peak. However, due to the very weak absorption (1.2%), trials to resolve the other lines failed.

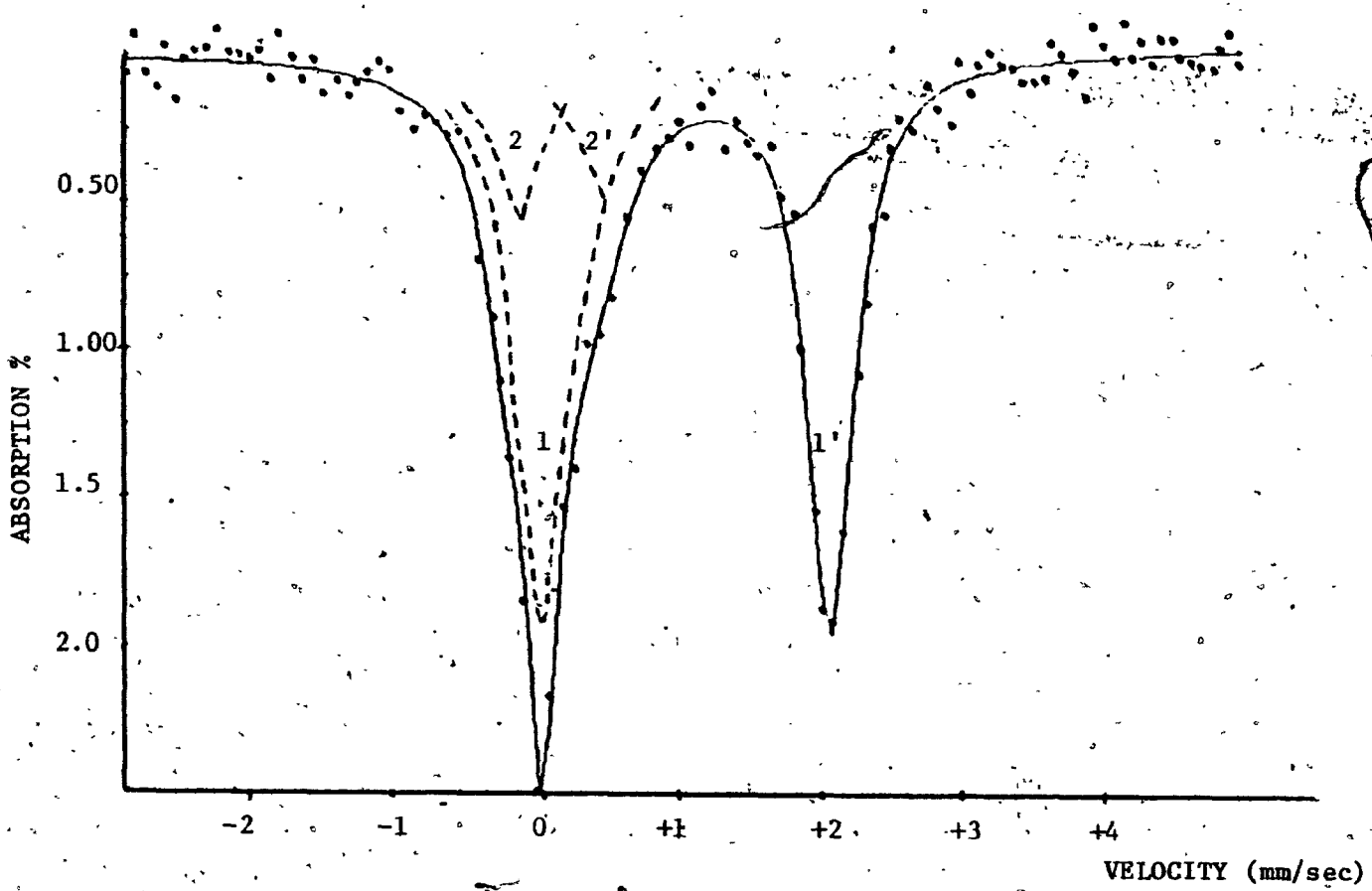

FIGURE 16

MÖSSBAUER SPECTRUM OF SAMPLE E288.C

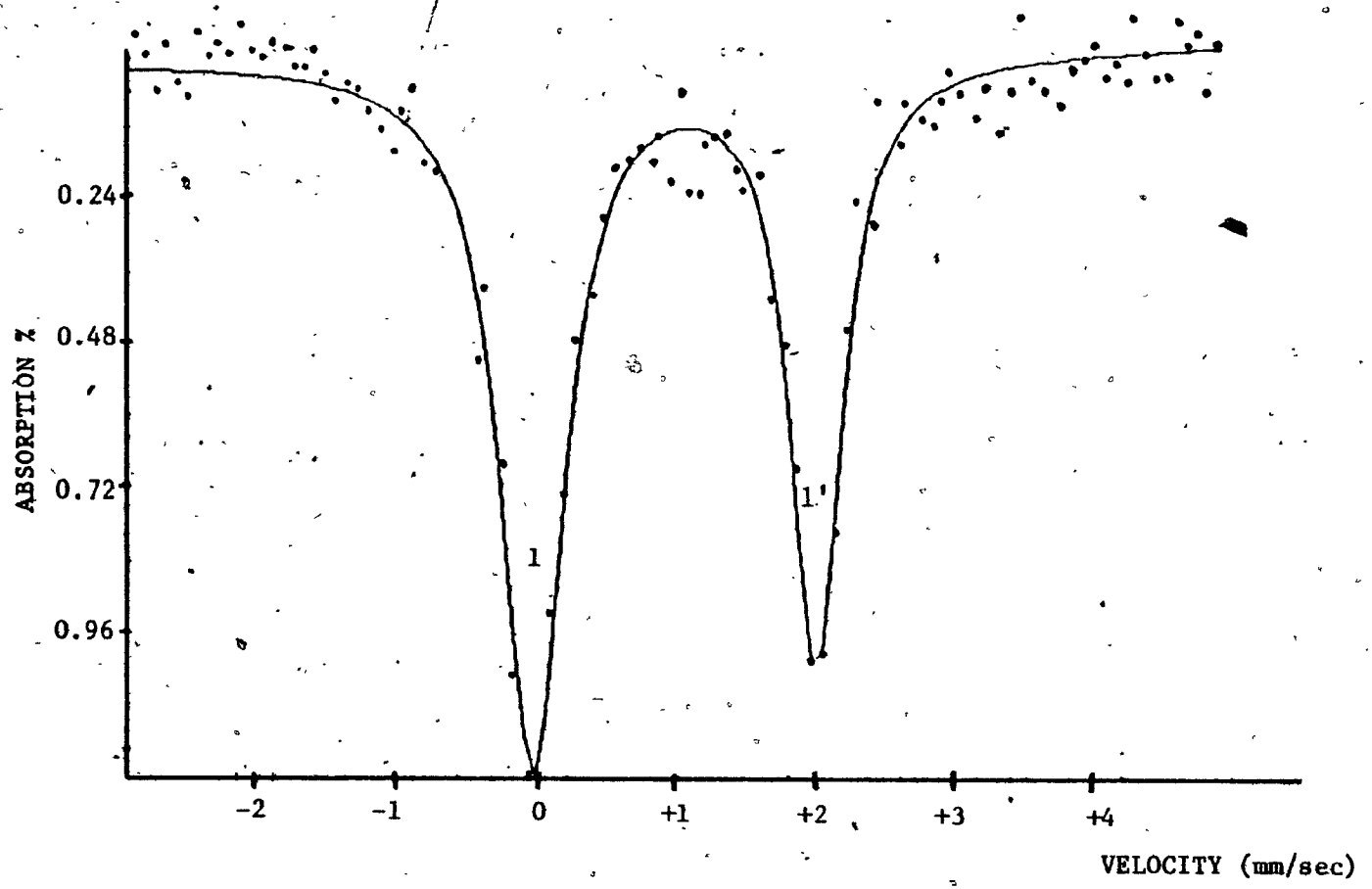

FIGURE 17

MÖSSBAUER SPECTRUM OF SAMPLE E282.b

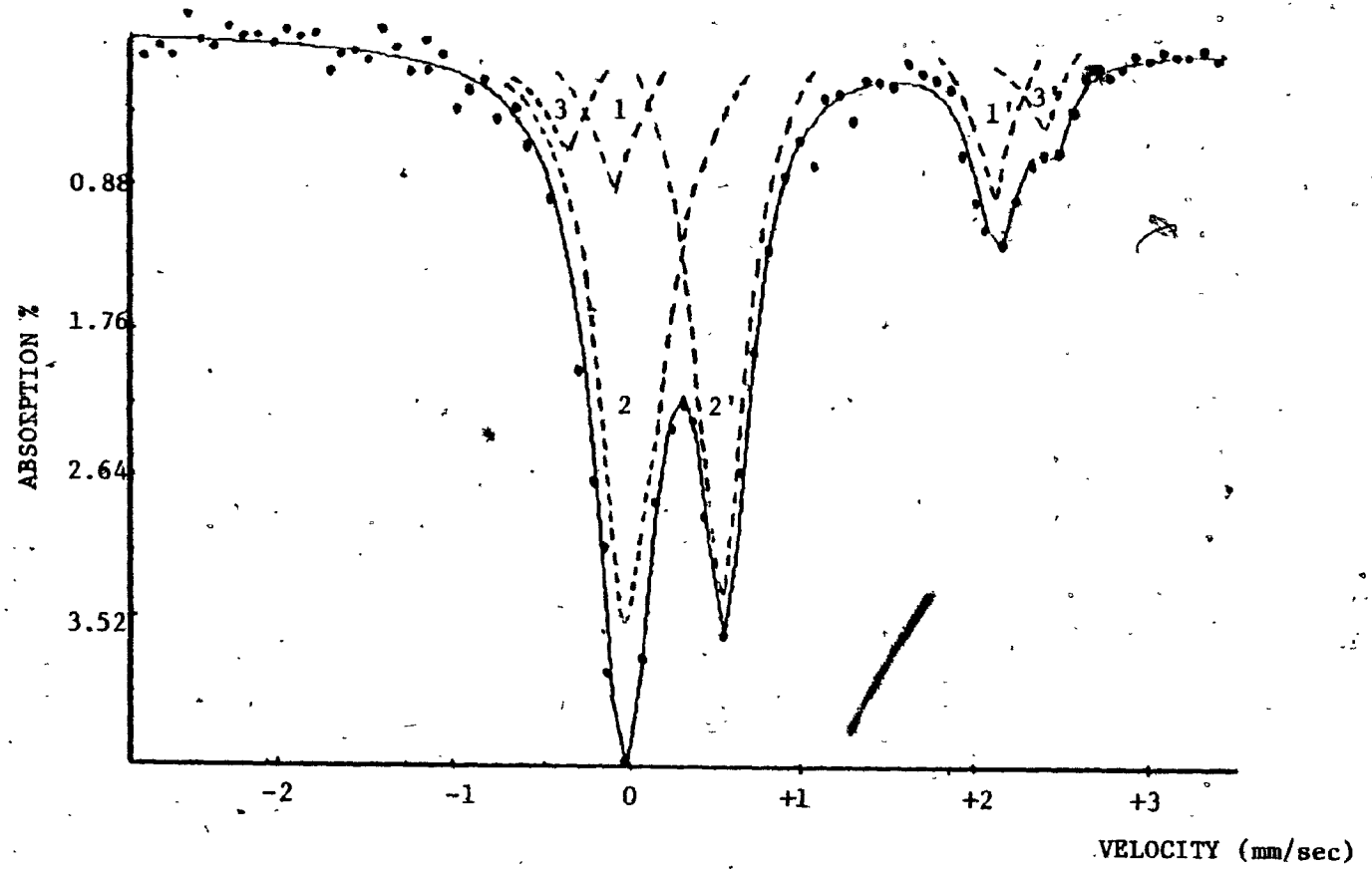

FIGURE 18

MÖSSBAUER SPECTRUM OF SAMPLE E294

TABLE 6

CALCULATED PARAMETERS OF THE BULK SAMPLES (Δ, δ and Γ ARE IN MM/SEC. NUMBERS IN PARANTHESES ARE ERRORS TO THE LAST DIGIT. ERROR IN IRON RATIOS IS UP TO 5%)

SAMPLE	E282.b	E288.C	E294
Δ(11')	1.98(2)	1.99(2)	2.03(2)
δ(11')	1.43(2)	1.46(2)	1.46(2)
Δ(22')	-	0.65(4)	0.56(2)
δ(22')	-	0.53(4)	0.66(2)
Δ(33')	-	-	2.66(4)
δ(33')	-	-	1.44(4)
Γ1, Γ1'	0.45, 0.39(2)	0.35, 0.35(2)	0.31, 0.31(2)
Γ2, Γ2'	- -	0.39, 0.39(4)	0.32, 0.32(2)
Γ3, Γ3'	- -	- -	0.27, 0.27(4)
Fe(11')/ΣFe	100	75	25
Fe(22')/ΣFe	-	25	68
Fe(33')/ΣFe	-	-	7
X^2	309	219	268
max ab.	1.2%	2%	4%

The spectrum of the sample E288.c was resolved into two quadrupole doublets. The isomer shift and the quadrupole splitting of the doublet labelled 11' are close to that of sample E282.b i.e. it is assigned to ferrous iron in pyroxenes. The weaker doublet 22' has its parameters close to the published parameters of pyrite[17,18] (Section 6.5).

The two outer doublets 11' and 33' of the three doublet spectrum of sample E294 were assigned to ferrous iron in pyroxenes, while the intense doublet 22' was assigned to ferric iron entering the silicate structure (see Chapter 7).

The percentage composition of the different iron sites was derived using area ratios.

6.2 PYROXENES - STRUCTURE

Pyroxenes are an important group of the rock-forming ferromagnesium silicates, which have a wide abundance in nature. The majority of the pyroxenes present in igneous and metamorphic rocks can be considered as members of the system shown in Figure 19.

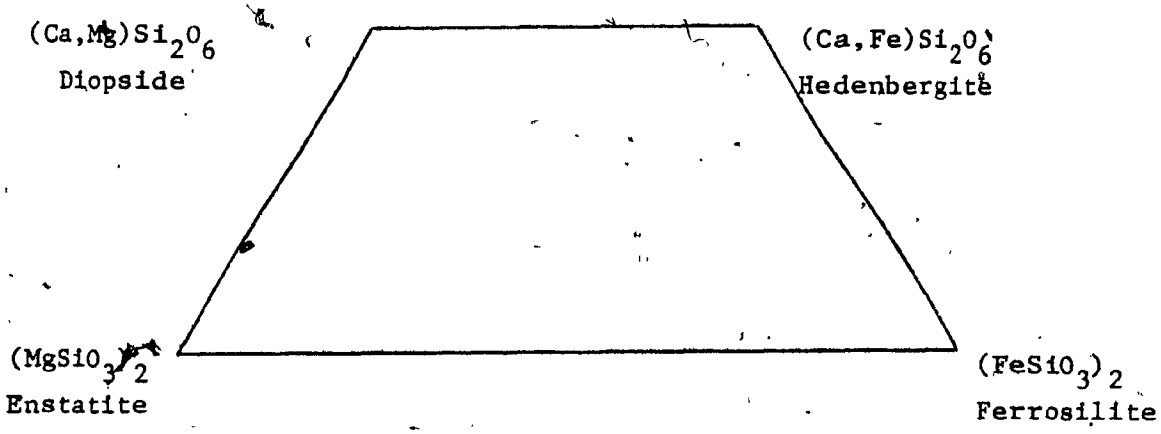

FIGURE 19

PYROXENES IN THE SYSTEM $CaFeSi_2O_6$ - $CaMgSi_2O_6$ - $Mg_2Si_2O_6$ - $Fe_2Si_2O_6$

The pyroxene crystal structure is roughly divided into two groups - a structure close to the diopside-Hedenbergite structure (clinopyroxenes) and a structure characteristic of pyroxenes lying on the Enstatite-Ferrosilite line (Orthopyroxenes).

The characteristic pyroxene structure, is the linkage of SiO_4 tetrahedra by sharing two out of four corners to form continuous chains of composition $(SiO_3)n$; see Figure 20. The chains are linked laterally by cations (Ca,Mg,Fe,...) but may have relative disposition; different arrangement of chains lead to the main subdivision of pyroxenes (monoclinic, orthorhombic)[19].

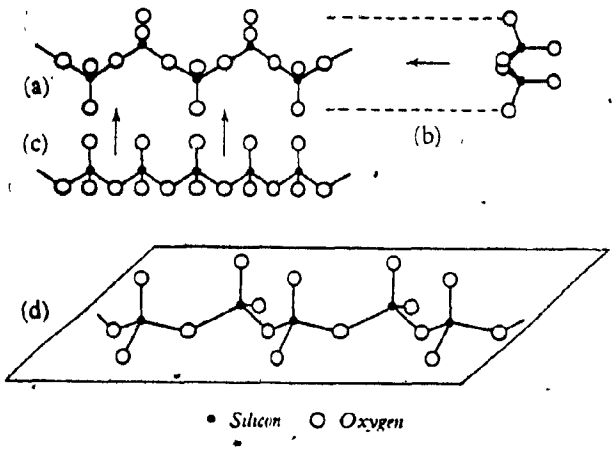

FIGURE 20

IDEALIZED ILLUSTRATION OF A SINGLE PYROXENE CHAIN $(SiO_3)n$ AS SEEN IN THREE PROJECTIONS (a) on (100), (b) ALONG THE z DIRECTION, (c) ALONG THE y DIRECTION, AND (d) IN PERSPECTIVE[19].

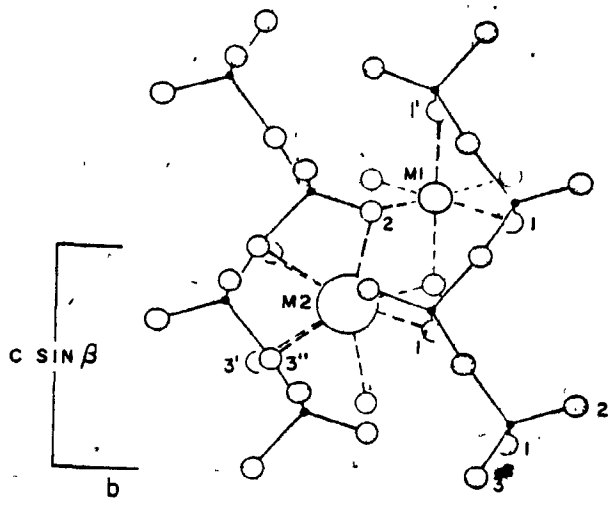

FIGURE 21

CRYSTAL STRUCTURE OF DIOPSIDE, $CaMg\ Si_2O_6$, VIEWED ALONG THE a AXIS.
M_1=Mg M_2=Ca[20].

A general chemical formula for the pyroxene group, proposed by Bermann (1937) and later slightly modified by Hess (1949) may be expressed as [19]

$$(W)_{1-p}(X,Y)_{1+p}Z_2O_6$$

where

W = Ca,Na; X = Mg , Fe^{2+}, Mn,Ni,Li;
Y = Aℓ, Fe^{3+}, Cr,Ti, and Z = Si,Aℓ,

In the orthopyroxene Series P ≈ 1 and the content of Y ions is small. In the clinopyroxene series; P varies from zero (eg. diopside; where y

is small, and Aegerine - Jadiete in which X is small) to 1 (eg. Spodumene). Normally, there are two crystallographically distinct positions in the pyroxene structure labelled M_1 and M_2. In the orthopyroxene structure, cations in the M_1 position are coordinated to six oxygen ions, each linked to one silicon atom in a nearly regular octahedron (six coordinates site), same as in the clinopyroxene diopside structure; see Figure 21. However, the M_1 octahedron in diopside is more distorted than in orthopyroxenes[21]. The M_2 position in the clinopyroxene diopside structure is an eight coordinated site occupied usually by Ca^{++} ions, while in the orthopyroxene hypersthene structure M_2 is a six coordinated site and may be a five coordinated one, same as that occurs in synthetic orthoferrosilite[22].

Though many pyroxenes have only one structural type, the space group changes from Pbca for orthopyroxenes to P21/c for Pigeonite to C2/c for diopside hedenbergite. In clinopyroxenes, the type of structure is determined by the charge and the size of cations entering the M_2 position[23]. Large univalent (Na^+) or bivalent (Ca^{2+}) cations are responsible for the diopside type structure (space group C2/c), small univalent cations (Li^+) are responsible for spodumene type structure (space group C_2) and small bivalent cations (Mg^{2+}) for the clinoenstatite type structure (space group P21/c).

In the next two sections determination of iron ions entering the different sites is discussed in detail.

6.3 ORTHOPYROXENES $(Mg,Fe)_2Si_2O_6$

Four orthopyroxene samples were studied. They are labelled CGW1;CG3; CG5 and CG12; (for sample description see Appendix A). Absorption

spectra are shown in Figure 22, 23, 24, and 25 for the above four samples respectively. The calculated parameters are listed in Table 7. Preparation of the absorbers followed the same procedure outlined in Section 6.1. However, the orthopyroxene samples were considered to be pure crystals; this was confirmed by their absorption spectra, which showed that the absorption peaks are due to one structural type only.

TABLE 7

CALCULATED PARAMETERS OF THE ORTHOPYROXENES (Δ,δ and Γ ARE GIVEN IN MM/SEC. THE NUMBERS IN PARANTHESES ARE ERRORS IN THE LAST DIGIT. ERROR IN PERCENTAGE COMPOSITION IS ± 3%).

SAMPLE	SGW1	CG3	CG5	CG12
$\Delta(11')$	2.50(5)	2.44(5)	-	-
$\delta(11')$	1.37(3)	1.40(3)	-	-
$\Gamma(1,1')$	0.31(2)	0.28(2)	-	-
$\Delta(22')$	2.11(2)	2.09(2)	2.11(2)	2.13(2)
$\delta(22')$	1.34(2)	1.34(2)	1.34(2)	1.35(2)
$\Gamma(2,2')$	0.33(1)	0.31(1)	0.36(1)	0.35(1)
$\Delta(33')$	0.49(5)	0.34(5)	0.35(5)	0.55(5)
$\delta(33')$	0.69(5)	0.68(5)	0.65(5)	0.74(5)
$\Gamma(3,3')$	0.31(2)	0.32(2)	0.27(2)	0.35(2)
$Fe11'/\Sigma Fe^{2+}$	8.6%	10.5%	-	-
$Fe22'/\Sigma Fe^{2+}$	91.4%	89.5%	100%	100%
$\Sigma Fe^{2+}/\Sigma Fe$	94%	96%	96%	95%
$\Sigma Fe^{3+}/\Sigma Fe$	6%	4%	4%	5%
X^2	209	250	257	286
max. abs.	9%	9%	8%	9%

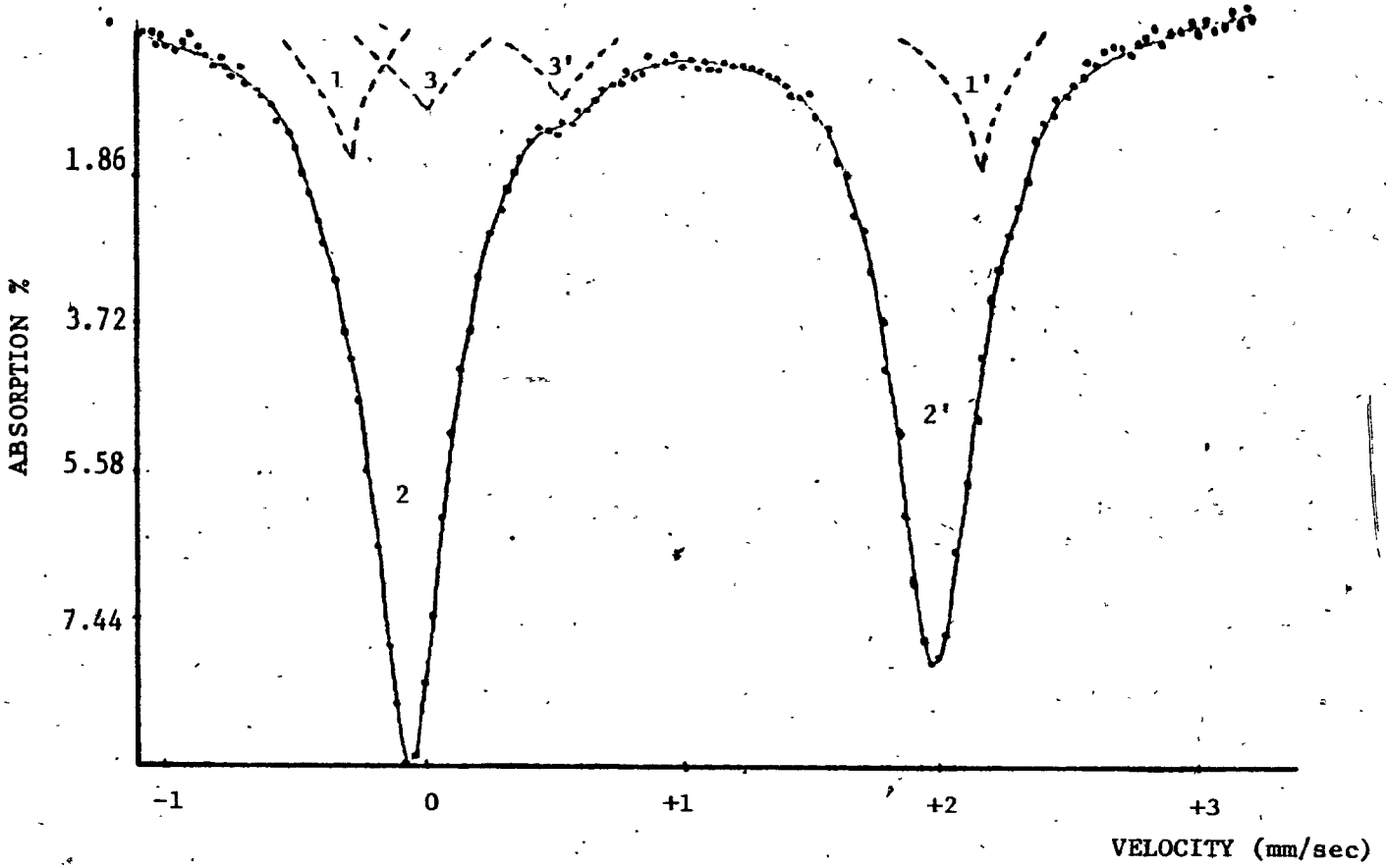

FIGURE 22

MÖSSBAUER SPECTRUM OF ORTHOPYROXENE CGW1

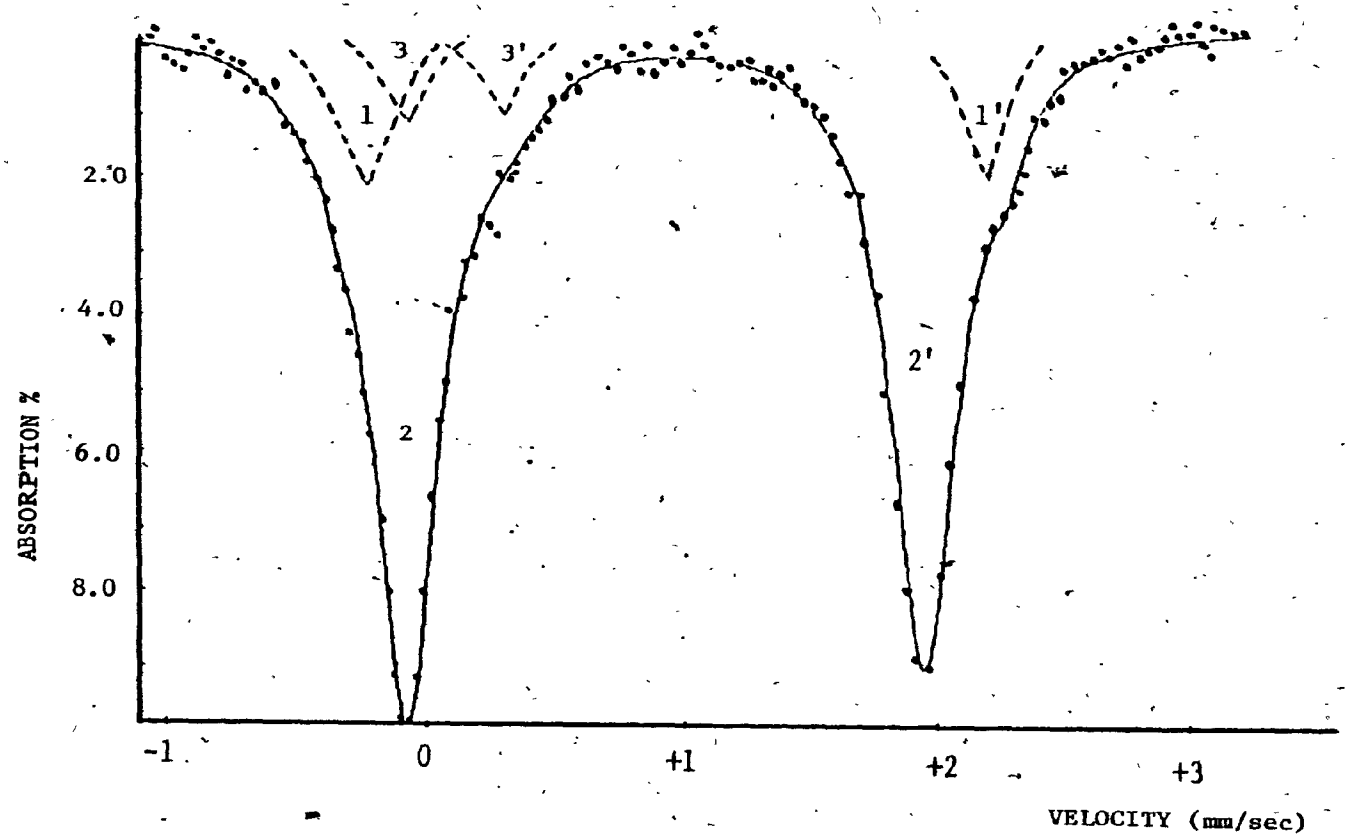

FIGURE 23

MÖSSBAUER SPECTRUM OF ORTHOPYROXENE CG3

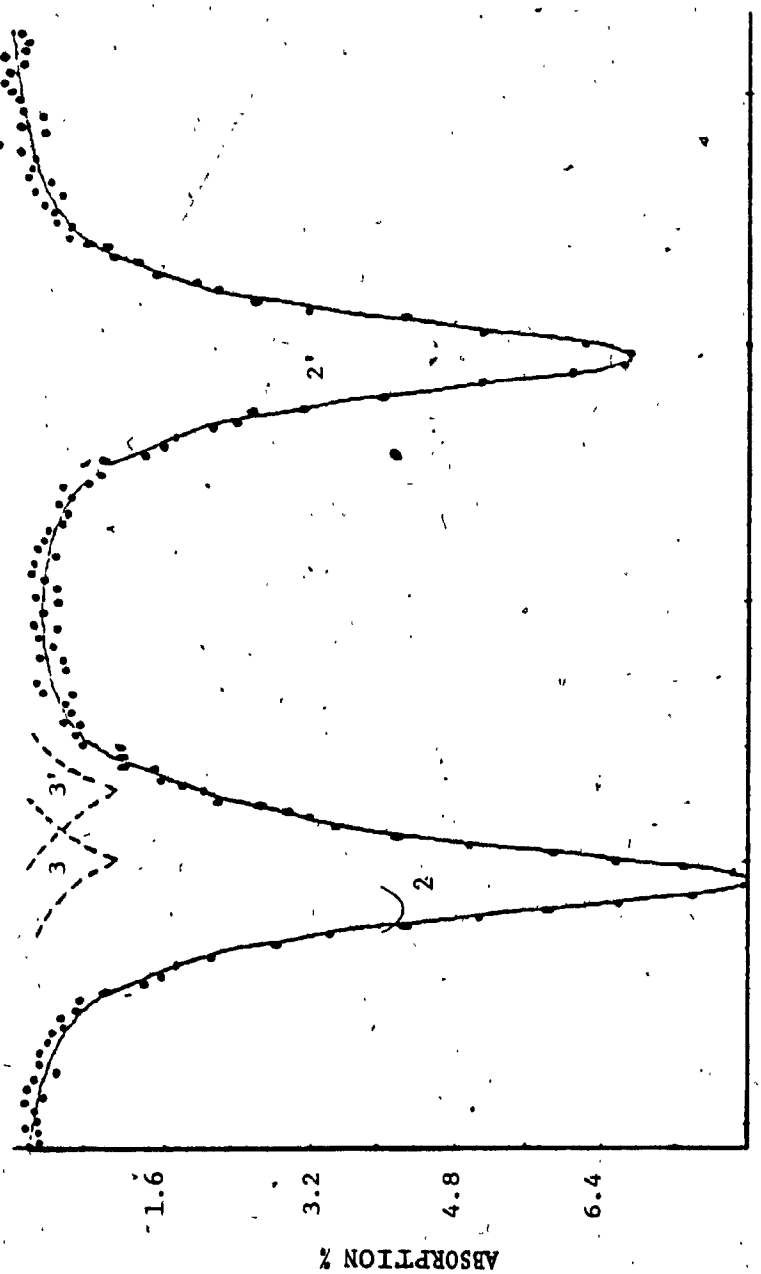

FIGURE 24

MÖSSBAUER SPECTRUM OF ORTHOPYROXENE CG5

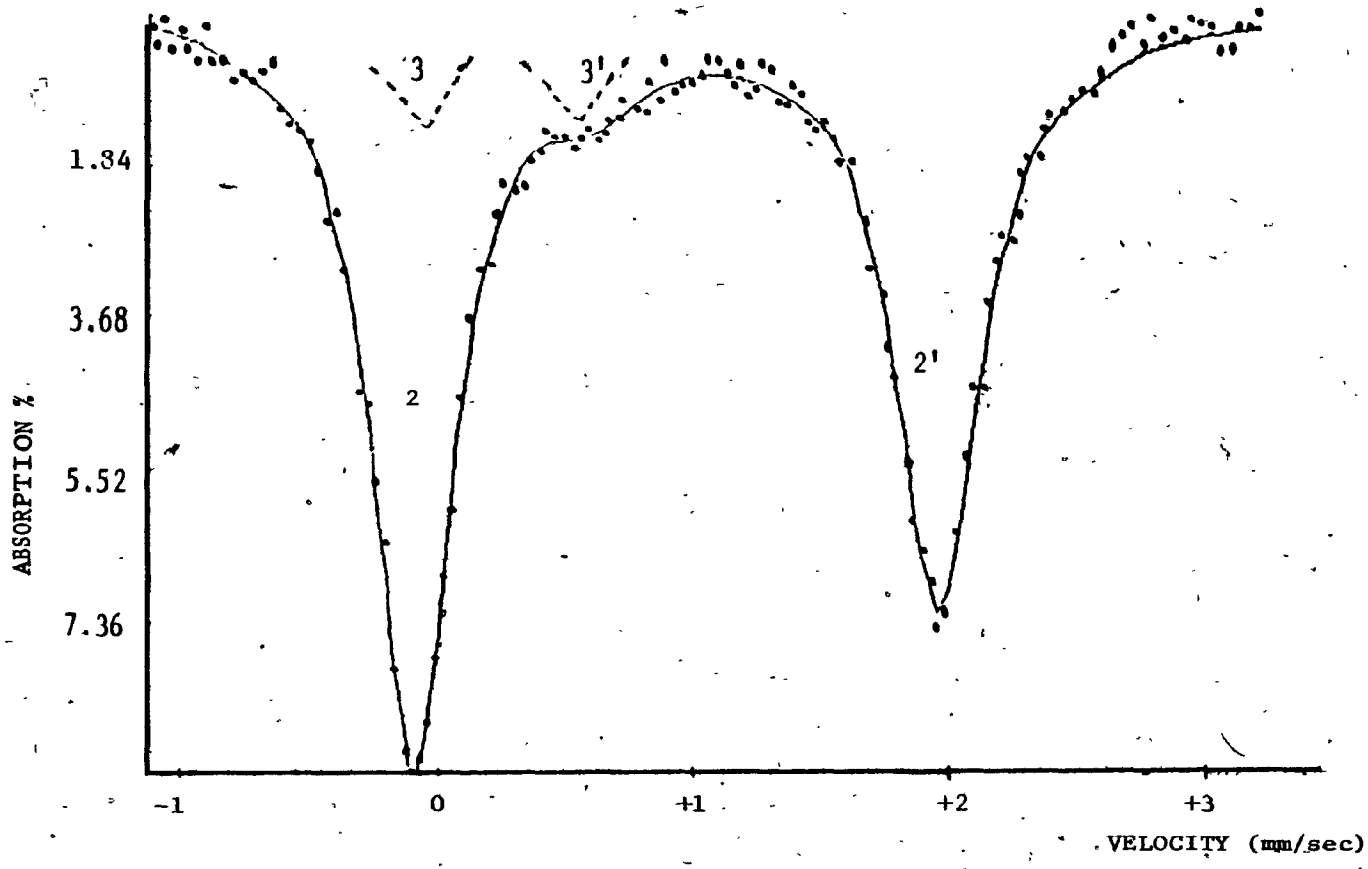

FIGURE 25

MÖSSBAUER SPECTRUM OF ORTHOPYROXENE CG12

The assignment of the orthopyroxene spectra follows the interpretation of Evans (1967)[12]. Fe^{3+} free orthopyroxenes give rise to two quadrupole doublets at most. One doublet due to ferrous iron entering the M_2 site while the other is due to ferrous iron entering the M_1 site. Our samples showed a weak doublet assigned to Fe^{3+} in the M_1 or M_2 sites, however, ferric iron accounted to no more than 6% of the total iron present (see Table 7). The intense doublet of the ferrous ions is assigned to the M_2 position because according to the preference criteria Mg preferably fills the M_1 crystal site. While iron enters the more distorted M_2 site. Since the quadrupole splitting decreases as the distortion from octahedral symmetry increases, the doublet due to the M_2 site has a smaller Δ[7]. Similar and varying explanations were given to the larger Δ of the M_1 site. Virgo and Hafner (1972)[24] interpreted the situation as "crystal site with the larger radial distortion index generally exhibits the smaller splitting". Greenwood and Gibb (1971)[25] interpretation is" at M_2 presumably there is a larger lattice term in the electric field gradient which partly cancels the contribution from the valence electrons".

The works of Nozik and Kaplan (1967)[26] showed that lattice contribution for Fe^{2+} is usually negligible or, in extreme cases, amounts to only 15% of the total quadrupole splitting, the major contribution being that of the ground state electron configuration.

Walsh and Donnay (1974)[22] dismissed the above explanations as not satisfactory; basing their argument on Nozik and Kaplan results concluded that "Since the ground orbital states at M_2 is different from that of M_1, the quadrupole splitting will also be different. The type of distortion controls the resulting ground orbital state and the

magnitude of distortion determines the temperature at which the excited orbital states becomes populated and the quadrupole splitting starts to decrease. So predictions about the ratio of the quadrupole splittings cannot be made without investigating the electronic states at M_1 and M_2".

Though there are many different arguments but the assignments of the quadrupole doublets has been agreed on by all previous works.

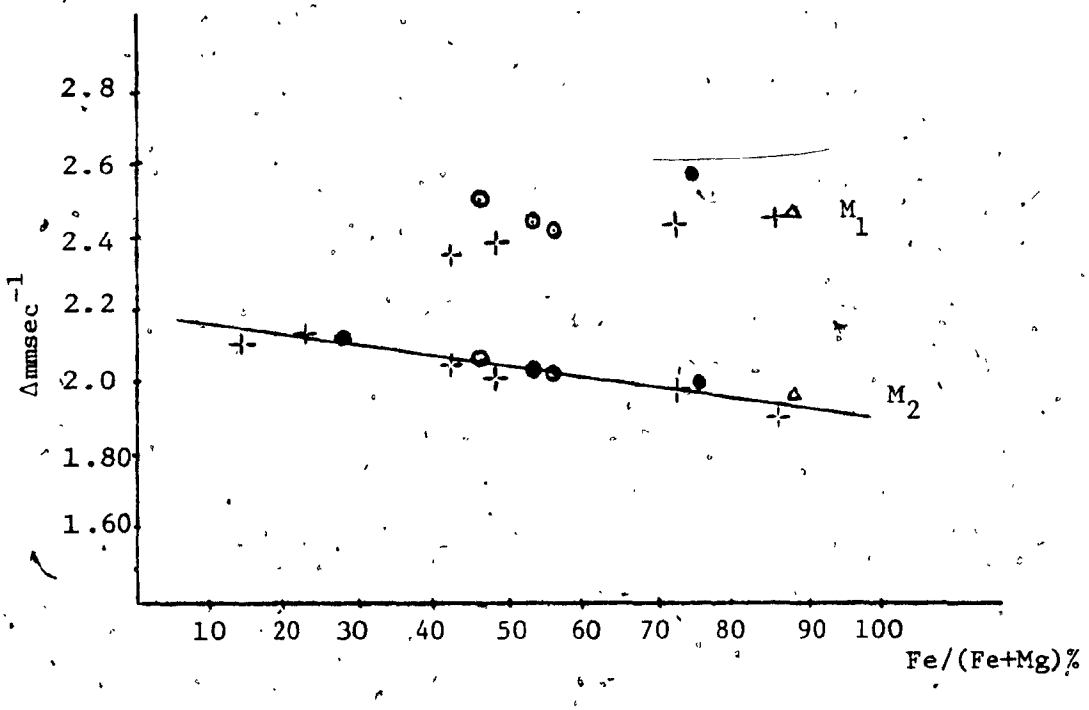

FIGURE 26

QUADRUPOLE SPLITTING AT M_1 AND M_2 VERSUS THE RATIO Fe/(Fe+Mg) IN ORTHOPYROXENES (VALUES ARE LISTED IN APPENDIX D)

Figure 26 shows the variation of Δ at M_1 and M_2 against the ratio Fe/(Fe+Mg). The variation of $\Delta(M_2)$ is found to be a linear one. This was noticed by Bancroft (1967)[13]. Though Bancroft suggested that $\Delta(M_1)$ follows a similar trend, but Figure 26 dismisses such a relation. However the values of $\Delta(M_1)$ usually have a much larger error than $\Delta(M_2)$ due to the difficulty in resolving its less intense doublet overlapping the M_2

doublet, especially when the ratio Fe/(Fe+Mg) is less than one half[15]. This is the case in the samples CG5 and CG12 where the doublet at M_1 could not be resolved, though the slightly larger line widths of the doublet due to M_2 in these samples suggest that a very small percentage of Fe^{2+} enters the M_1 site.

The distribution of iron at the M_1 and M_2 crystal sites in orthopyroxenes with a varying ratio Fe/(Fe+Mg) was studied in details by Virgo and Hafner (1969, 1970)[15,27] (fractions of iron at the M_1 and M_2 sites for different iron ratios as derived from Mossbauer analysis at liquid nitrogen temperature, are listed in Appendix D). Their analysis shows that site M_1 has usually less than 12% of total iron in orthopyroxenes where Fe/(Fe+Mg) is less than one half. As Fe/(Fe+Mg) decreases the ratio of iron in the site M_1 decreases; it becomes very difficult to resolve that doublet, especially at room temperature. The isotherms derived from heating experiments on natural orthopyroxene crystals in the range 500-1000C^0 are shown in Figure 27. Virgo and Hafner found that an Fe^{2+},Mg distribution is close to ideal (ordered) in the region $0 \leq x \leq 0.6$ where $X=Fe^{2+}/(Fe^{2+}+Mg)$. Figure 27 shows that orthopyroxenes from granulites and plutonic rocks have an equilibirium temperature of 480^{0}C while volcanic pyroxenes show a disordered Fe^{2+}, Mg distribution of 500^{0}C - 600^{0}C equilibirium temperature.

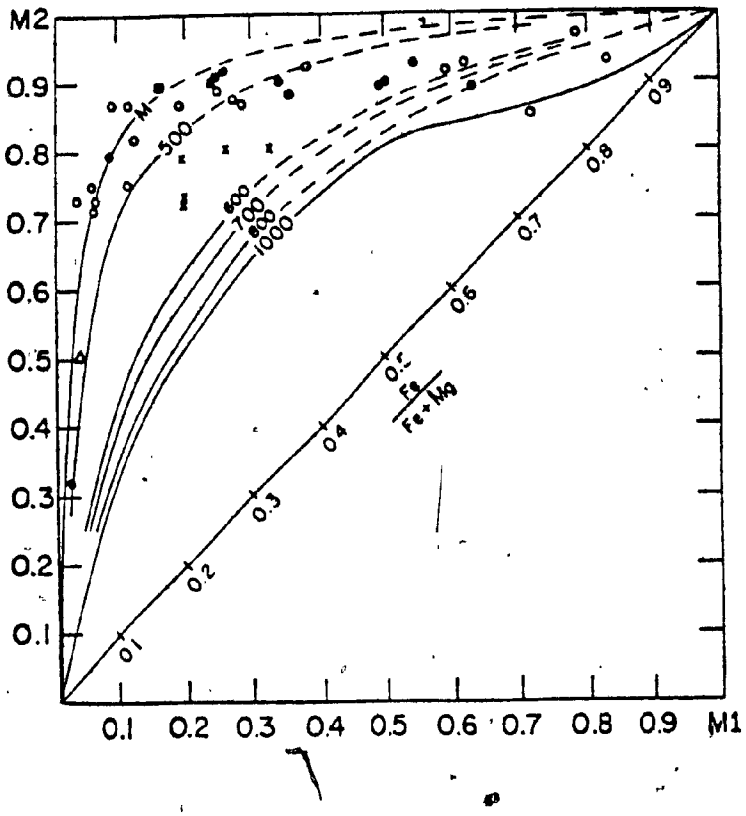

FIGURE 27

PLOT OF Fe^{2+} SITE OCCUPANCY AT M_1 AGAINST M_2 OF NATURAL ORTHOPYROXENES THE SOLID LINES REFER TO EXPERIMENTALLY DETERMINED ISOTHERMS AT THE INDICATED TEMPERATURES; ●-ORTHOPYROXENES FROM METAMORPHIC IRON FORMATIONS IN QUEBEC;■-FROM GRANULITES IN CEYLON AND MADRAS AREA;0 - FROM GRANULITES; X - FROM VOLCANIC ROCKS[15].

The M_1, M_2 distribution in the four samples studied suggest that their (Fe/Fe+Mg) is less than 30% and are ordered in the range 480°C-500°C.

6.4 CLINOPYROXENES

Six clino pyroxene samples labelled CG1;CG6;CG8;CG11;CG14; CGW3 (See Appendix A) were studied. Their absorption spectra are shown in Figures 28, 29, 30, 31, 32 and 33 respectively. While the calculated

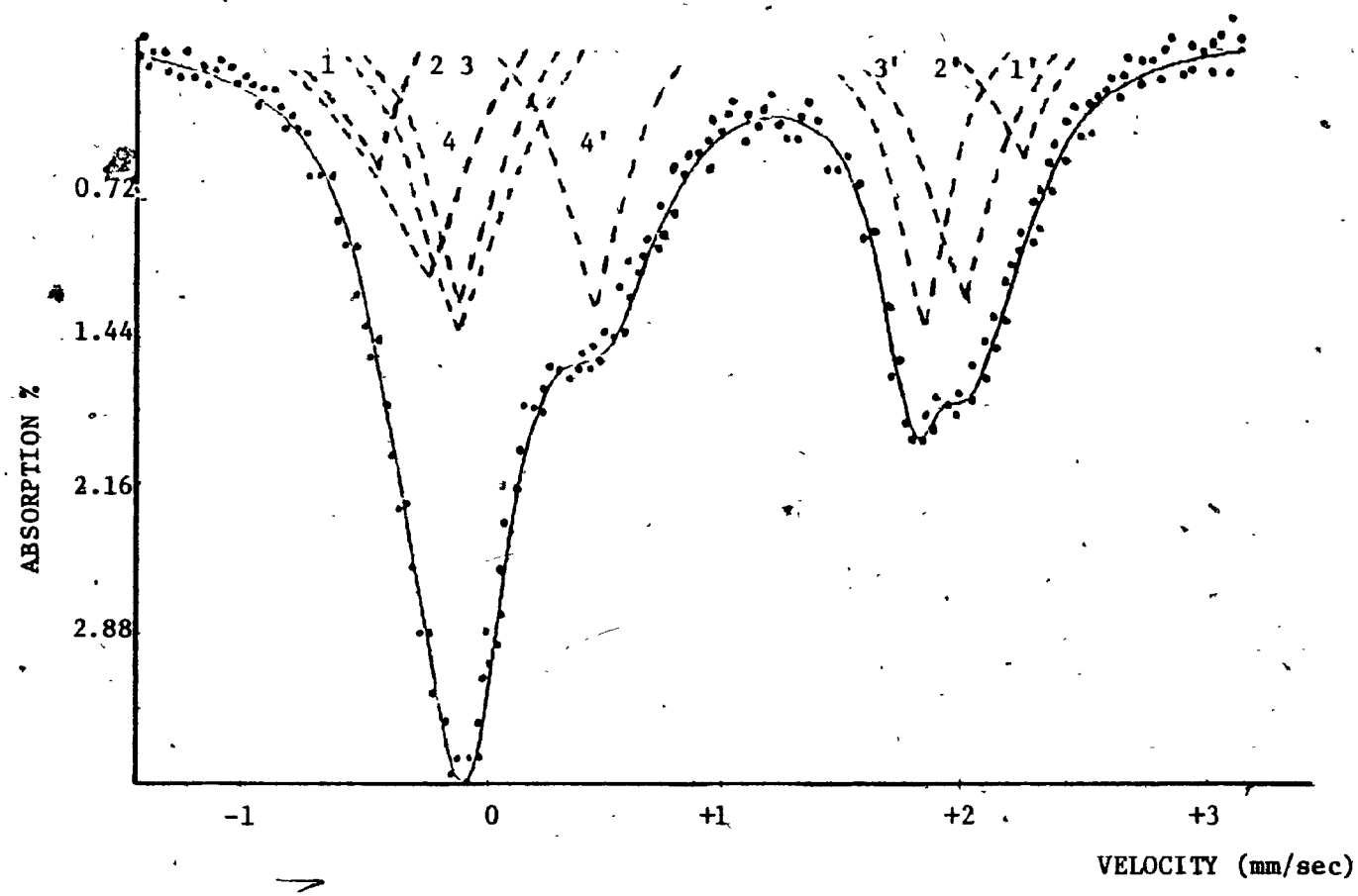

FIGURE 28

MÖSSBAUER SPECTRUM OF CLINOPYROXENE CG1

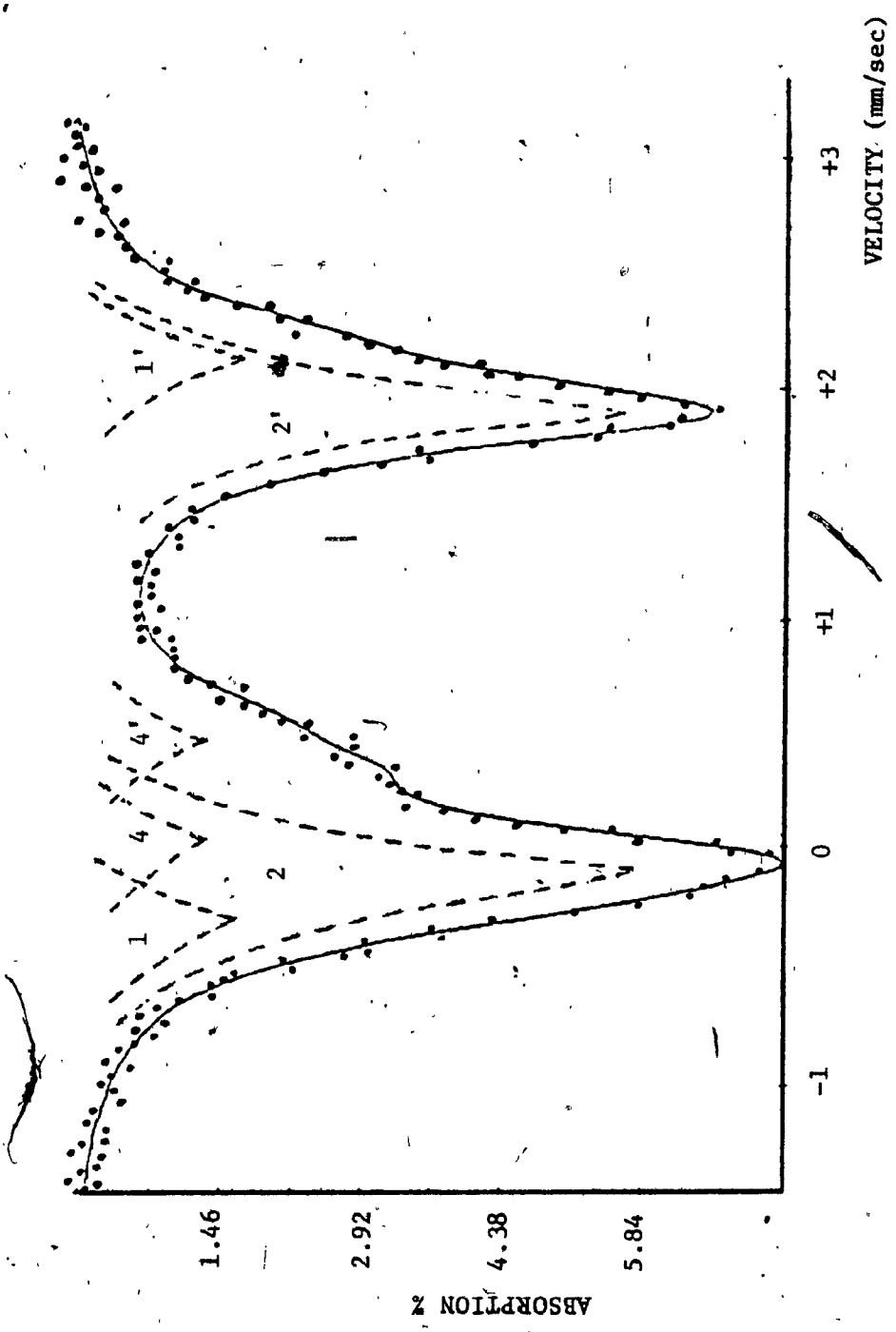

FIGURE 29

MÖSSBAUER SPECTRUM OF CLINOPYROXENE CG6

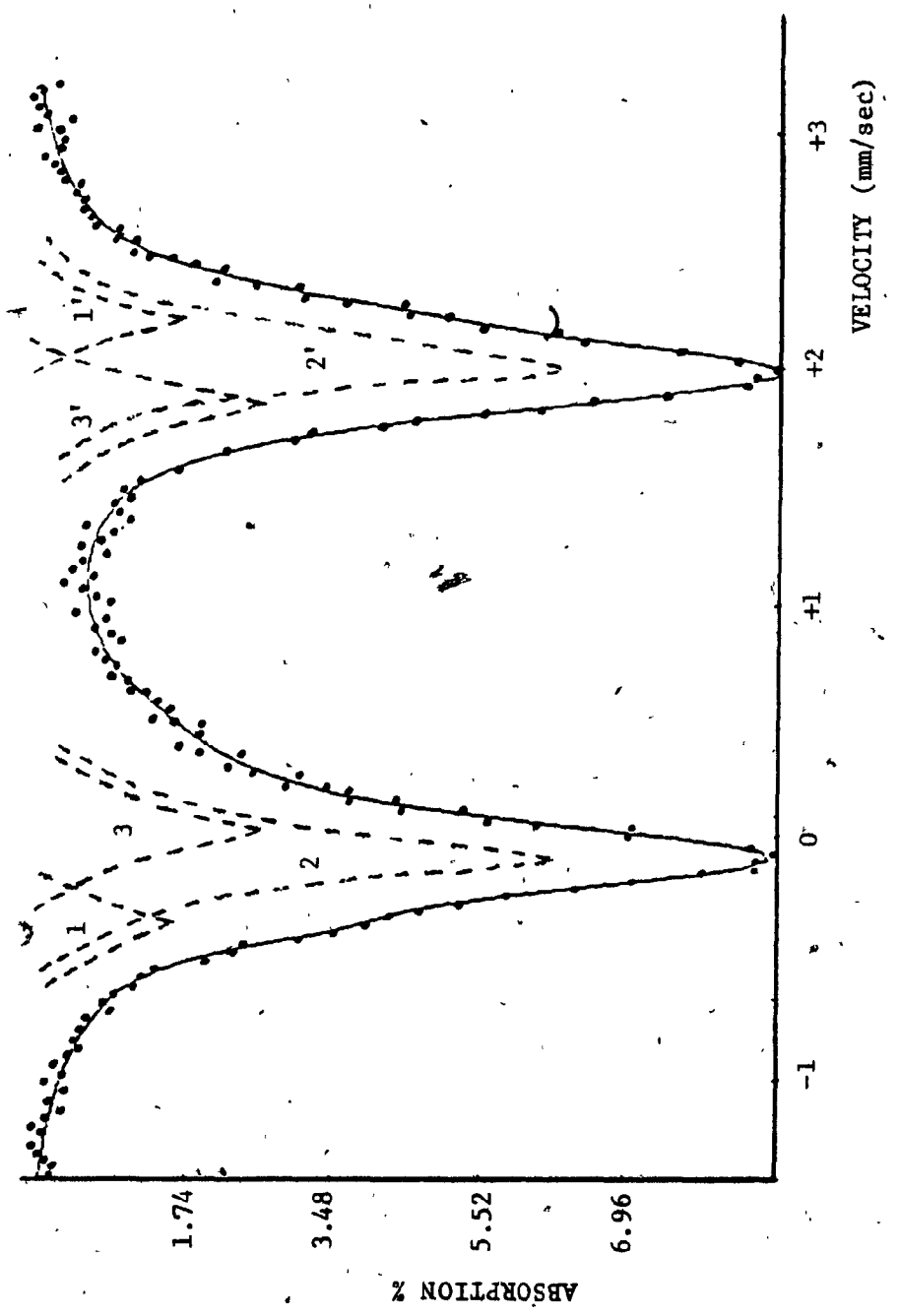

FIGURE 30

MÖSSBAUER SPECTRUM OF CLINOPYROXENE CG8

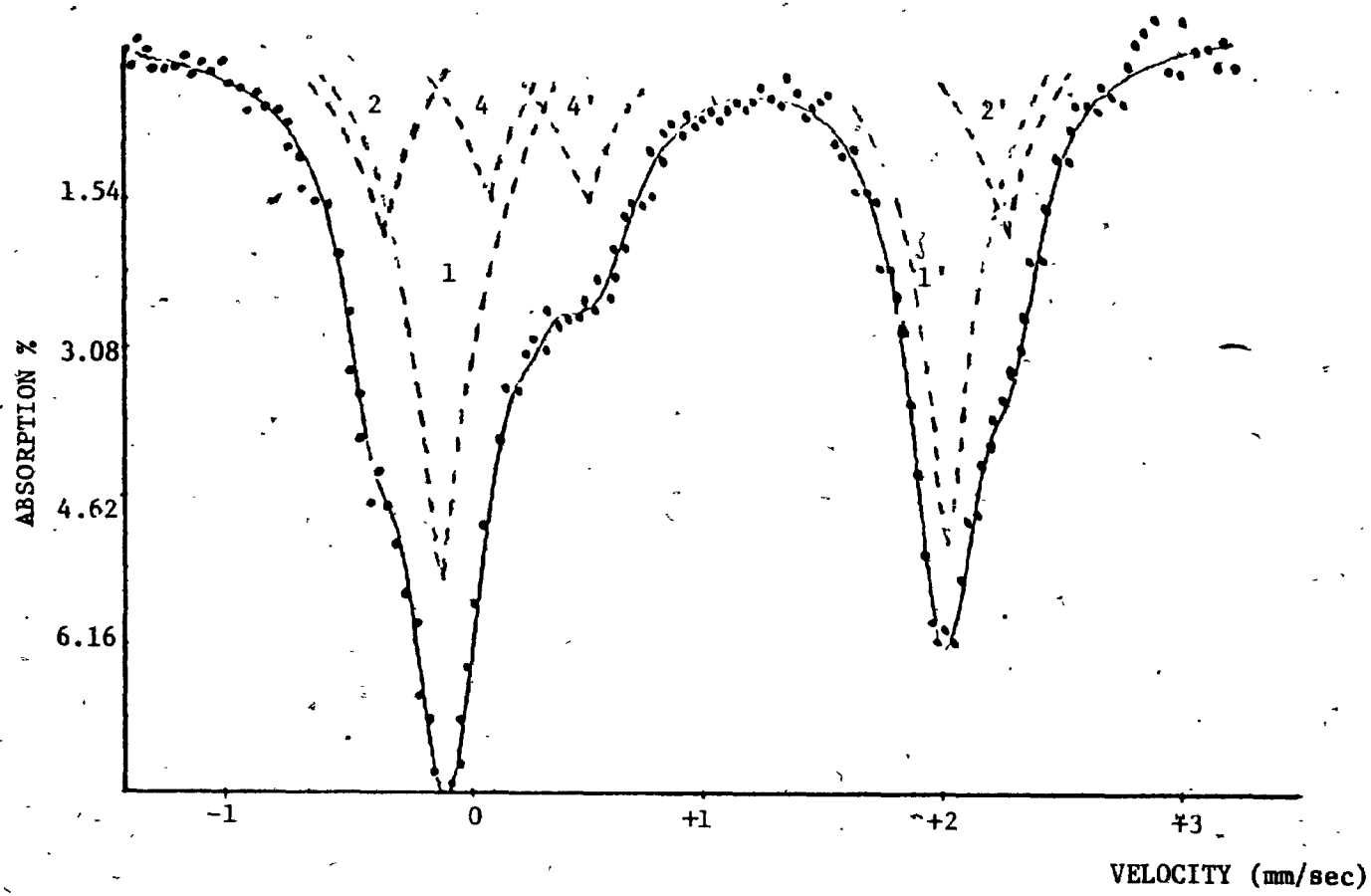

FIGURE 31

MÖSSBAUER SPECTRUM OF CLINOPYROXENE CG11

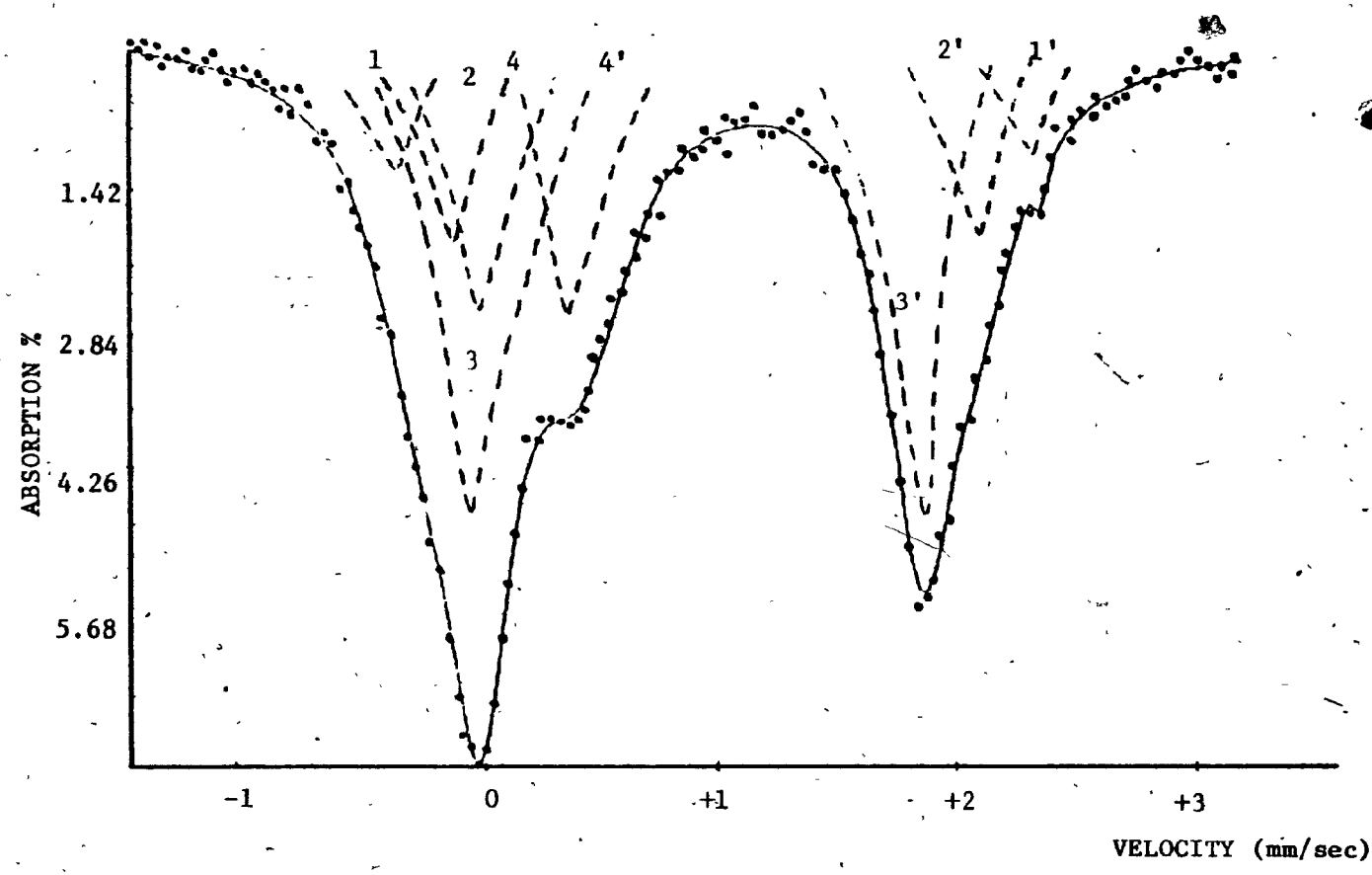

FIGURE 32

MÖSSBAUER SPECTRUM OF CLINOPYROXENE CG14

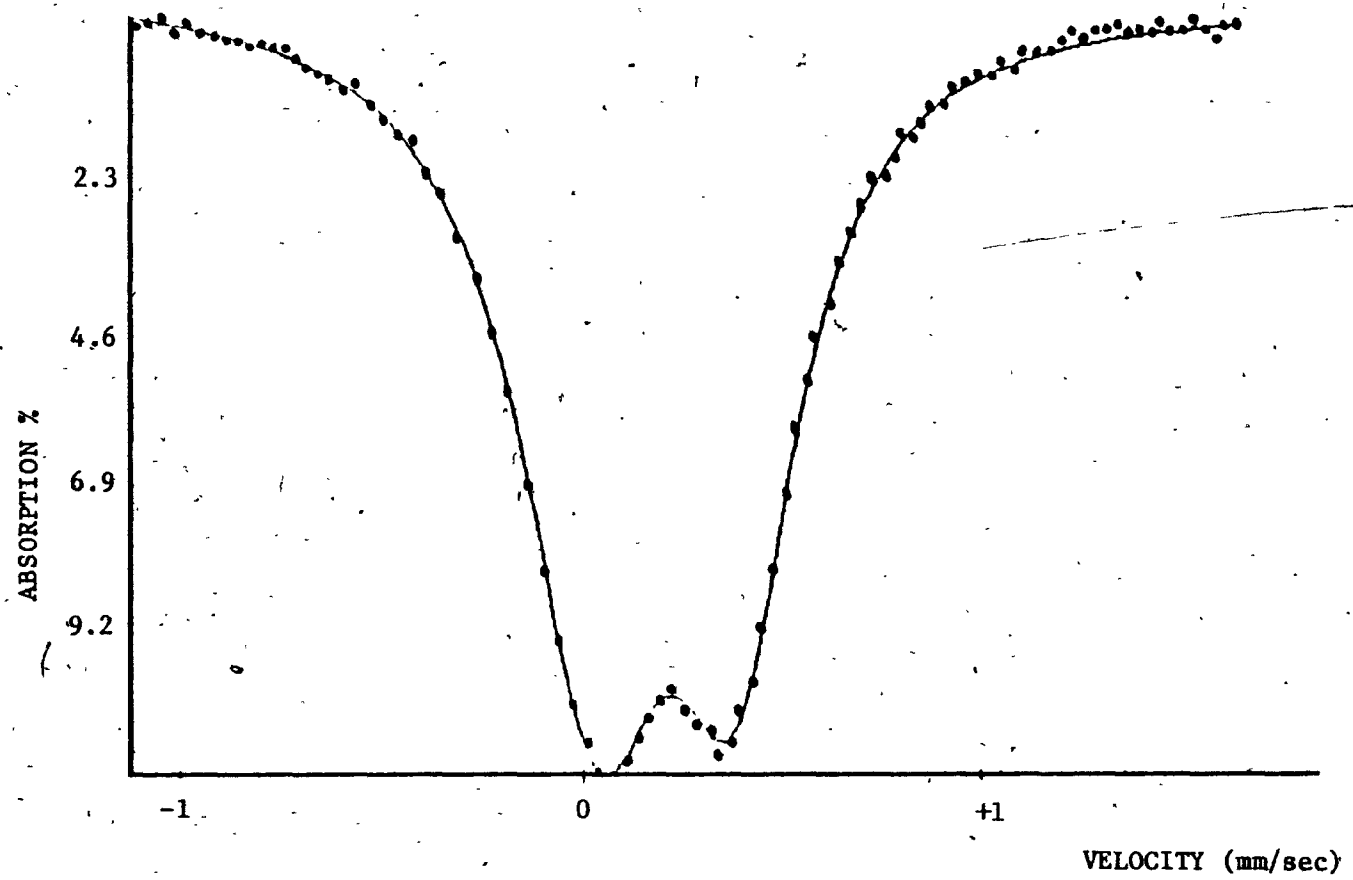

FIGURE 33

MÖSSBAUER SPECTRUM OF CLINOPYROXENE CGW3

parameters are listed in Table 8.

Unlike the orthopyroxene series, where structural changes are due to variation in the Fe/(Fe+Mg) ratio, clinopyroxenes usually have other numerous substitutions. In calcic clinopyroxenes (diopside-hedenbergite line), only the ratio of iron to magnesium is variable. The spectra obtained are analyzed easily because iron is expected to occupy the M_1 site. Since site M_2 is filled by calcium, and if there is no calcium deficiency, the spectra should consist of one doublet due to Fe^{2+} pesent at site M_1. This has been affirmed in natural samples very close to the diopside-hedenbergite line[28] and in synthetic pure samples[29]. If there is no calcium deficiency and more than one quadrupole doublet is present - one doublet must be due to impurities[28]. Figure 34 shows the variation in $\Delta(M_1)$ against the ratio Fe/(Fe+Mg) (Sources of data are listed in Appendix D). The variation is noticed to be linear, the non-smoothness of the curve is attributed to the effects of different cations especially in natural samples on the quadrupole splitting.

Sample CGW_3 spectrum was resolved into one doublet only. It is due to ferric iron in the M_1 site as expected from the chemical structure of aegerine (acmite), $NaFe^{3+}Si_2O_6$. The parameters are analogus to those given by Angelis and Sgarlata (1979)[30] in their study of pyroxenes from central Sweden, where it is reported that ferric iron enters the M_1 position only in the crystal structure, which is similar to the diopside structure.

TABLE 8

CLINOPYROXENES CALCULATED PARAMETERS (Δ, δ AND Γ ARE IN MM/SEC, VALUES IN PARENTHESES ARE ERRORS IN THE LAST DIGIT, ERRORS IN IRON RATIOS ARE UP TO 5%

SAMPLE	CG11	CG6	CG14	CG8	CG1	CGW[3]
$\Delta(11')$	2.15(2)	2.47(2)	2.80(2)	2.62(2)	2.75(2)	-
$\delta(11')$	1.38(2)	1.46(2)	1.40(4)	1.38(2)	1.40(3)	-
$\Gamma(1,1')$	0.36(2)	0.36(2)	0.27(2)	0.29(2)	0.35(2)	-
$\Delta(22')$	2.72(2)	1.93(2)	2.40(2)	2.18(2)	2.46(2)	-
$\delta(22')$	1.36(2)	1.40(2)	1.35(2)	1.39(2)	1.35(2)	-
$\Gamma(22')$	0.28(2)	0.37(2)	0.30(2)	0.34(2)	0.35(2)	-
$\Delta(33')$	-	-	1.99(2)	1.85(2)	2.01(3)	-
$\delta(33')$	-	-	1.33(2)	1.38(2)	1.37(3)	-
$\Gamma(2'2)$	-	-	0.32(2)	0.34(2)	0.33(2)	-
$\Delta(44')$	0.48(3)	0.54(4)	0.43(4)	-	0.55(3)	0.35(2)
$\delta(44')$	0.71(3)	0.74(4)	0.62(4)	-	0.71(3)	0.63(2)
$\Gamma(2'2)$	0.38(3)	0.32(2)	0.36(2)	-	0.35(3)	0.40(2)
$Fe(11')/\Sigma Fe^{2+}$	76%	22%	10%	13.2%	10%	-
$Fe(22')/\Sigma Fe^{2+}$	24%	78%	20%	63.4%	45%	-
$Fe(33')/\Sigma Fe^{2+}$	-	-	70%	23.4%	45%	-
$Fe^{3+}/\Sigma Fe$	19%	10%	29%	-	32%	100%
$Fe^{2+}/\Sigma Fe$	81%	90%	71%	100%	68%	-
X^2	272	238	249	252	286	330
max a.b.	7.7	7.3	7.1	8.7	3.6	11.5

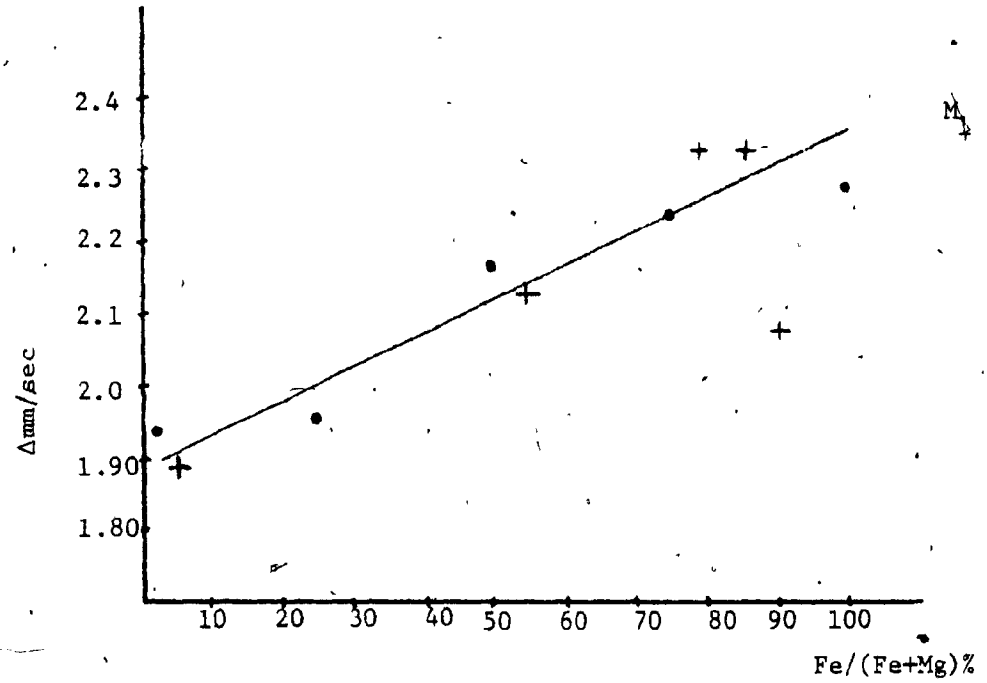

FIGURE 34

VARIATION OF $\Delta(M_1)$ AGAINST Fe/(Fe+Mg) IN DIOPSIDE-HEDENBERGITE

In subcalcic pyroxenes, (Ca/(Fe+Mg))<1), the assignment of Mossbauer spectra has followed different explanations, confusion is mostly due to the comparison with orthopyroxenes and calcic clinopyroxenes assignments. It is also due to the supposition that Mg is favorable to fill the calcium deficiency at the M_2 site[29,31]. However, studies on calcium-poor pyroxenes by Walsh et.al. (1974)[22] showed that Fe^{2+} is more likely to fill the calcium deficiency at the more distorted site M_2.

The spectra of sampels CG6, CG8 and CG14 is assigned in a similar way to the assignment of the spectra of augites in 1971 by Williams et.al[32]. The inner doublet (smaller Δ) is assigned to ferrous iron at site M_2; the outer doublet (less intense) to ferrous iron at site M_1.

The weak doublet (11') in CG14 is assigned to impurities, while CG8 spectrum, one different from other augites and clinopyroxenes;(since there is no detected presence of ferric iron also the high velocity peak is almost more intense than the low velocity one), has two doublets of quadrupole splitting 1.85 and 2.18 mmsec^{-1} assigned to the M_2 site. An anomalous behaviour attributed to a fine domain structure of pyroxenes close to the composition $Ca_{0.8}Fe_xMg_{1-x}Si_2O_6$ $(0 \leq x \leq 1.2)$[32].

Sample CG1 spectrum is very close to that of ordered omphacites, where ferrous iron enters four M_1 positions[33]. Though only three ferrous doublets were resolved, the similarity of the spectra and the large percentage of ferric iron (32%) present allows the suggestion that CG1 is an ordered omphacite where the structure space group is P2.

6.5 PYRITES

Two naturally occuring pyrite sample labelled SS7P and SS8P were studied (see Appendix A). Their absorption spectra are shown in Figures 35 and 36 respectively, while the parameters are listed in Table 9. Sample SS7P consisted of small cubic crystals (∿ 3mm edge) that were seperated from a host rock, Sample SS8 had no specific shape. The two samples yielded almost identical isomer shifts and quadrupole splitting, which are consistent with those previously published (see Appendix D). The Δ and δ values are characteristic of low spin iron II.

TABLE 9

CALCULATED PARAMETERS OF PYRITE SAMPLES

	Δ mmsec^{-1}	δ mmsec^{-1}
SS7P	0.60±0.02	0.57±0.02
SS8P	0.60±0.02	0.58±0.02

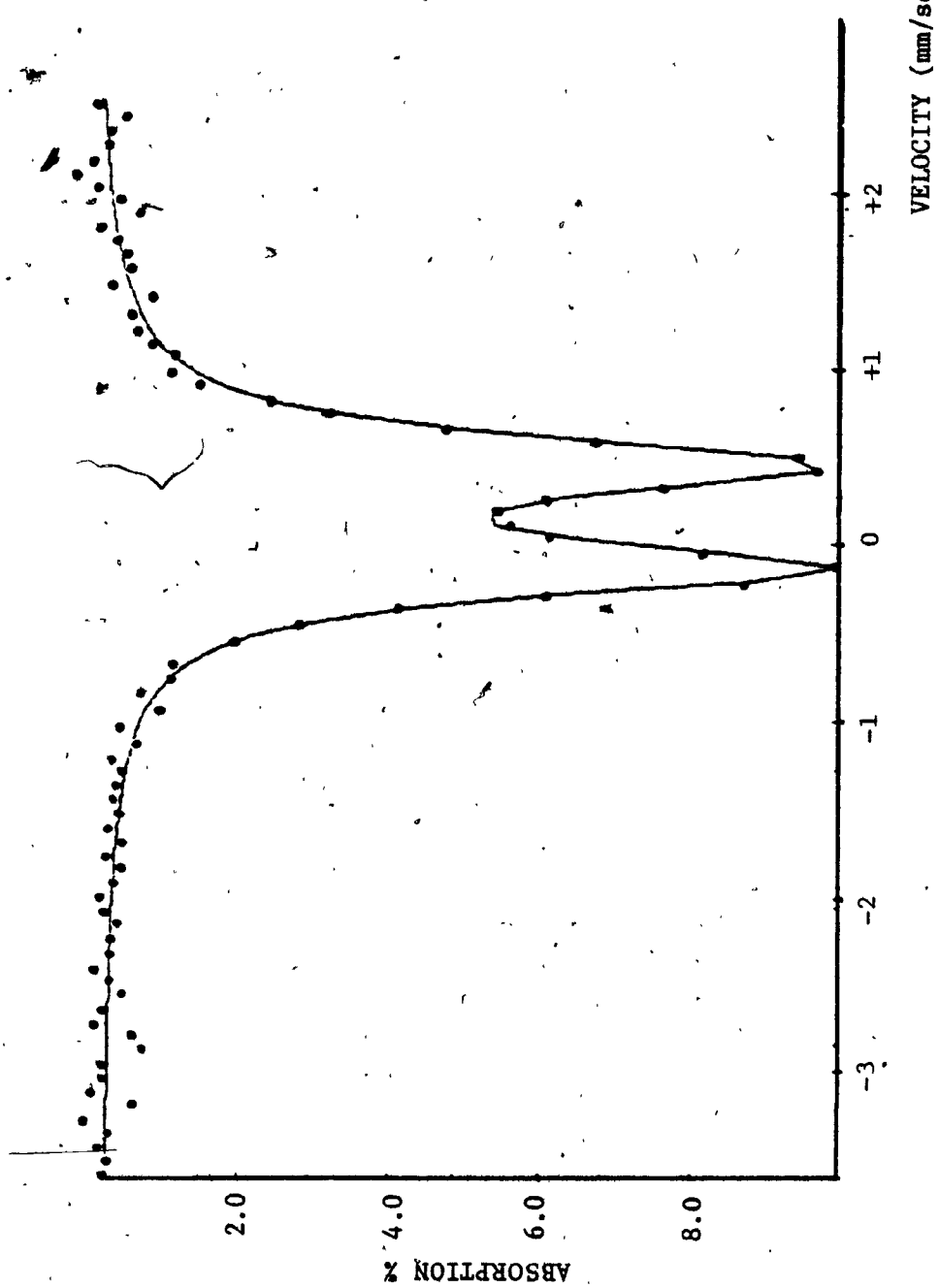

FIGURE 35

MÖSSBAUER SPECTRUM OF PYRITE SS7P.

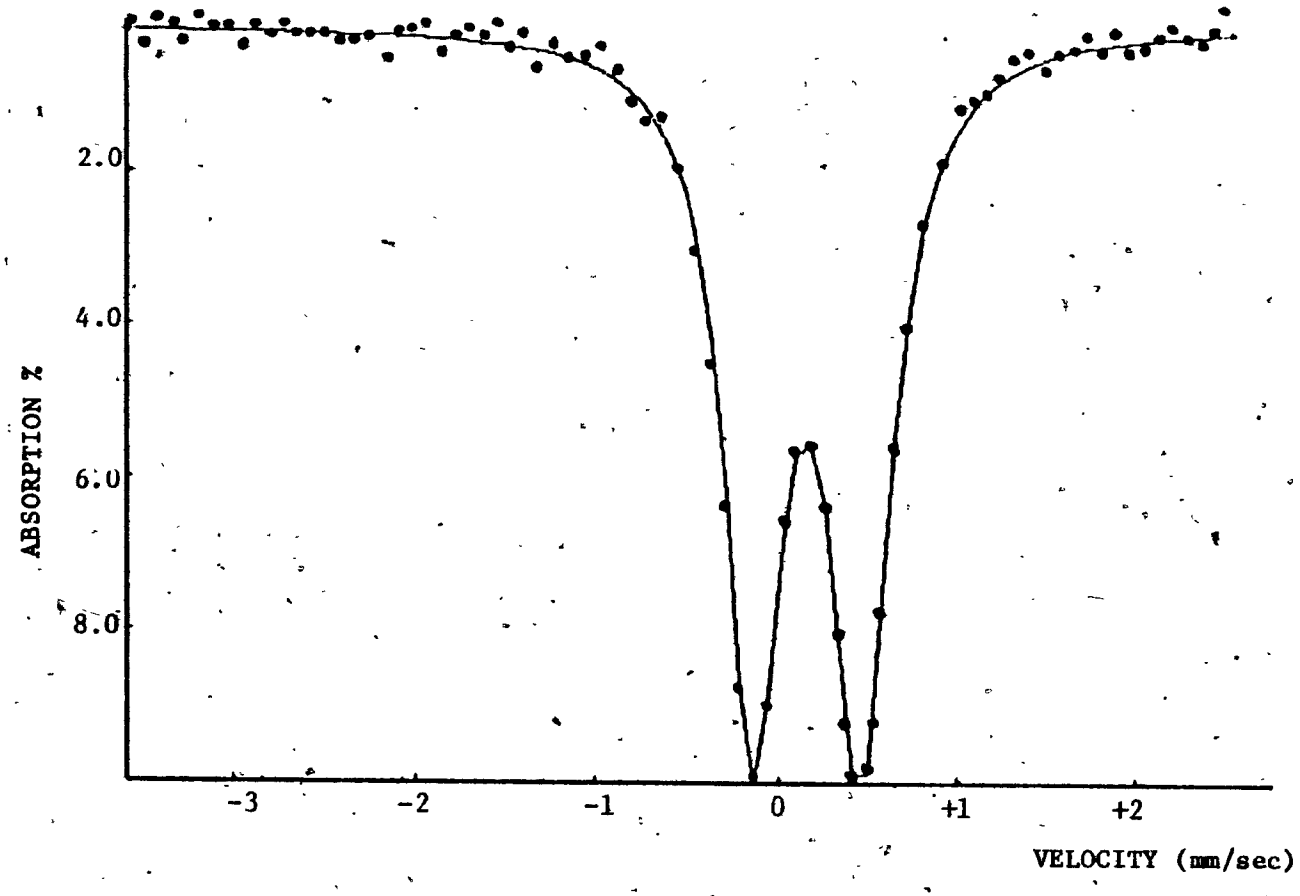

FIGURE 36

MÖSSBAUER SPECTRUM OF PYRITE SS8P

CHAPTER VII

MÖSSBAUER SPECTROSCOPY AS A GEOCHEMICAL PROSPECTING TECHNIQUE - STUDY OF SOME SAMPLES FROM GASPÉ COPPER MINES

7.1 INTRODUCTION

The possible use of Mössbauer spectroscopy as a geochemical prospecting technique for ore deposits was suggested by Bancroft[3] in 1973. Since then, the only published works related to the subject are by Amirkhanov et.al.[34,35] in 1974-75, where tracing some thermodynamic conditions of the ore-forming process and estimation of the potential of ore zones, were deduced from a proposed relation between the absolute age of iron containing rocks and mudstones and the corresponding quadrupole splitting.

The results presented earlier in Chapter 6, and Mössbauer data from various references on silicate minerals, correlate mostly the variation in the quadrupole splitting of a specific mineral to the variation in the contents of iron or other ions; as in the diopside - hedenbergite line, where the quadrupole splitting is found to increase linearly as the ratio Fe/(Fe+Mg) increases, in both synthetic and natural samples.

In this chapter, an investigation of the possible use of Mossbauer spectroscopy in geochemical prospecting is carried out by studying six samples from specific locations in the Gaspé Copper mines area, the approach is outlined in Chapter 1. Information on the different formations in the area is given in Figure 37. A previous geological study of the area by J. Allcock[36] is used as a guide and a background for this study.

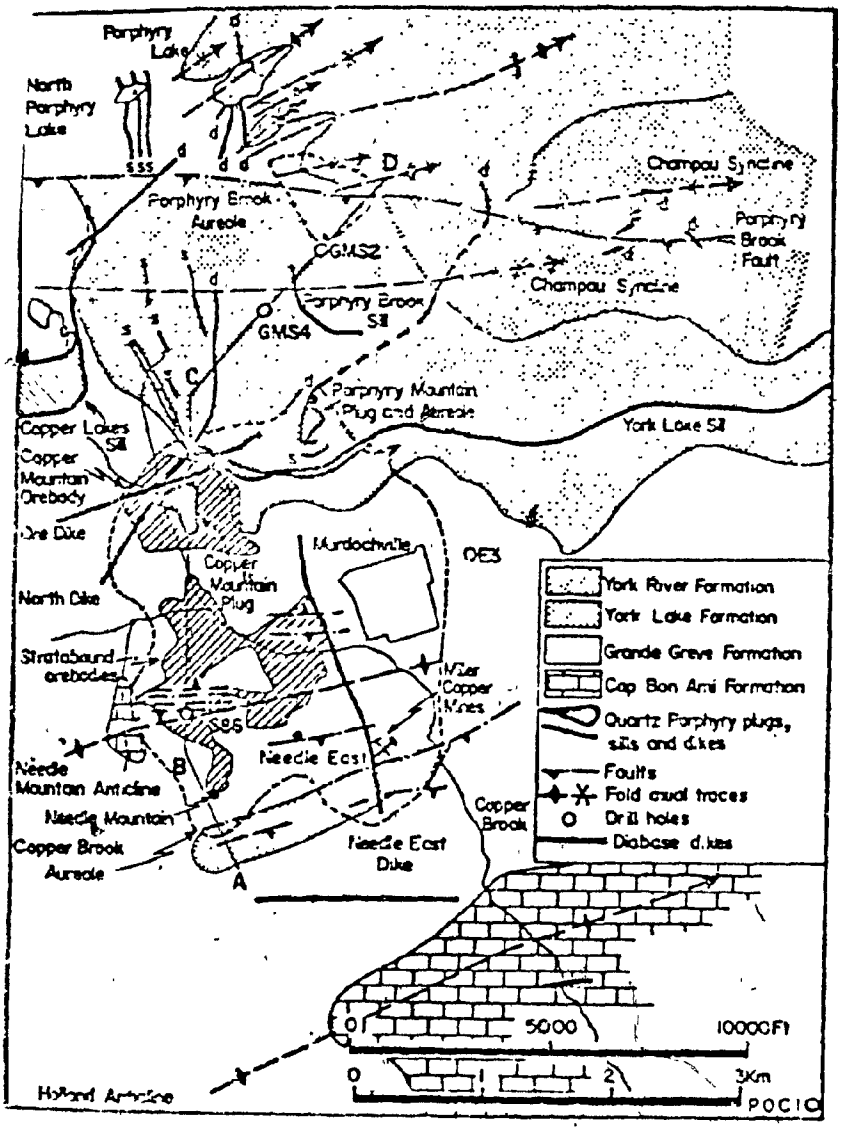

FIGURE 37

GEOLOGICAL MAP OF THE GASPÉ COPPER MINES AREA[36]

7.2 THE FORMATION AND THE SAMPLES

A cross section of the Copper mountain plug is shown in Figure 38 with the distribution of metamorphic zones and iron metasomatism. As is clear from the Figure, the Cap Bon Ami formation is divided into several units (Q_1, T_1, ...) which differ in general composition. The

L1 unit, to which the samples belong, refer to a calcareous layer that is mostly formed of an intergrowth of grossular and diopside with minor idocrase and wollastonite[36]. The samples are specified as follows, (see also Appendix A).

A - S675 - 2612

B - S678 - 2761

C - S258 - 2027

D - U3587 - 1552.5

E - U1467 - 240

F - S674 - 2313

A,B,...,F refer to the sample number, the second part of each label refer to to the drill hole position, whereas the last part refer to the depth in feet from the surface. The drill holes mentioned are shown in Figure 39.

7.3 ABSORBERS PREPARATION - RESULTS

Polished thin sections were prepared from the six samples and were studied under a microscope (to help in identifying the minerals present and their proportions). The absorbers were prepared by crushing each piece of rock (Sample) to a coarse grain; grains free of pyrite were only picked (Pyrite is easily detected by its glitter, it is present in the samples in very small quantities). The picked grains were ground and then freed from magnetite by use of a hand magnet (magnetite showed a very weak presence < 0.001% wt. also). Thereafter, each sample was powdered, absorbers were then made by enclosing about 100mg of powder between two thin circular plastic discs of an inch diameter. The thickness of absorbers was about 0.2 mm except that for sample F, for which it was 0.4mm.

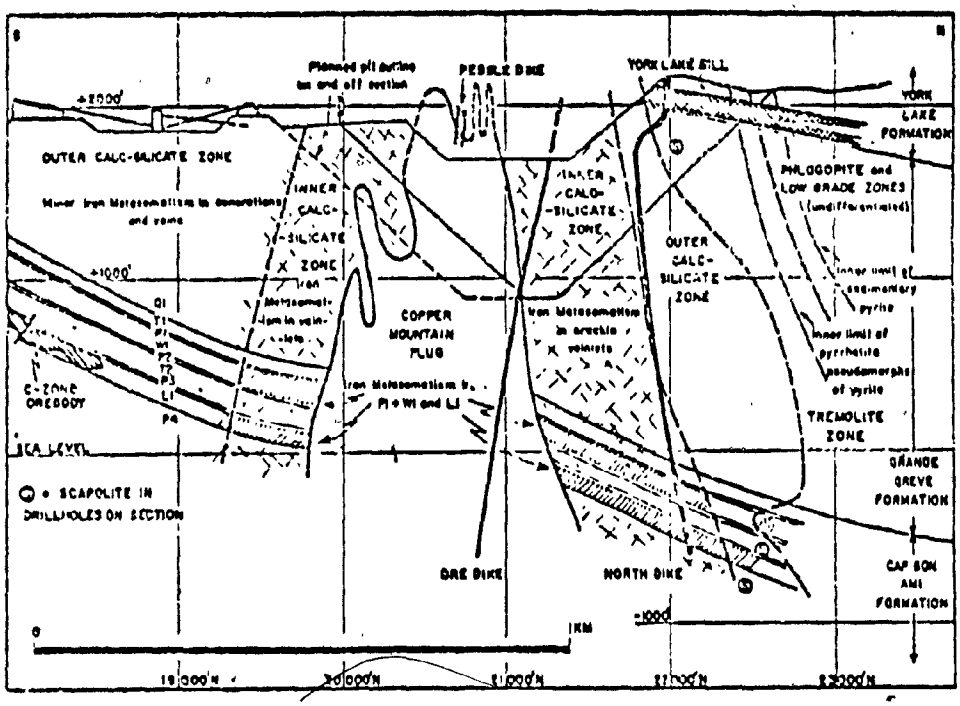

FIGURE 38

CROSS SECTION THROUGH THE COPPER MOUNTAIN PLUG ON 254QOE SHOWING DISTRIBUTION OF METAMORPHIC ZONES AND IRON METASOMATISM[36].

The absorption spectra of the samples are shown in Figures 40-45; Table 10 gives the calculated parameters. The main feature of the absorption spectra of the six samples, is that they are composed of two quadrupole doublets in varying proportions (see absorption spectra). The doublet labelled 11' of Δ around 0.53 mm/sec and δ = 0.63 mm/sec is assigned to ferric iron entering the structure of the garnet andradite of chemical composition $Ca_3(Fe^{3+},Al)_2\ Si_3O_{12}$. The garnet structure consists of independent SiO_4 tetrahedra linked by trivalent ions in octahedral coordination and divalent ions in eightfold coordination[43]. The octahedron of one Fe and 60 atoms is reported to be regular in andradite[13] and the

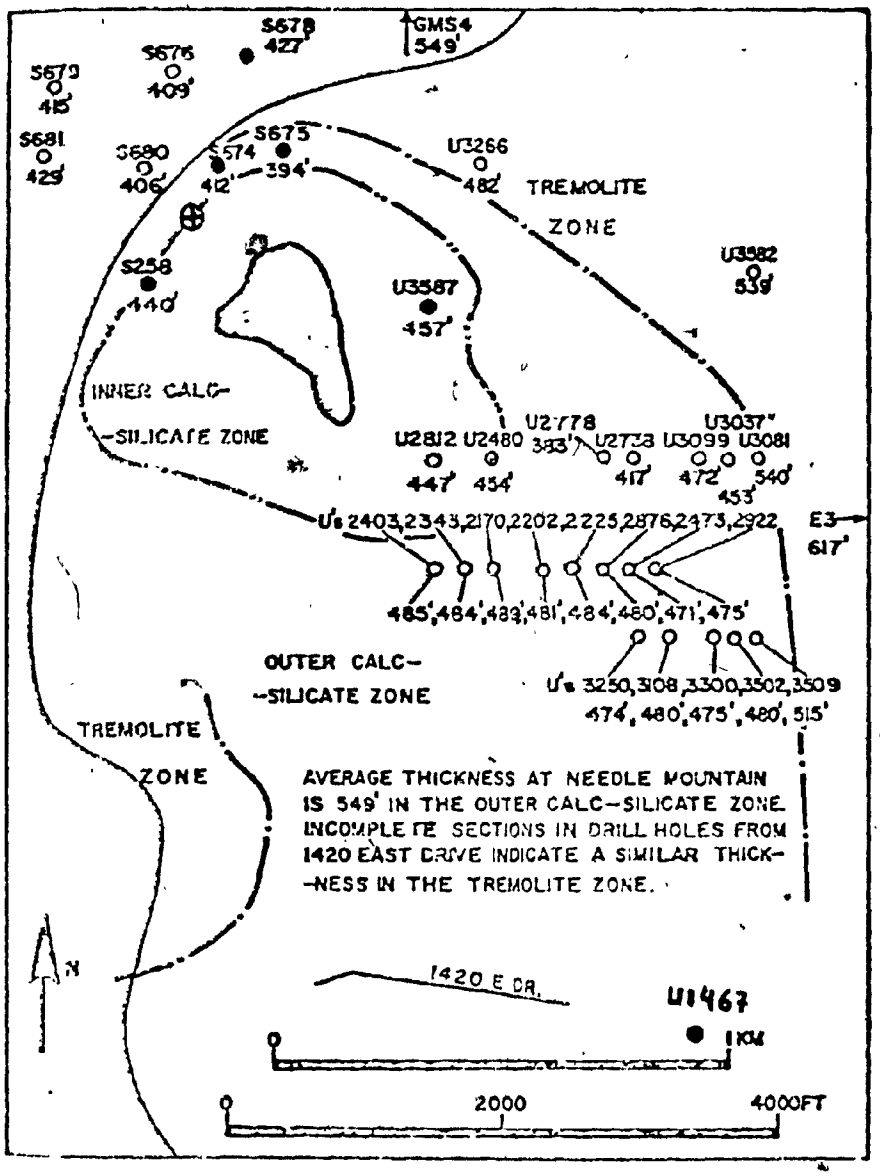

FIGURE 39

DRILL HOLES AND THE VARIATION OF THICKNESS OF THE SECTION T10-P40 IN THE CAP BON AMI FORMATION[36]

parameters are consistent with Fe^{3+} being in a slightly distorted octahedral configuration. The doublet labelled (22') in the absorption spectra is assigned to ferrous iron of the hedenbergite structure of chemical composition $Ca(Fe^{2+},Mg)\ Si_2O_6$. The hedenbergite structure is similar to

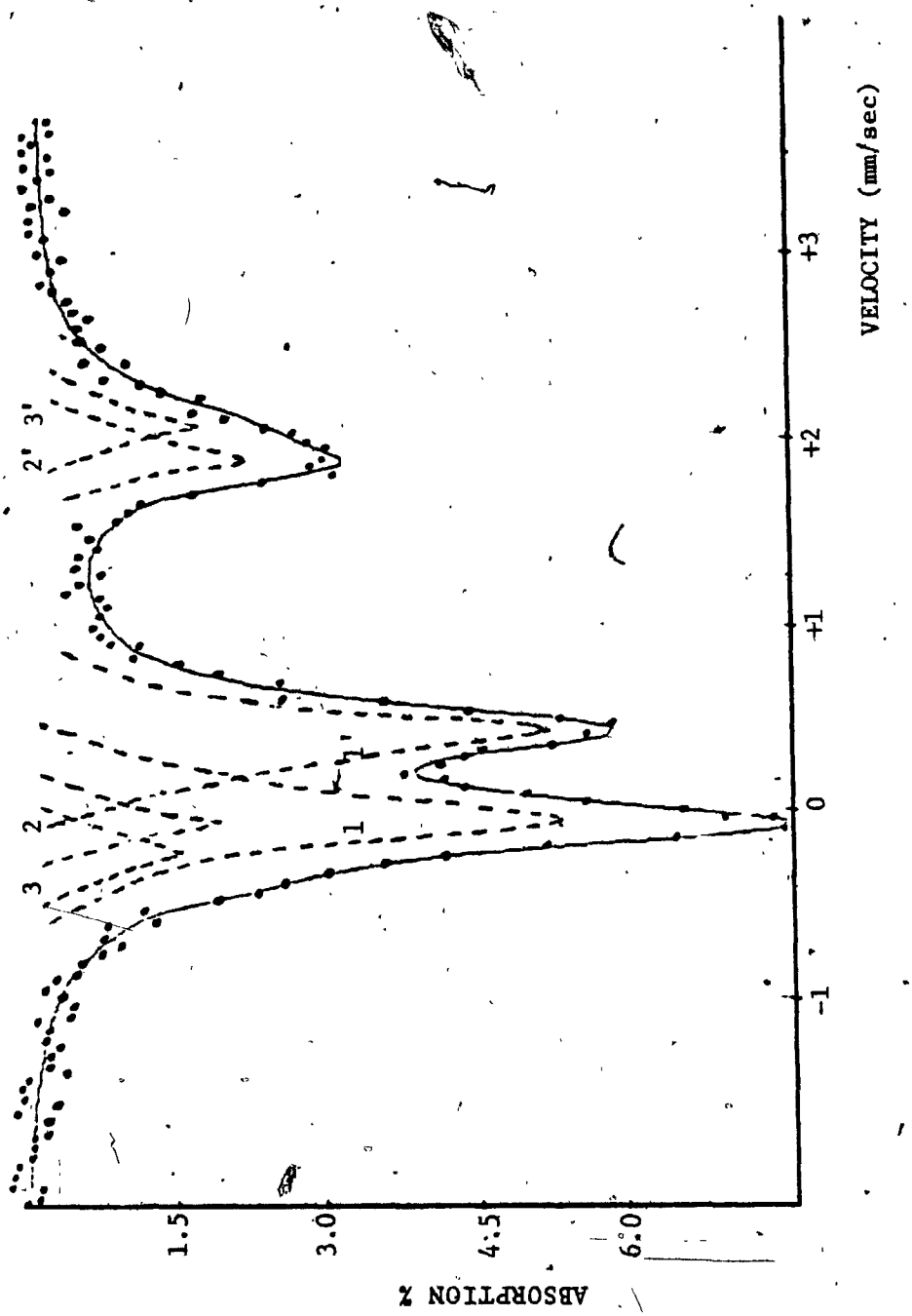

FIGURE 40

MÖSSBAUER SPECTRUM OF SAMPLE A (S675-2612)

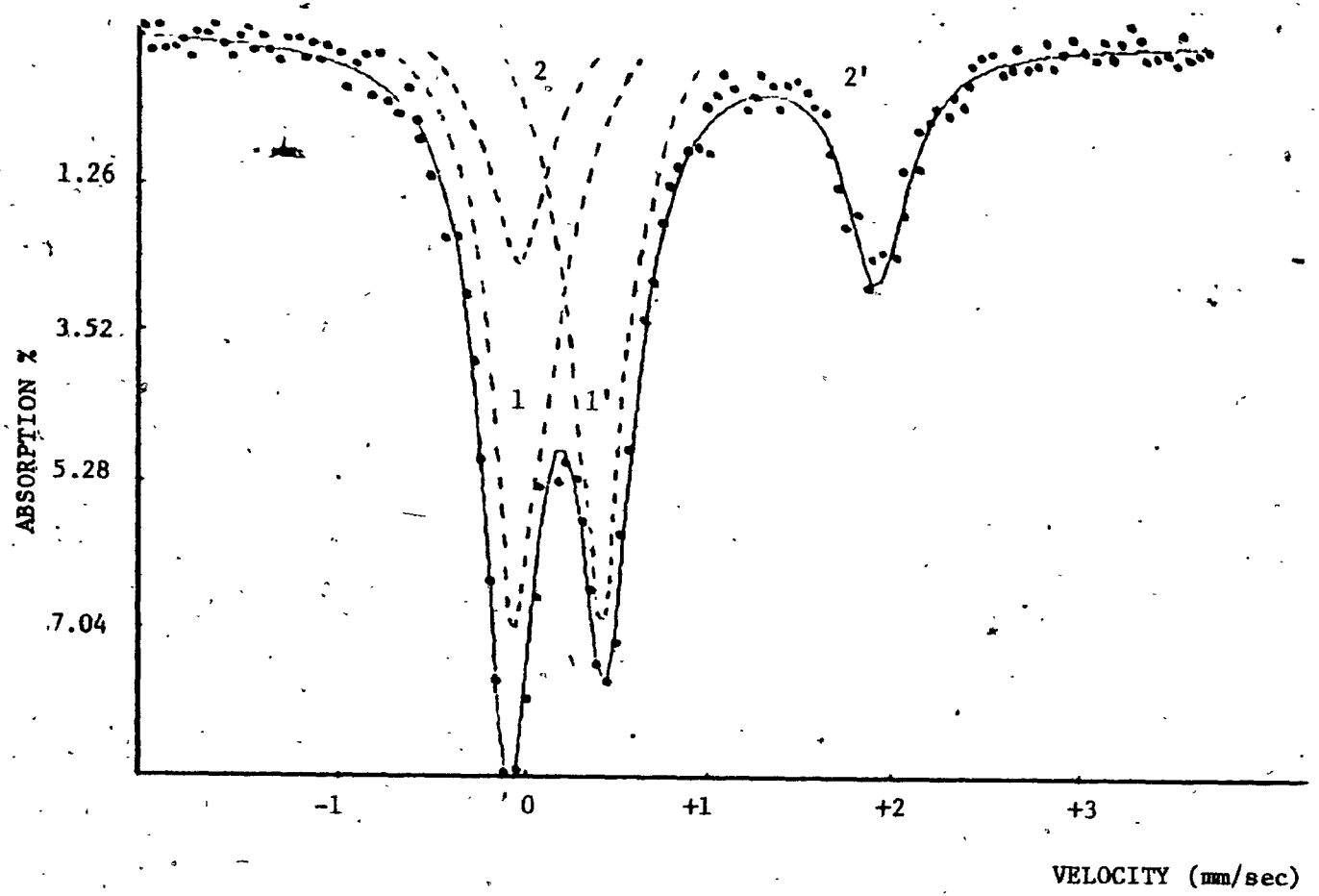

FIGURE 41

MÖSSBAUER SPECTRUM OF SAMPLE B (S678-2761)

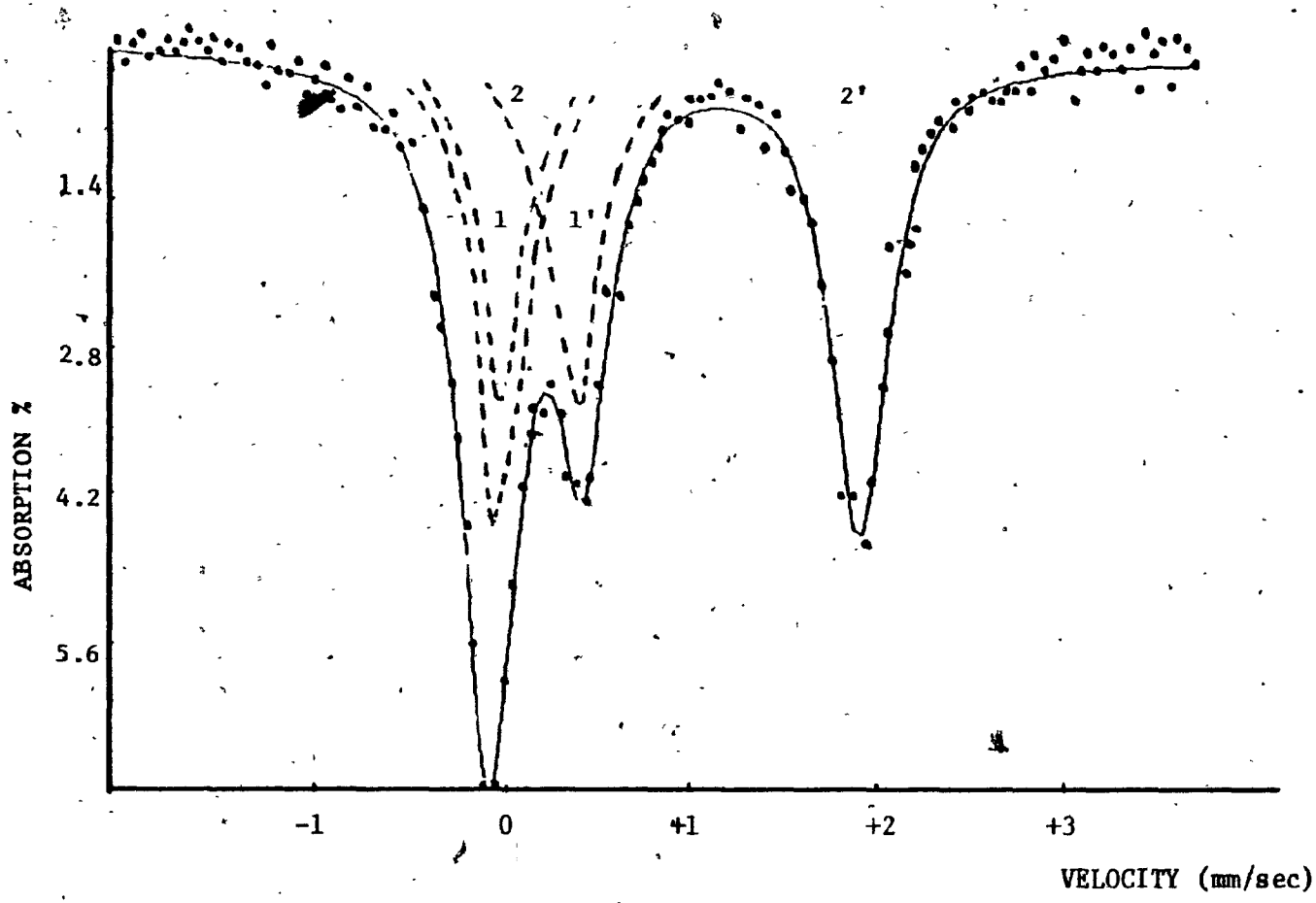

FIGURE 42

MÖSSBAUER SPECTRUM OF SAMPLE C(S258-2027)

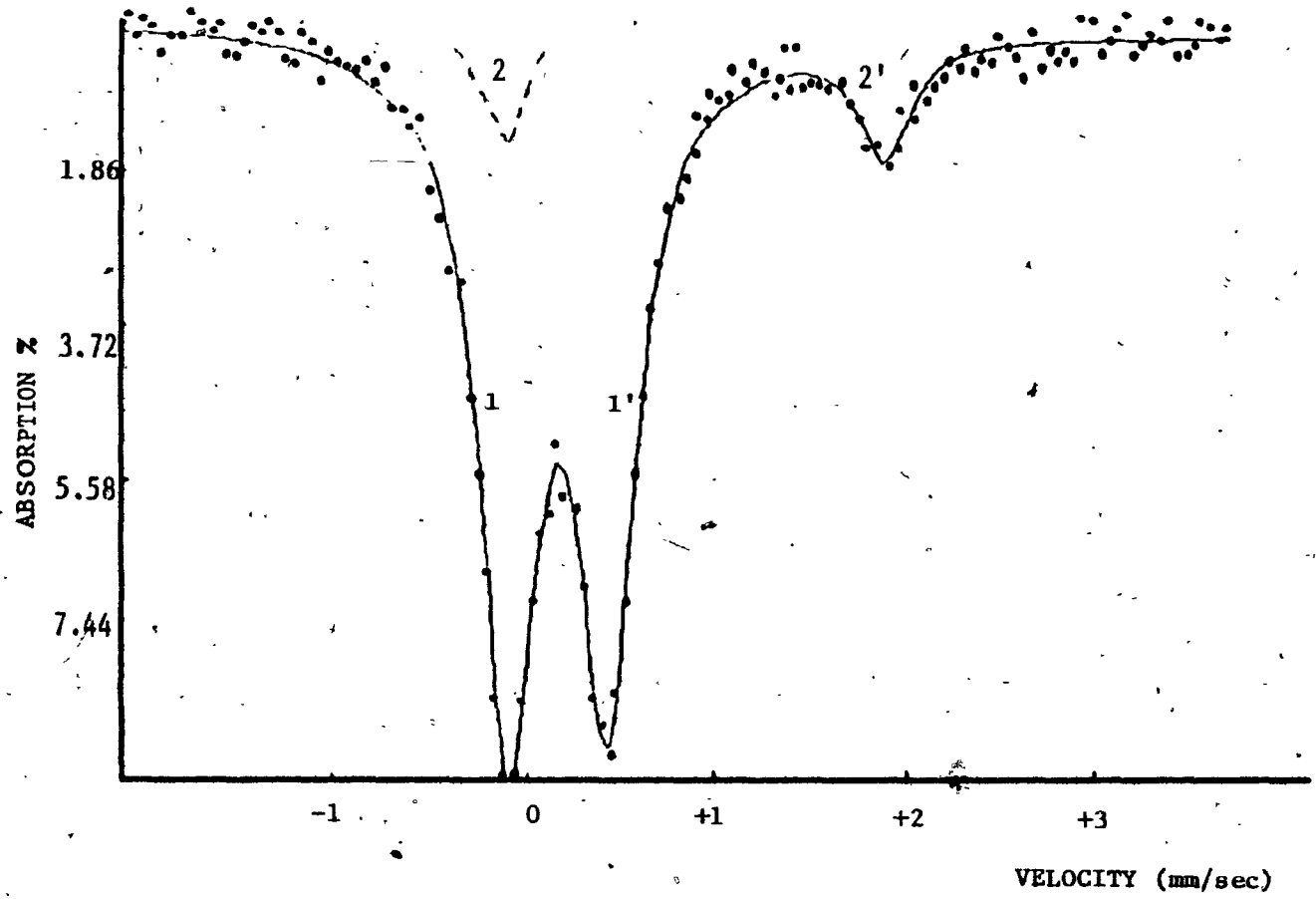

FIGURE 43 -

MÖSSBAUER SPECTRUM OF SAMPLE D (U3587-1552.5)

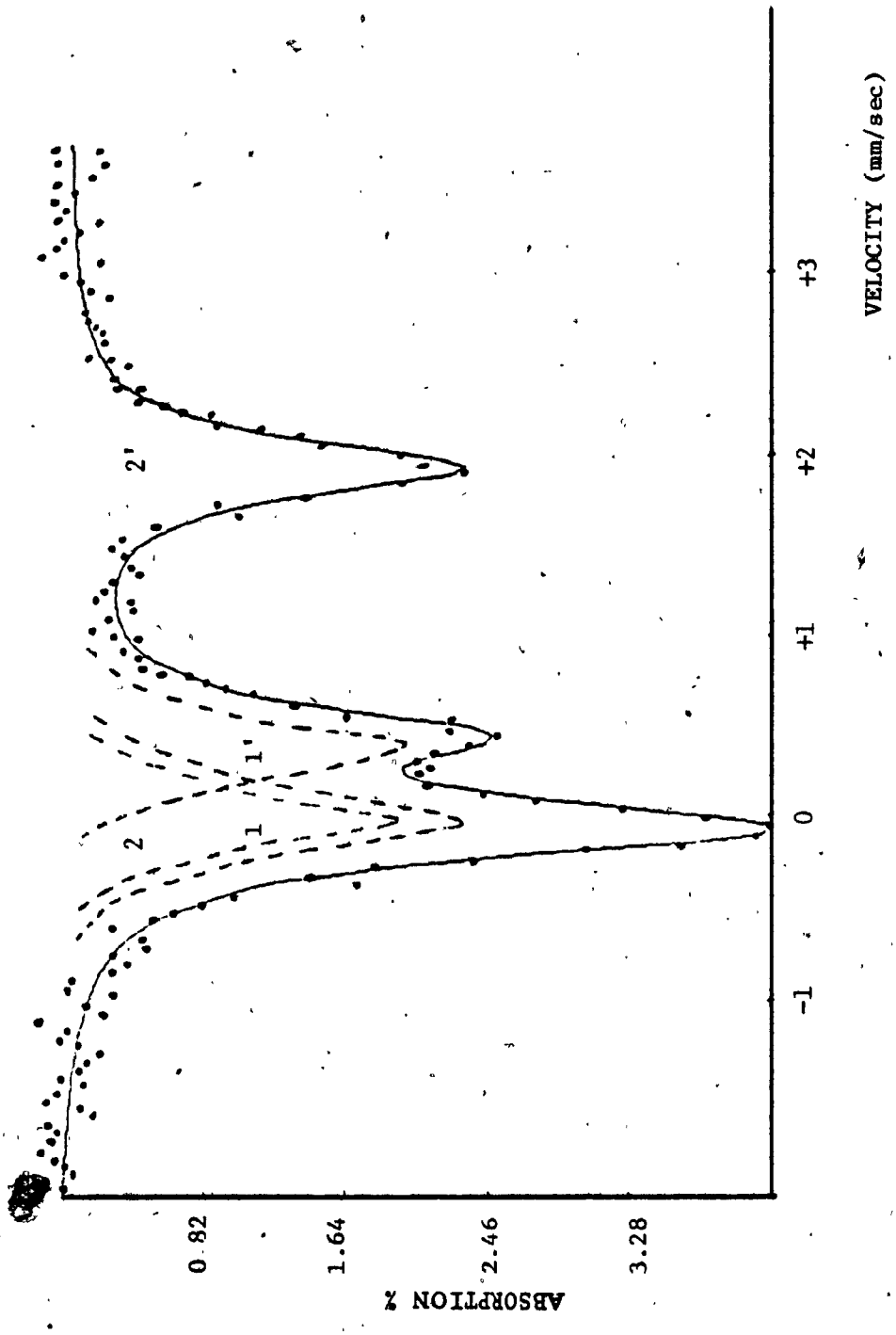

FIGURE 44

MÖSSBAUER SPECTRUM OF SAMPLE E(U1467-240)

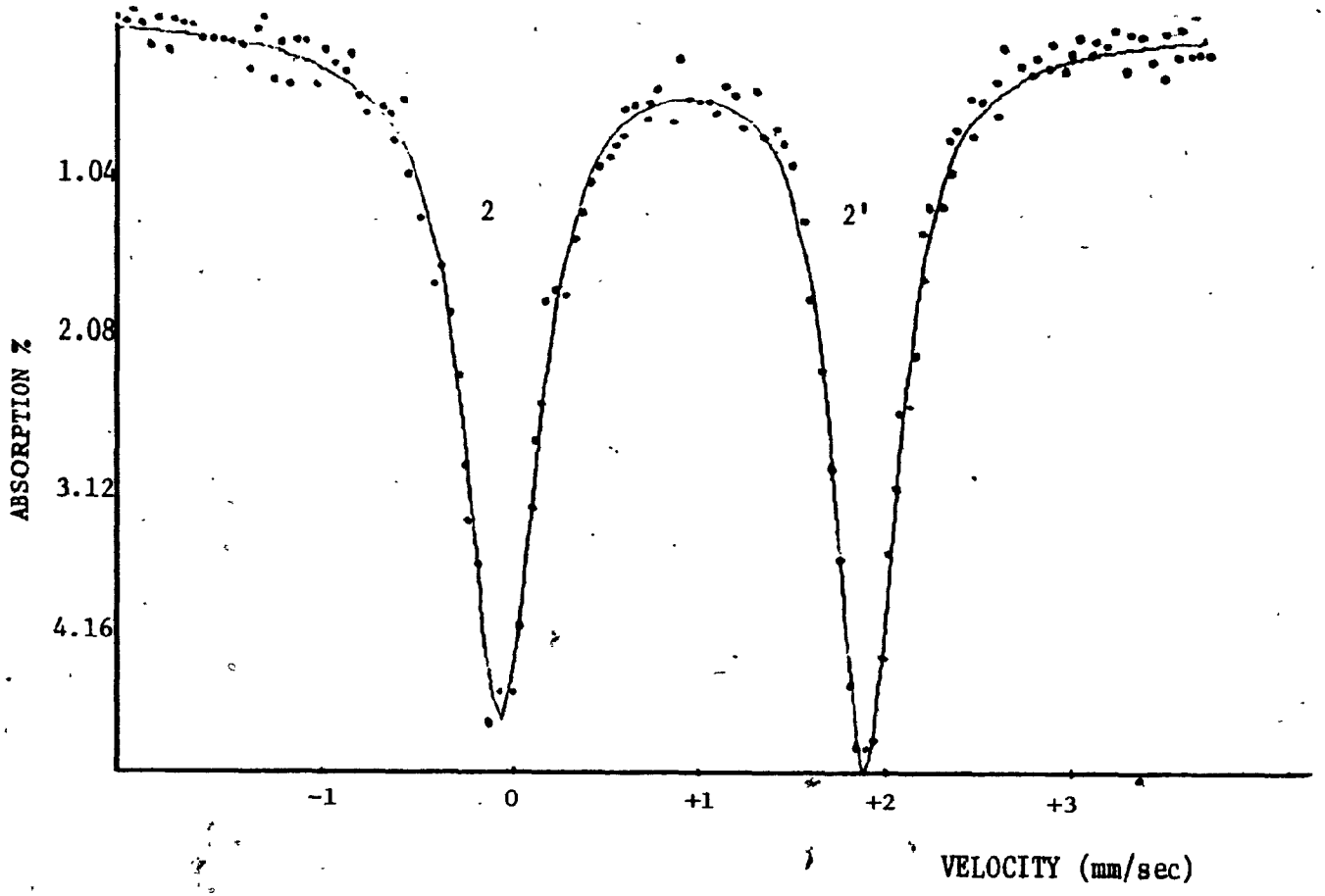

FIGURE 45

MÖSSBAUER SPECTRUM OF SAMPLE F (S674-2313)

that of diposide (see Section 6.2, Figure 21). The extra ferrous doublet (33') in the spectrum of Sample A (S675-2612) is probably due to an impurity of another pyroxene or silicate mineral. The percentages of ferrous and ferric iron, as calculated from area ratios (Section 5.3), the percentage absorption calculated using the formula

$$\text{Absorption} = \frac{\text{peak height (counts)}}{\text{background (counts)}}$$

and the total absorption, calculated using the formula.

$$\text{Total absorption} = \frac{\text{absorption area}}{\text{background area}}$$

are given in Table 10 along with the X^2 values.

TABLE 10

CALCULATED PARAMETERS OF THE GASPÉ COPPER MINES SAMPLES (NUMBERS IN PARANTHESES REPRESENT THE MAXIMUM EXPERIMENTAL ERROR, Δ AND δ ARE GIVEN IN mm/sec)

SAMPLE	A	B	C	D	E	F
Δ(11')	0.53(3)	0.54(3)	0.52(3)	0.54(3)	0.54(3)	-
δ(11')	0.63(3)	0.63(3)	0.63(3)	0.63(3)	0.63(3)	-
Δ(22')	2.00(3)	2.03(3)	2.06(3)	2.02(3)	2.05(3)	2.02(3)
δ(22')	1.40(3)	1.40(3)	1.40(3)	1.40(3)	1.40(3)	1.40(3)
Δ(33')	2.50(3)	-	-	-	-	-
δ(33')	1.35(3)	-	-	-	-	-
$\Sigma Fe^{2+}/\Sigma Fe\%$	42(5)	29(5)	60(5)	14(5)	54(5)	100(5)
$\Sigma Fe^{3+}/\Sigma Fe\%$	58(5)	71(5)	40(5)	86(5)	46(5)	0(5)
max. abs.%	7.64	8.88	7.17	9.40	4.18	5.24
Total abs.x10^3	7.88	8.93	7.31	8.78	4.26	5.97
X^2	247	247	271	300	262	256

7.4 INTERPRETATION OF RESULTS

Hedenbergite and andradite in the inner calcic-silicate zone and in viens and crackles extending into the outer calcic-silicate zone (Figure 46), were formed by iron metasomatism (caused by the emplacement of the plug in its present position). Introduction of iron to diopside and grossular, the main constituents of the calcic-silicate zone formed hedenbergite and andradite as follows:

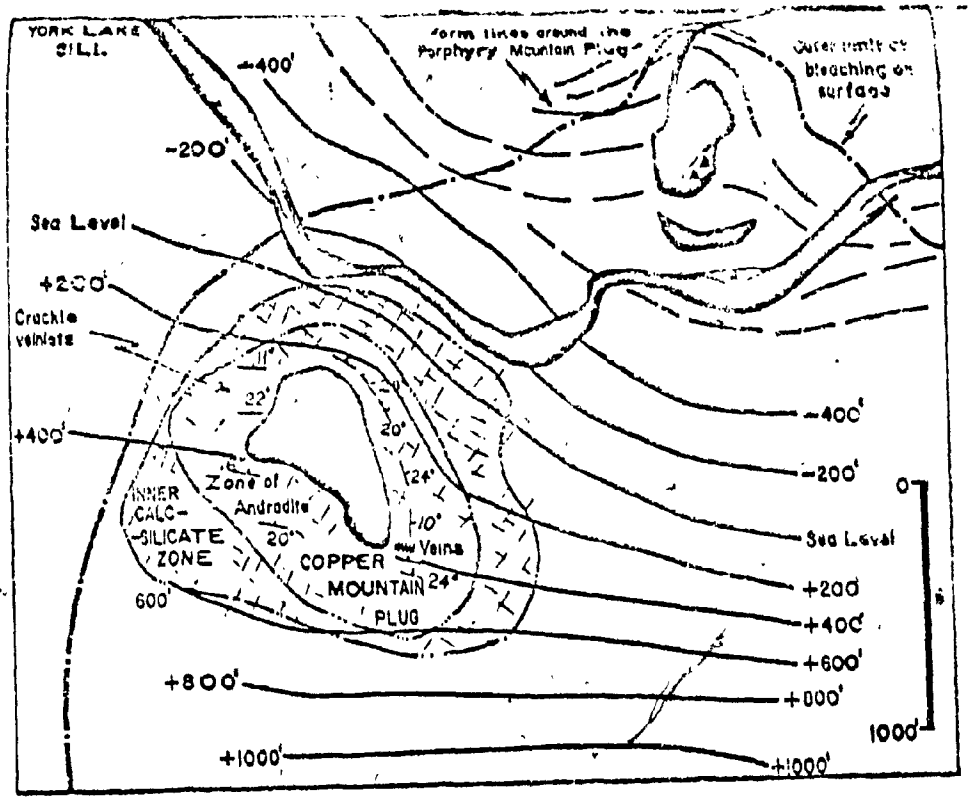

FIGURE 46

THE COPPER MOUNTAIN PLUG AND METASEDIMENTS, CONTOURS DRAWN ON UPPER SURFACE OF THE CAP BON AMI FORMATION. OUTLINE OF COPPER MOUNTAIN PLUG AT 500 FEET A.S.L. METAMORPHIC ZONES AT 1200-1500 FEET A.S.L.

$CaMgSi_2O_6$ (diopside) + Fe → $Ca(Fe^{2+},Mg)Si_2O_6$ (hedenbergite)

$Ca_3Al_2Si_3O_{12}$ (grossular) + Fe → $Ca_3(Fe^{3+},Al)_2Si_3O_{12}$ (andradite)

There is no consensus upon the origin of iron and other metals[36] (Cu,Mo,...). According to one argument "it has been leached from a large volume of surrounding rocks and redeposited by a circulating hydrothermal system". While according to another one it is due to" similar hydrothermal systems that occured during the emplacement of the igneous rocks".

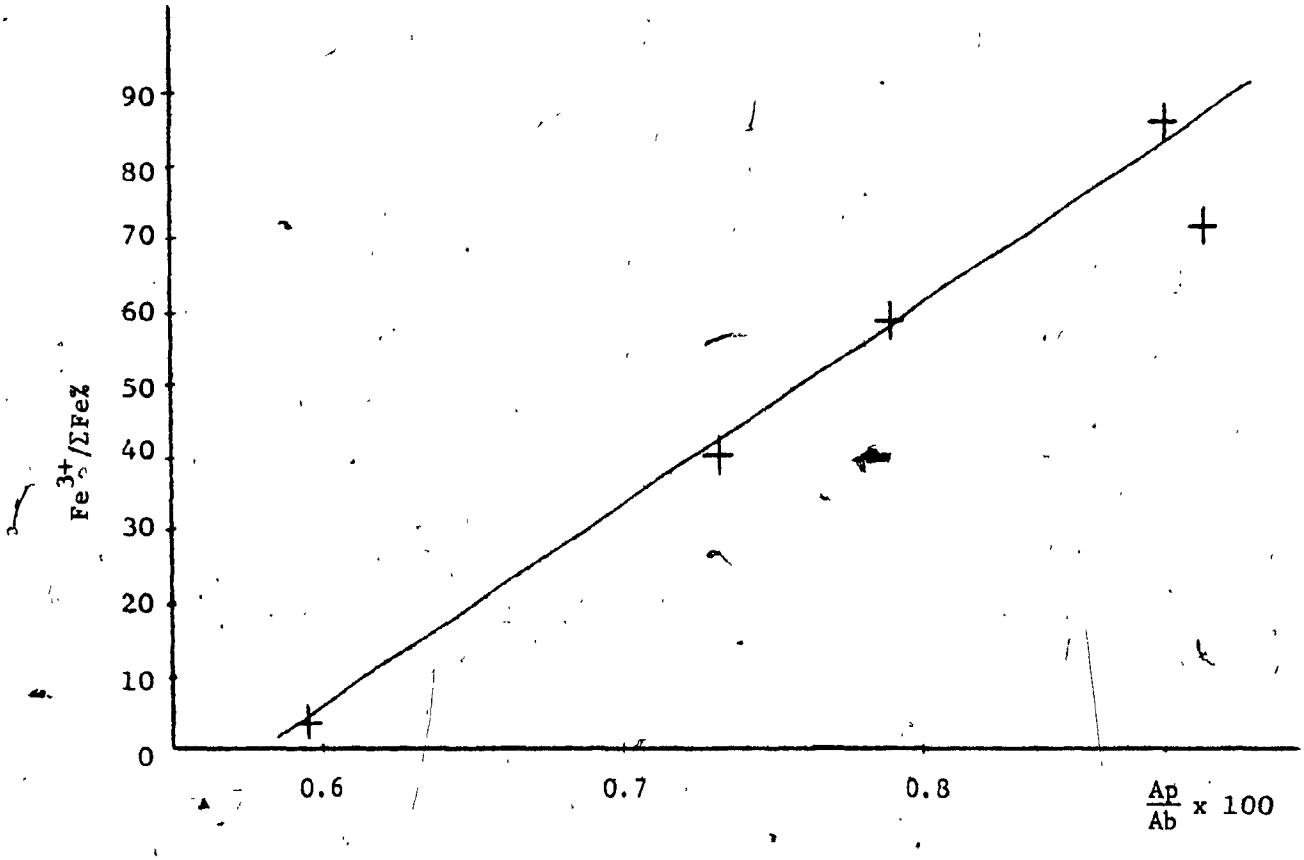

FIGURE 47

VARIATION OF THE RATIO ($\frac{Fe^{3+}}{\Sigma Fe}$) AGAINST TOTAL ABSORPTION ($\frac{Ap}{Ab}$ x 100).

Figure 47 represents the variation of andradite in the samples, with the total absorptions (the increase in the resonant absorption, is a

direct consequence of the increase in the iron contents). As the contents of iron increase in the rocks, a higher andradite content is noticed, while hedenbergite follows a reverse trend. Sample E (U1467 - 240) is not included in Figure 47 because its location is far away from the rest (Figure 39), and its thin section revealed that it is mostly formed of calcite while the others are mostly intergrowths of diopside and grossular.

The result of Figure 47 is a direct consequence of one fact; the andradite zone is closer to the mountain plug, i.e. the andradite ratio decreases as one moves toward the outer calcic-silicate zone, where the iron content fall rapdily (neglecting the veinlets and crackles).

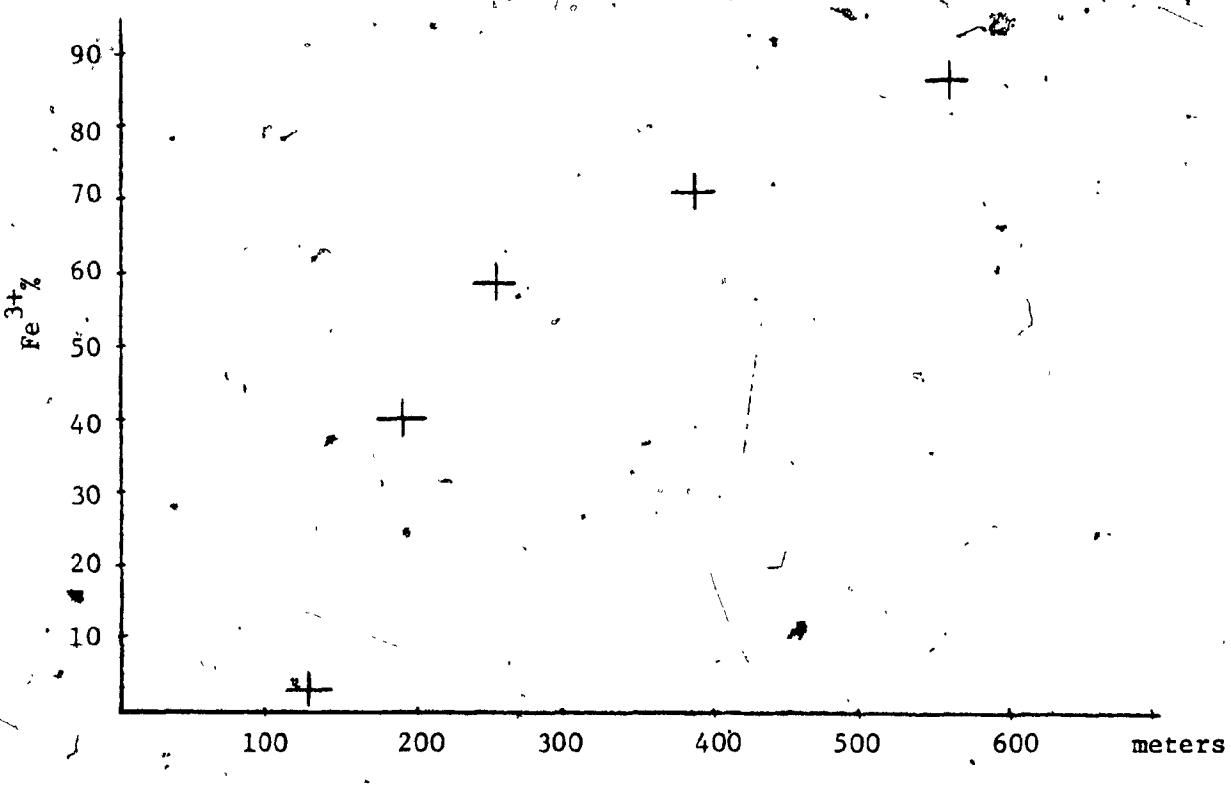

FIGURE 48

Fe^{3+} VERSUS DISTANCE FROM CENTER OF PLUG (THEORETICAL), SHOWN IN FIGURE 39 AS A CROSSED CIRCLE (⊕).

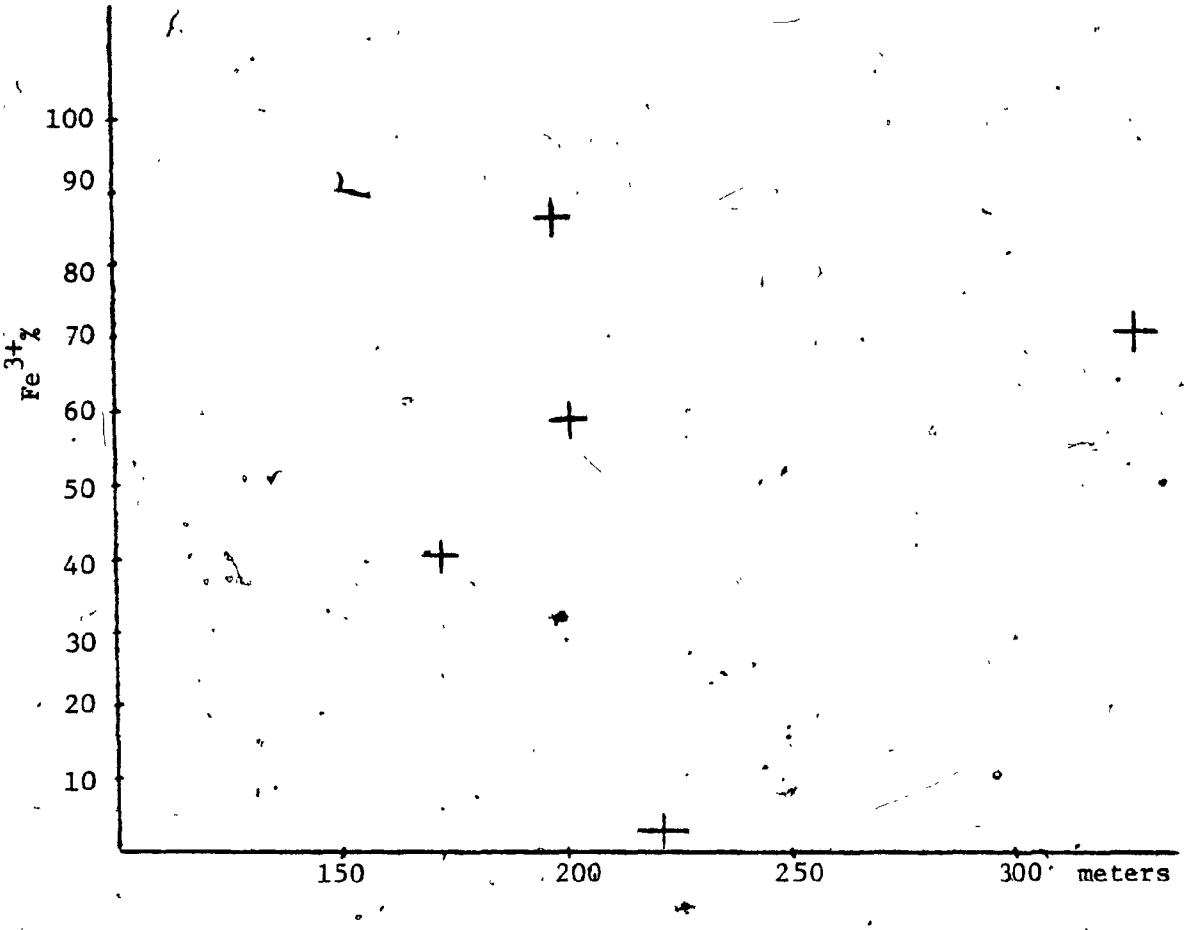

FIGURE 49

Fe^{3+} VERSUS DISTANCE FROM BOUNDARY OF MOUNTAIN PLUG (FIGURE 39).

Figures 48 and 49, are two attempts to correlate the variation of Fe^{3+} with the distance from the mountain plug. In the first the center of the plug is taken outside the given boundaries of Figure 39 and this hypothetical center gives somewhat a close to linear variation of Fe^{3+} with distance. In Figure 49 the distance of the drill holes (Figure 39) to the nearest boundary of the plug is taken, the points are scattered in a similar manner if the center of the plug is taken anywhere inside the boundaries.

7.5 DISCUSSION OF RESULTS

In the previous Section (7.4), the trials done to correlate the variation of Fe^{3+} (which is also an indicator to the variation of iron contents as a whole) with distance, were not successful, due to two factors:

1 - The lack of precise shape of the plug in three dimensions, which prevented the estimation of the distance seperating the samples from the plug.

2 - Since the Mössbauer spectroscopy deals with samples on a very small scale, studied samples should represent to a good degree the location, the layer or the formation to which they belong. Taking into consideration the inhomogeneity of geological formations, a larger number of samples would yield more detailed results.

CHAPTER VIII

CONCLUSION

8.1 CONCLUSION

The valuable use of the Mössbauer effect in semiquantitative analysis, is illustrated by the results of the study on bulk rocks and the Gaspe Copper Mines samples, where the identification of iron bearing minerals and their proportions (using the finger print technique and area ratios) is successful.

In studying the bulk rocks, though the iron contents were minimal and the absorption very weak, peaks accounting to less than ten percent of the total absorption were solved.

In studying the orthoand clinopyroxenes, the Mössbauer spectra obtained and the parameters derived from computer analysis, indicate to a good degree the purity and uniformity of their structure. Predictions about the iron contents (Fe/(Fe+Mg)) could be made only qualitatively, due to the limited variation of the quadrupole splitting.

The results derived from samples of Gaspe Copper Mines (Chapter 7) where a linear relation is found to hold between the ferric or ferrous iron proportions and the total iron contents, is a basic step toward the study of better chosen samples, other locations and reaction aureoles. There is a good degree of evidence in the derived results (Chapter 7), that MÖssbauer spectroscopy will prove to be valuable and useful in geochemical prospecting.

8.2 RECOMMENDATION FOR FUTURE WORK IN GASPÉ COPPER MINES AREA

i - independent checks of results (chemical, X-ray analysis etc.)

ii - closer representative sampling

iii - better controlled sample preparation (using more advanced techniques in the separation of Fe containing minerals, present in the samples studied but regarded as impurities).

APPENDIX A

SAMPLES DECRIPTION

1. E288.c Diopside Limy quartzite, Gaspé Copper Mines, Quebec, Ref. A.
2. E282.b Porcellenite, Gaspé Copper Mines, Quebec, Ref. A.
3. E294 Chalcopyrite in altered limy quartzite, Gaspé Copper Mines, Quebec, Ref. A.
4. CGW1 Bronzite (St. Agathe), Ref. B.
5. CG3 Enstatite, Ref. C.
6. CG5 Bronzite, (MRD-606), Ref. C.
7. CG12 Enstatite (St. Set. 131B), Ref. C.
8. CG1 Clinopyroxene (from Alaska), Ref. C.
9. CG6 Augite (MRD-608), Ref. C.
10. CG8 Augite (MRD-614), Ref. C.
11. CG11 Hedenbergite ($MRD-622_2$), Ref. C.
12. CG14 Augite (St. Set. 134B.), Ref. C.
13. CGW2 Aegerine, Ref. C.
14. SS7P Pyrite, Eastern Townships, Quebec, Ref. D.
15. SS8P Pyrite, Eastern Townships, Quebec, Ref. D.
16. Samples from Gaspé Copper Mines (S675-2612; S678-2761; S258-2027; 43587-1552.5;U1467-240;S674-2313), Ref. E.

References:

A. P.S. Kumarapeli, Department of Geology, Concordia University, Montreal, Quebec.

B. E. Procyshin, Department of Geology, Concordia University, Sir George Williams Campus, Montreal, Quebec.

C. J.T. Jenkins, Department of Geology, Concordia University, Loyola Campus, Montreal, Quebec.

D. I.Y. Eladas.

E. Kevin Shelton, Department of Geology and Geophysics, Yale University, New Haven, Connecticut.

APPENDIX B

```
      PROGRAM LOSSBA (INPUT,OUTPUT,TAPE5,TAPE6=OUTPUT,TAPE66)
C
C              CURVE FITTING  LINE + LORENTZIANS
C       N      =NUMBER OF PARAMETERS
C       NG     =NUMBER OF LORENTZIANS UP TO SIX
C       L4     =NUMBER OF ITERATIONS ALLOWED
C       NC     =INITIAL CHANNEL OF THE GROUP
C       M      =NUMBER OF CHANNELS IN THE GROUP
C       B(3*NG+2)=SLOPE
C       B(3*NG+1)=BACKGROUND
C       B(3*J)   =CHANNEL NUMBER OF PEAK
C       B(3*J-1) =HALF WIDTH AT HALF MAXIMUM
C       B(3*J-2) =HEIGHT OF THE PEAK
C       KONG=PROVIDES 12 SPACES FOR SPECIFYING THE DATE OF EXPERIMENT
C       SAMPLE=PROVIDES 72 SPACES FOR SPECIFYING THE SAMPLE
C       TIME=PROVIDES 12 SPACES FOR SPECIFYING THE DURATION OF EXPERIMENT
C     ******ALL INPUT DATA IS READ IN SUBROUTINE READA ******
C
      DIMENSION Z(256),FH(256),FL(256),BF(256),ERR(256),B(20),B1(20),
     1B2(20,20),BB(2000),S(6),DAT(256),KONG(5),S1(6),P(6),PE(6),PH(6),
     2PHE(6),PW(6),PWE(6),A(6),AE(6),SAMPLE(5),ABC(2),Y(4),TIME(5),
     3DATA(256),YFIT(256),FDATA(512),IDATA(512)
      COMMON/DATA/ABC,Y
      COMMON BB
      EQUIVALENCE (Z,BB),(FH,BB(257)),(FL,BB(513)),(BF,BB(769)),
     1(ERR,BB(1025)),(B1,BB(1281)),(B2,BB(1301)),(N,BB(1701)),
     2(L4,BB(1703)),(G1,BB(1704)),(G2,BB(1705)),(T,BB(1706)),
     3(S,BB(1715)),(Y1,BB(2100)),(L,BB(2179)),(NG,BB(2182)),
     4(IDATA,BB(2200)),
     5(NC,BB(2720)),(M,BB(2721)),(SAMPLE,BB(2722)),(TIME,BB(2727)),
     6(KONG,BB(2732))
      DATA(ABC=2HBC,3HYES),(Y=1H ,1HC,1H*,1HM)
C
C     READ IN SPECTRUM
C     DATA= MOSSBAUER DATA CORRECTED LATER FOR CURFIT
C     G1 AND G2 ARE THE PRECISIONS OF THE CURVE FITTING
C
      WRITE(6,100)
      CALL READA
    7 FORMAT(2F5.2)
      WRITE(6,8) G1,G2
    8 FORMAT (1X,4HG1 = ,F5.2,5X,4HG2 = ,F5.2)
      DO 301 IA=1,512
  301 FDATA(IA)=FLOAT(IDATA(IA))
      WRITE(6,56)
   56 FORMAT(10X,*INITIAL  DATA*,//)
   55 FORMAT(10X,10F9.0)
      FDATA(1)=FDATA(2)
      FDATA(512)=FDATA(511)
      FDATA(256)=FDATA(255)
      FDATA(257)=FDATA(256)
```

```
C     THE FOLLOWING FOR REMOVING ANY DATA POINT SCATTERED TOO FAR
      DO 50 J=3,512
      D1=FDATA(J-1)*0.8
      D2=FDATA(J-1)*1.2
   54 CONTINUE
      IF(FDATA(J).LT.D1.AND.FDATA(J).LT.D2) GO TO 51
      FDATA(J)=(FDATA(J-1)+FDATA(J-1))/2.
   53 FORMAT(5X,*ERRATIC CHANNEL CORRECTED AGAIN*)
      GO TO 54
   51 CONTINUE
   50 CONTINUE
   52 FORMAT(5X,*ERRATIC CHANNEL NUMBER=*,I4)
C
C
   32 FORMAT (12X,10F6.0)
      PRINT 100
  100 FORMAT (1H1)
    4 FORMAT(10X,10F9.0)
      WRITE(6,100)
C     SS=0. ONLY ANALYSE CHANNEL 1 TO 256
C     SS=1. OVERLAP CHANNELS 257 - 512 ON CHANNELS 1- 256
      SS=1.
      IF(SS)56,56,59
   59 CONTINUE
      DO 66 J=1,256
      DATA(J)=(FDATA(J)+FDATA(513-J))/2.
   66 CONTINUE
      GOTO71
   56 CONTINUE
      DO70 J=1,256
   70 DATA(J)=FDATA(J)
   71 CONTINUE
   88 FORMAT(10X,10F9.0)
  100 FORMAT (1H1)
      WRITE (6,100)
    1 FORMAT(10A1)
      WRITE(6,2)RUNNO
    2 FORMAT (1X,14H RUN NUMBER=  ,5A10/)
  226 FORMAT (5A10)
      WRITE (6,222) SAMPLE
  222 FORMAT(1X,14H SAMPLE    =  ,5A10/)
  150 FORMAT (2A6)
      WRITE(6,151) TIME
  151 FORMAT(1X,14H TIME      = ,5A10/)
  999 FORMAT (4I3)
      WRITE(6,10)NC,N,KG
   10 FORMAT(1X20H*INITIAL CHANNEL=    I3,25H   *NUMBER OF CHANNE
     1I3,29H    NUMBER OF LORENTZIANS=   I2/)
      DO 111 J=1,256
      DAT(J)=DATA(J)
  111 CONTINUE
```

```
      N=3*KG+2
      NN=N
      DO 115 J=1,NN
      KNG=J+NG
      Z(J)=(KNG-1)
      FR(J)=EAT(KNG-1)
  115 ERR(J)=SQRT(FR(J))
   69 FORMAT (1F6.0)
      WRITE(6,11)B(3*KG+1)
   11 FORMAT (1X14H BACKGROUND=  F6.0/)
      B(3*KG+2)=0.0
  122 FORMAT(6F5.0)
    5 FORMAT(6F6.2)
      WRITE(6,13)(B(3*J-2),J=1,KG)
   13 FORMAT(1X,16H PEAK HEIGHTS=  6F15.0/)
   12 FORMAT(1X,16H PEAK POSITIONS=  6(F15.0)/)
      WRITE(6,12)(B(3*J),J=1,KG)
  126 FORMAT(6F5.3)
      WRITE(6,14)(B(3*J-1),J=1,KG)
   14 FORMAT(1X,9H SIGMA=  6F15.3///)
      KG1=KG
      DO 21 J=1,KG1
   21 B(3*J-2)=B(3*J-2)*B(3*J-1)**2/10000.0
      B(3*KG+1)=B(3*KG+1)/10000.0
      DO 22 J=1,NN
      FR(J)=FR(J)/10000.0
   22 ERR(J) = ERR(J)/10000.
      WRITE (6,1661)
 1661 FORMAT (39H0 CURVE FITTING        LINE+GAUSSIANS //)
      CALL CURFIT
      WRITE(6,166)
      WRITE (6,135)
  135 FORMAT(1X,11H PARAMETERS//3X,1HJ, 10X,4HB(J),27X,6HERRORS//)
      WRITE (6,140)(J,B(J),B1(J),J=1,N)
  140 FORMAT(3X,I2,5X,E16.6,15X,E16.6 /)
      DO 200 J=1,KG
      P(J)=B(3*J)
      PE(J)=B1(3*J)
      PH(J)=10000.0*B(3*J-2)/B(3*J-1)**2
      T=2.0*(B1(3*J-1)/B(3*J-1))**2
      W=(B1(3*J-2)/B(3*J-2))**2
      PHE(J)=PH(J)*SQRT(T+W)
      PW(J)=2.0*B(3*J-1)
      PWE(J)=2.0*B1(3*J-1)
      A(J)=31415.9265*B(3*J-2)/B(3*J-1)
      TT=(B1(3*J-1)/B(3*J-1))**2
      WW=(B1(3*J-2)/B(3*J-2))**2
      AE(J)=A(J)*SQRT(TT+WW)
  200 CONTINUE
      WRITE(6,188)
      WRITE (6,201)
```

```
 201  FORMAT    (1X,15H LINE POSITIONS,6X,7H ERRORS/)
      WRITE (6,202) (P(J),PE(J),J=1,KG)
 202 FORMAT     (3X,1F10.5,6X,1F11.6/)
      WRITE (6,203)
 203 FORMAT (/,1X,13H LINE HEIGHTS,6X,7H ERRORS/)
      WRITE (6,204) (PH(J),PHE(J),J=1,KG)
 204 FORMAT(2X,F10.3,10X,F10.4/)
      WRITE (6,205)
 205  FORMAT (/,1X,14H WIDTH OF LINES,7X,7H ERRORS/)
      WRITE (6,206) (PW(LL),PWE(LL),LL=1,KG1)
 206  FORMAT     (3X,1F10.6,6X,1F10.7/)
      WRITE (6,207)
 207  FORMAT (/,5X,11H LINE AREAS,6X,7H ERRORS/)
      WRITE (6,208) (A(J),AE(J),J=1,KG)
 208  FORMAT (1X,1F16.6,2X,1F16.6/)
      WRITE (6,188)
      CALL PLOTB(NG,N,FL,FH)
      NN=N
      DO  46 KK=1,NN
      FL(KK) = FL(KK)*100000
      FH(KK) = FH(KK)*100000
  46  CONTINUE
      WRITE(6,188)
      WRITE(6,935)  (FH(KJ),KJ=1,NN)
      WRITE(66,935) (FH(KJ),KJ=1,NN)
      WRITE(6,935)  (FL(KJ),KJ=1,NN)
      WRITE (66,935) (FL(KJ),KJ=1,NN)
 935 FORMAT(5X,10F7.6)
9461  FORMAT (5H"""N=,I5,5H/"NG=,I5,2H//)
  16 FORMAT (I1)
      STOP
      END
      SUBROUTINE NDATA
      DIMENSION IDATA(512),DD(2000),IIDATA(512),D(20),C(20),
     1SAMPLE(5),TIME(5),RUNNO(5),SAM(5),TIM(5),RUN(5)
      COMMON DD
      EQUIVALENCE (IDATA,DD(2200)),(G1,DD(1704)),(G2,DD(1705)),
     1(N,DD(1701)),(KG,DD(2102)),(L4,DD(1703)),(D,DD(1719)),
     2(NG,DD(2720)),(JG,DD(2721)),(SAMPLE,DD(2722)),(TIME,DD(2727)),
     3(RUNNO,DD(2732))
      READ(5,1150) (IIDATA(I),I=1,512)
      DO 145 K3=1,512
      IIDATA(K3)=IIDATA(K3)
 145  CONTINUE
1150 FORMAT(16,917)
      DATA(RUN(J),J=1,2)/10HSEP.20-OCT,8H.20,1977/
      DATA(SAM(J),J=1,2)/10HCO-5750URL,1HE/
      DATA TIM(1)/9HONE MONTH/
      DATA(C(I),I=1,11)/
     5-10000.,4.,127.,-5500.,4.,130.,-6500.,4.,170.,
     5242000.,0.0001/
```

```
      DO 100 IA=1,512
  100 IDATA(IA)=IIDATA(IA)
      DO 200 J=1,11
  200 B(J)=C(J)
      DO 300 J=1,5
      RUNNO(J)=RUN(J)
      SAMPLE(J)=SAM(J)
  300 TIME(J)=TIM(J)
      NO=1
      N=256
      KO=3
      L4=16
      Q1=0.
      Q2=.01
      JO=1.
      RETURN
      END

      SUBROUTINE CURFIT
C          F U N T N A N  4
      DIMENSION Z(256),FN(256),FC(256),DF(256),ERR(256),X(256),
     1D(20),D1(20),D2(20,20),GRAD(20),B1(20),B2(20,20),DC(2000),B3(20,20
     2),AA(20),BB(20),WE(20),W2(20),ABC(2),DD(20,20),Y(4)
      COMMON/DATA/ABC,Y
      COMMON DC
      EQUIVALENCE (Z,DD),(FN,DC(257)),(FC,DC(513)),(DF,DC(769)),
     1(ERR,DC(1025)),(B1,DC(1281)),(B2,DC(1301)),(N,DC(1761)),
     2(L4,DC(1763)),(Q1,DC(1764)),(Q2,DC(1765)),(R,DC(1766)),
     3(D,DC(1719)),(GRAD,DC(1739)),(D1,DC(1759)),(D2,DC(1779)),
     4(I,DC(2100)),(L,DC(2179))
      DATA(ABC=2HNO,3HYES),(Y=1H ,1HC,1H*,1HM)
      L1 = 0
      SA = 0.0
      DO 1000 J=1,20
      B1(J)=0.0
      DO 1000 K=1,20
 1000 B2(J,K)=0.0
      NN=N
      MM=M
      DO 100 K = 1, NN
      X(K) = ERR(K)**2
      L=1
      I=K
      CALL FUNC(Z)
      DF(K) =FN(K) - FC(K)
      DO 101 J=1,MM
      B1(J)=B1(J)-(2.0*DF(K)*D1(J))/X(K)
      DO 101 KK=1,MM
  101 B2(J,KK)=B2(J,KK)-(2.0*(DF(K)*D2(J,KK)-D1(J)*D1(KK)))/X(K)
  100 SA = SA + DF(K)**2/X(K)
      GMOD=0.0
```

```
      DO 102 J=1,N
  102 GNOO=GNOO+B1(J)**2
      WRITE(6,243)SA,GNOO
  243 FORMAT (1X,26H*INITIAL VALUE SUM OF SQ.=E13.5,20X,17H*SQ ROO OF GR
     1AD =E13.5)
      WRITE(6,1751)
 1751 FORMAT(14HO DERIVATIVES-)
      WRITE(6,240)(B1(J),J=1,N)
  240 FORMAT (15X,5(E13.5,6X)/)
      IF (SA - G1) 110, 110, 200
  110 LE = 1
      GO TO 600
  200 S = 0.0
      GNOO = 0.0
      BNOO = 0.0
      PNOO = 0.0
      A2=ALO(1)
      DO 210 J = 1, NN
      B1(J) = 0.0
      DO 210 K = 1, NN
  210 B2(J,K) = 0.0
      DO 220 JJ = 1, NN
      L=1
      I=JJ
      CALL FUNC(2)
      DF(JJ) = FN(JJ) - FO(JJ)
      DO 220 J = 1, NN
      B1(J) = B1(J) - (2.0*DF(JJ)*B1(J))/X(JJ)
      DO 220 K = 1, NN
  220 B2(J,K) = B2(J,K) - (2.0*(DF(JJ)*B2(J,K) -B1(J)*B1(K)))/X(JJ)
      DO 230 J = 1, NN
  230 GRAD(J) = B1(J)
      L1 = L1 + 1
      CALL EXAM (B2,B1,N,LF)
      IF (LF)  250, 250, 305
  250 DO 231 II=1,N
      DO 231 JJ=1,N
  231 B3(II,JJ)=B2(II,JJ)
      CALL JACOBI (N,B3,1,NR,B2)
      NN=N
      DO 235 JJ=1,NN
  235 B1(JJ)=B3(JJ,JJ)
      A2=ALO(2)
      DO 260 J = 1, NN
  260 B1(J) = 0.0
      DO 270 J = 1, NN
      DO 270 K = 1, NN
  270 B1(K) = B1(K) + B2(J,K) *GRAD(J)
      DO 275 J = 1, NN
      IF (B1(J))  280, 290, 285
  280 B1(J) = - B1(J)
```

```
285 B1(J) = B1(J)/B1(J)
    GO TO 275
290 B1(J) = 0.0
275 CONTINUE
    DO 295 J = 1, MM
295 B1(J) = 0.0
    DO 300 J = 1, MM
    DO 300 K = 1, MM
300 B1(J) = B1(J) + B2(J,K)*B1(K)
305 DO 310 J=1,M
    GMOO = GMOO + GRAL(J)**2
    BMOO = BMOO + B1(J)**2
310 PROO = PROO + GRAL(J)*B1(J)
    IF (GMOO - G2)  315, 315, 320
315 LE = 2
    GO TO 600
320 C=PROO/SQRT(BMOO*GMOO)
    IF (C) 335, 335, 400
335 LE = 4
    GO TO 600
400 LL = 0
    L3 = 0
    DO 410 J = 1, MM
410 GRAL(J) = B(J) - B1(J)
450 DO 420 II = 1, MM
    L=2
    I=II
    CALL FUNC (1)
    DF(II) = FM(II) - FC(II)
420 S = S + DF(II)**2/X(II)
    IF (SA - S) 435, 500, 500
435 LL = LL + 1
430 DO440 J = 1, MM
    B1(J) = B1(J)/2.0
440 GRAL(J) = B(J) - B1(J)
    S = 0.0
    L3 = L3 + 1
    IF (L3 - 256) 450, 460, 460
460 LE = 5
    GO TO 600
500 IF (LL) 505, 505, 506
506 LL = 0
    GO TO 430
505 DO 510 J = 1, MM
510 B(J) = GRAL(J)
    SA = S
    IF (SA - Q1) 507, 507, 530
507 LE = 1
    GO TO 600
A
```

```
530 IF (L4) 200, 200, 900
900 WRITE(6,920)L1,L2,L3,S,GNORM,(B(J),J=1,N)
920 FORMAT(//,15H ITERATION NO.=I5,10X,43H   TRANSFORMATION MADE TO PR
   1INCIPAL AXES = A4,10X,   18H BINARY CHOP USED=I3,6H TIMES/1X,27H W
   2EIGHTED SUM OF SQUARES = E14.7,25X,32H   SQUARE MODULUS OF GRADIEN
   3T = E14.7/20H . PARAMETERS B(J) -/(6E17.6)/)
    IF (L1 - L4) 200, 910, 910
910 LE = 6
    GO TO 666
666 DO 710 J=1,MM
    B1(J) = 0.0
    DO 710 K=1,MM
710 B2(J,K) = 0.0
    L=1
    DO 720 JJ = 1, NN
    CALL FUNC(2)
    DF(JJ) = FM(JJ) - FC(JJ)
    DO 720 J = 1, MM
    B1(J) = B1(J) - (2.0*DF(JJ)*B1(J))/X(JJ)
    DO 720 K = 1, MM
720 B2(J,K) = B2(J,K) - (2.0*(DF(JJ)*B2(J,K) -B1(J)*B1(K)))/X(JJ)
    CALL MATINV(B2,M,B1,1,DETERM)
    DO 730 J=1,MM
    IF (B2(J,J)) 2001,2001,2002
2001 B1(J) = -SQRT(-B2(J,J))
    GO TO 730
2002 B1(J)= SQRT(B2(J,J))
 730 CONTINUE
    DO 740 J=1,MM
    DO 740 K=1,MM
 740 B2(J,K)=B2(J,K)/(B1(J)*B1(K))
    WRITE(6,591)LE,SA
 591 FORMAT(//,13H EXIT NUMBER=I3,20X,25H WEIGHTED SUM OF SQUARES=E15.6
   1//)
    RETURN
    END

    SUBROUTINE FUNC (LX)
C   SUBROUTINE FUNC
    DIMENSION BC(2163),B(20,2),B1(20),B2(20,20),FC(256),Z(256),E(6)
    COMMON BC
    EQUIVALENCE (Z,BC),(FC,BC(513)),(B,BC(1719)),(B1,BC(1759)),
   1(B2,BC(1779)),(M,BC(1706)),(L,BC(2179)),(I,BC(2180)),(KG,BC(2182))
    MM=M
    DO 50 J=1,MM
    B1(J)=0.0
    DO 50 K=1,MM
 50 B2(J,K)=0.0
    FC(1)=B(M,L)*Z(1) + B(M-1,L)
    KG1=KG
    DO 60 J=1,KG1
```

```
   60 FC(I)=FC(I) + C(3*J-2 ,L)/((Z(I)-B(3*J,L))**2 + B(3*J-1,L)**2)
      IF(LX-1)110,110,120
  120 D1(M-1)=1.0
      D1(M)=Z(I)
      DO 70 J=1,KG1
      XI=(Z(I)-B(3*J,L))**2
      ETA=B(3*J-1,L)**2
      DEN=XI+ETA
      D1(3*J-2)=1.0/DEN
      D1(3*J-1)=-2.0*B(3*J-1,L)*B(3*J-2,L)/DEN**2
      D1(3*J)=2.0*(Z(I)-B(3*J  ,L))*B(3*J-2,L)/DEN**2
      D2(3*J-1,3*J-2)=-2.0*B(3*J-1,L)/DEN**2
      D2(3*J-2,3*J-1)=D2(3*J-1,3*J-2)
      D2(3*J,3*J-2)=2.0*(Z(I)-B(3*J,L))/DEN**2
      D2(3*J-2,3*J) = D2(3*J,3*J-2)
      D2(3*J-1,3*J-1)=-2.0*B(3*J-2,L)*(XI -3.0*ETA)/DEN**3
      D2(3*J-1,3*J)=-8.0*B(3*J-2,L)*B(3*J-1,L)*(Z(I)-B(3*J,L))/DEN**3
      D2(3*J,3*J-1)=D2(3*J-1,3*J)
   70 D2(3*J,3*J)=2.0*B(3*J-2,L)*(3.0*XI-ETA)/DEN**3
  110 CONTINUE
      RETURN
      END

      SUBROUTINE EXAM(A,B,N,LF)
C     SUBROUTINE EXAM
C       F O R T R A N  4
      DIMENSION A(20,20),B(20),C(20)
      DO 80 J=1,N
   80 C(J)=A(J,J)
      IF(A(1,1)) 60,200,70
   60 A(1,1) =-SQRT(-A(1,1))
      GO TO 300
   70 A(1,1) =SQRT(A(1,1))
      GO TO 100
  100 IF(N-1)400,400,110
  110 DO 115 K=2,N
  115 A(1,K)=A(1,K)/(A(1,1)          )
      DO 120 J=2,N
      J1=J-1
      S=A(J,J)
      DO 125 L=1,J1
  125 S=S-A(L,J)**2
      IF (S) 50,200,40
   50 A(J,J) =-SQRT(-S)
      GO TO 300
   40 A(J,J) =SQRT(S)
      GO TO 130
  130 IF(J-N)135,400,400
  135 J2=J+1
      DO 120 K=J2,N
      S=A(J,K)
```

```
      DO 145 L=1,J1
  145 S=S-A(L,J)*A(L,K)
  120 A(J,K)=S/A(J,J)
  400 B(1)=B(1)/A(1,1)
      IF(N-1)420,420,405
  405 DO 410 J=2,N
      S=B(J)
      J1=J-1
      DO 415 L=1,J1
  415 S=S-A(L,J)*B(L)
  410 B(J)=S/A(J,J)
  420 B(N)=B(N)/A(N,N)
      J=N-1
  435 IF(J)450,450,425
  425 S=B(J)
      J2=J+1
      DO 430 L=J2,N
  430 S=S-A(J,L)*B(L)
      B(J)=S/A(J,J)
      J=J-1
      GO TO 435
  450 LF=1
      GO TO 460
  200 LF=0
      GO TO 460
  300 LF=-1
  460 DO 465 J=1,N
      A(J,J)=C(J)
      IF(J-N)470,475,475
  470 J2=J+1
      DO 465 K=J2,N
  465 A(J,K)=A(K,J)
  475 RETURN
      END

      SUBROUTINE MATINV(A,N,B,M,DETERM)
C     SUBROUTINE MATINV
C       F O R T R A N  4
C     MATRIX INVERSION WITH ACCOMPANYING SOLUTION OF LINEAR EQUATIONS
      DIMENSION IPIVOT(20),A(20,20),B(20,1),INDEX(20,2),PIVOT(20)
      EQUIVALENCE (IROW,JROW),(ICOLUM,JCOLUM),(AMAX,T,SWAP)
      DETERM=1.0
      DO 20 J=1,N
   20 IPIVOT(J)=0
      DO 550 I=1,N
      AMAX=0.0
      DO 105 J=1,N
      IF(IPIVOT(J)-1)60,105,60
   60 DO 100 K=1,N
      IF(IPIVOT(K)-1)80,100,740
   80 IF(ABS(AMAX)-ABS(A(J,K)))85,100,100
```

```
      IROW=J
      ICOLUM=K
      AMAX=A(J,K)
  100 CONTINUE
  105 CONTINUE
      IPIVOT(ICOLUM)=IPIVOT(ICOLUM)+1
      IF (IROW-ICOLUM)140,260,140
  140 DETERM=-DETERM
      DO 200 L=1,N
      SWAP=A(IROW,L)
      A(IROW,L)=A(ICOLUM,L)
  200 A(ICOLUM,L)=SWAP
      IF(M)200,200,210
  210 DO 250 L=1,M
      SWAP=B(IROW,L)
      B(IROW,L)=B(ICOLUM,L)
  250 B(ICOLUM,L)=SWAP
  260 INDEX(I,1)=IROW
      INDEX(I,2)=ICOLUM
      PIVOT(I)=A(ICOLUM,ICOLUM)
      DETERM=DETERM*PIVOT(I)
      A(ICOLUM,ICOLUM)=1.0
      DO 350 L=1,N
  350 A(ICOLUM,L)=A(ICOLUM,L)/PIVOT(I)
      IF(M)380,380,360
  360 DO 370 L=1,M
  370 B(ICOLUM,L)=B(ICOLUM,L)/PIVOT(I)
  380 DO 550 L1=1,N
      IF (L1-ICOLUM)400,550,400
  400 T=A(L1,ICOLUM)
      A(L1,ICOLUM)=0.0
      DO 450 L=1,N
  450 A(L1,L)=A(L1,L)-A(ICOLUM,L)*T
      IF(M)550,550,460
  460 DO 500 L=1,M
  500 B(L1,L)=B(L1,L)-B(ICOLUM,L)*T
  550 CONTINUE
      DO 710 I=1,N
      L=N+1-I
      IF(INDEX(L,1)-INDEX(L,2))630,710,630
  630 JROW=INDEX(L,1)
      JCOLUM=INDEX(L,2)
      DO 705 K=1,N
      SWAP=A(K,JROW)
      A(K,JROW)=A(K,JCOLUM)
      A(K,JCOLUM)=SWAP
  705 CONTINUE
  710 CONTINUE
  740 RETURN
      END
```

```
      SUBROUTINE PLOTL (NG,N,AA,BB)
C     SUBROUTINE PLOT B
C     A= LARGEST OF FC AND FM, B= SMALLEST
      DIMENSION X(116),AA(512),BB(512),Y(4),ABC(2)
      COMMON/DATA/ABC,Y
      DATA(ABC=2HNG,3HYES),(Y=1H ,1HC,1H*,1HM)
      A=AA(1)
      B=A
      DO 900 I=1,N
      IF(AA(I)-A)905,905,910
  910 A=AA(I)
  905 IF(BB(I)-A)915,915,920
  920 A=BB(I)
  915 IF(AA(I)-B)930,925,925
  930 B=AA(I)
  925 IF(BB(I)-B)935,900,900
  935 B=BB(I)
  900 CONTINUE
      FACTOR = 1.0
  520 IF (A-B-100.0) 500, 510, 510
  500 A = 2.0*A
      B = 2.0*B
      FACTOR = 2.0*FACTOR
      GO TO 520
  510 KD = (A-B)/112.0 + 1.0
      KS = IFIX(B) - 2*KD
      WRITE (6,1)
    1 FORMAT(1H0...0.....1.....2.....3.....4.....
     15.....6.....7.....8.....9.....10.....11...)
      DO 100 I=1,N
      DO 110 K=1,116
  110 X(K)=Y(1)
      K = AA(I)*FACTOR
      K = (K-KS)/KD
      X(K) = Y(2)
      L = BB(I)*FACTOR
      L = (L-KS)/KD
      IF(L-K)120,130,120
  130 X(L)=Y(3)
      GO TO 105
  120 X(L)=Y(4)
  105 ING=I+NG-1
  100 WRITE (6,90)ING,X
   90 FORMAT(1X13,116A1)
      WRITE (6,1)
      RETURN
      END
      SUBROUTINE JACOBI (N,Q,JVEC,M,V)
C     SUBPROGRAM FOR DIAGONALIZATION OF MATRIX Q BY SUCCESSIVE ROTATIONS
      DIMENSION Q(20,20),V(20,20),X(20),TH(20)
C
C
```

```
C     NEXT 6 STATEMENTS FOR SETTING INITIAL VALUES OF MATRIX V
C
      IF(JVEC) 16,15,16
   16 DO 14 I=1,N
      DO 14 J=1,N
      IF(I-J) 12,11,12
   11 V(I,J)=1.0
      GO TO 14
   12 V(I,J)=0.
   14 CONTINUE
C
   15 IM=0
C     NEXT 6 STATEMENTS SCAN FOR LARGEST OFF DIAG. ELEM. IN EACH ROW
C     X(I) CONTAINS LARGEST ELEMENT IN ITH ROW
C     IH(I) HOLDS SECOND SUBSCRIPT DEFINING POSITION OF ELEMENT
C
      NM1=N-1
      DO 30 I=1,NM1
      X(I)=0.
      MJ=I+1
      DO 30 J=MJ,N
      IF (X(I)-ABS (Q(I,J))) 20,20,30
   20 X(I)=ABS (Q(I,J))
      IH(I)=J
   30 CONTINUE
C
C     NEXT 7 STATEMENTS FIND FOR MAXIMUM OF X(I)S FOR PIVOT ELEMENT
   40 DO 70 I=1,NM1
      IF(I-1) 60,60,45
   45 IF (XMAX-X(I)) 60,70,70
   60 XMAX=X(I)
      IP=I
      JP=IH(I)
   70 CONTINUE
C
C     NEXT 2 STATEMENTS TEST FOR XMAX,IF LESS THAN 1E**-6,GO TO 1000
C
      EPS1=1.E-6
      IF (XMAX-EPS1) 1000,1000,140
C
  140 IM=IM+1
C
C     NEXT 11 STATEMENTS FOR COMPUTING TANG,SINE,COSN,Q(I,I),Q(J,J)
C
      IF (Q(IP,IP)-Q(JP,JP)) 150,151,151
  150 TANG =-2.*Q(IP,JP)/(ABS(Q(IP,IP)-Q(JP,JP))+SQRT((Q(IP,IP)-Q(JP,JP)
     1)**2+4.*Q(IP,JP)**2))
      GO TO 160
  151 TANG =+2.*Q(IP,JP)/(ABS(Q(IP,IP)-Q(JP,JP))+SQRT((Q(IP,IP)-Q(JP,JP)
     1)**2+4.*Q(IP,JP)**2))
  160 COSN=1.0/SQRT(1.0+TANG**2)
```

```
      SINE=TANG*COSN
      QII=Q(IP,IP)
      Q(IP,IP)= COSN**2*(QII+TANG*(2.*Q(IP,JP)+TANG*Q(JP,JP)))
      Q(JP,JP)= COSN**2*(Q(JP,JP)-TANG*(2.*Q(IP,JP)-TANG*QII))
C
      Q(IP,JP)=0.
C
C     NEXT 4 STATEMENTS FOR PSEUDO RANK OF THE EIGENVALUES
      IF (Q(IP,IP)-Q(JP,JP)) 152,153,153
  152 TEMP=Q(IP,IP)
      Q(IP,IP)=Q(JP,JP)
      Q(JP,JP)=TEMP
C
C     NEXT 6 STATEMENTS ADJUST SIN,COS FOR COMPUTATION OF Q(I,K),V(I,K)
C
      IF(SINE) 154,155,155
  154 TEMP=+COSN
      GO TO 170
  155 TEMP=-COSN
  170 COSN=ABS(SINE)
      SINE=TEMP
C
C     NEXT 10 STATEMENTS FOR INSPECTING  THE I'S BETWEEN I+1 AND N-1 TO
C     DETERMINE WHETHER A NEW MAXIMUM VALUE SHOULD BE COMPUTED SINCE
C     THE PRESENT MAXIMUM IS IN THE I OR J ROW
C
  153 DO 350 I=1,II
      IF (I-IP) 210,350,200
  200 IF (I-JP) 210,350,210
  210 IF (IH(I)-IP) 230,240,230
  230 IF (IH(I)-JP) 350,240,350
  240 K= IH(I)
      TEMP=Q(I,K)
      Q(I,K)=0.
      MU=I+1
      X(I)=0.
C
C     NEXT 5 STATEMENTS SEARCH IN DEPLETED ROW FOR NEW MAXIMUM
C
      DO 320  J=MU,N
      IF (X(I)-ABS(Q(I,J))) 300,300,320
  300 X(I)=ABS(Q(I,J))
      IH(I)=J
  320 CONTINUE
      Q(I,K)=TEMP
  350 CONTINUE
C
      X(IP)=0.
      X(JP)=0.
C
C     NEXT 30 STATEMENTS FOR CHANGING THE OTHER ELEMENTS OF Q
```

```
C
      DO 530 I=1,N
C
      IF (I-IP) 370,530,420
  370 TEMP=Q(I,IP)
      Q(I,IP)=COSN*TEMP+SINE*Q(I,JP)
      IF (X(I)-ABS(Q(I,IP))) 380,390,390
  380 X(I)=ABS(Q(I,IP))
      IN(I)=IP
  390 Q(I,JP)=-SINE*TEMP+COSN*Q(I,JP)
      IF (X(I)-ABS(Q(I,JP))) 400,530,530
  400 X(I)=ABS(Q(I,JP))
      IN(I)=JP
      GO TO 530
C
  420 IF (I-JP) 430,530,400
  430 TEMP =Q(IP,I)
      Q(IP,I)=COSN*TEMP+SINE*Q(I,JP)
      IF (X(IP)-ABS(Q(IP,I))) 440,450,450
  440 X(IP)=ABS(Q(IP,I))
      IN(IP)=I
  450 Q(I,JP)=-SINE*TEMP+COSN*Q(I,JP)
      IF (X(I)-ABS(Q(I,JP))) 400,530,530
C
  400 TEMP=Q(IP,I)
      Q(IP,I)=COSN*TEMP+SINE*Q(JP,I)
      IF(X(IP)-ABS(Q(IP,I))) 490,500,500
  490 X(IP)=ABS(Q(IP,I))
      IN(IP)=I
  500 Q(JP,I)=-SINE*TEMP+COSN*Q(JP,I)
      IF (X(JP)-ABS(Q(JP,I))) 510,530,530
  510 X(JP)=ABS(Q(JP,I))
      IN(JP)=I
  530 CONTINUE
C
C     NEXT 6 STATEMENTS TEST FOR COMPUTATION OF EIGENVECTORS
C
      IF (JVEC) 540,40,540
  540 DO 550 I=1,N
      TEMP=V(I,IP)
      V(I,IP)= COSN*TEMP+SINE*V(I,JP)
  550 V(I,JP)=-SINE*TEMP+COSN*V(I,JP)
      GO TO 40
 1000 RETURN
      END
 > ?
```

COMPUTER SYSTEM 6809 TRANSFER PROGRAMS

PROGRAM MCAREAD

```
8E E030      LDX#$E030      PIA BASE ADDRESS=PIAAD
6F 01        CLR 1,X        ACCESS DDRA
6F 03        CLR 3,X        ACCESS DDRB
10
8E F004      LDY#$F004      DDRA,B HAVE UPPER NYBBLE=OUTPUT,
                            LOWER NYBBLE=INPUT,THEN ACCESS PIAD'S
10
AF 21        STY ,X++       F0 INTO DDRA ,04 INTO CRA
10
AF 21        STY ,X++       F0 INTO DDRB, 04 INTO CRB
A6 83        LDA ,--X       READ PIABD TO CLEAR INTERRUPTS
A6 83        LDA ,--X       LIKEWISE FOR PIAAD, X NOW=$E030
10
8E C400      LDY#BEGA
86 70READY 2 LDA#$70        =READY2+SHFT+SP=HI
A7 02        STA 2,X        PIABB
C6 06        LDB#6          B=#DIGITS/CHANNEL
34 READ                     FIRST READ FOLLOWS READY2
04           PSHS B         SAVE DIGIT COUNTER
C6 10        LDB#$10
12           NOP
5A DELAY     DECB           WAIT FOR ADC TO PRESENT DATA
26 FD        BNE DELAY
35           PULS B         RETRIEVE DIGIT COUNTER
04
A6 84        LDA ,X         INPUT DATA VIA PIAAD
84 0F        ANDA#$0F       ONLY LOWER NYBBLE SIGNIFICANT
8A 30        ORA#$30        CONVERT TO ASCII
A7 A0        STA ,Y+        STORE DIGITCY AND INCREMENT Y BY 1
10
8C DC01      CMPY#ENDA+2    ENDA=BEGA+6*1024=BEGA+$1800
27 11        BEQ STOP       (DO READ PAST ENDA TO GENERATE ECHO
                            WHICH RESETS ADC FOR "DISPLAY")
5A           DECB READY 2
27 DF        BEQ            CALL OUT NEXT CHANNEL AFTER 6 DIGITS
C6 40        LDA#$40        =SP
A7 02        STA 2,X        2,X=PIABB. SHFT LO ,SP HI
6F 02        CLR 2,X        SP LO
A7 02        STA 2,X        SHFT LO ,SP HI
C6 60        LDA#$60        =SHFT +SP
A7 02        STA 2,X        SHFT,SP HI
20 D7        BRA READ       READ FOLLOWS NEXT 5 SHIFTS
3F   STOP    SWI
50
55           READY2 =$10
94 67        SHFT   =$20
36           SP     =$40
```

PROGRAM PUNCH

```
8E E024     LDX#PORTØB     =$E024
86 03       LDA#3          MASTER RESET
A7 84       STA ,X
86 11       LDA#%0001 0001 8 BIT ,NO PAR ,2 STOP BITS-MOST
                           ERROR FREE
A7 84       STA ,X         WRITE FORMAT (2 SE HELP LOCATE
                           FOLLOWING START BITS )
8E CC1D     LDX#RENTRY     PLACE RE-ENTRY PC ON STACK TO BE
                           PULLED BY RTS AT END OF SBUG
                           PUNCH ROUTINE
34 10       PSHS ,X
6F E2       CLR ,-S        FOLLOWING SLUG
BD FD20     JSR IN2ADR     INPUT BEGA,ENDA,SAVE ON STACK
C6 24       LDB#$24        LSBYTE OF PORT2B
F7 DFE1     STB  CPORT+1   I/O NOW VIA PORT2B(TAPE RECORDER)
7E FC69     JMP  PUN1      ENTER SBUG PUNCH ROUTINE AFTER
80 53       LDA's          ACCEPTING BEGA,ENDA FROM PORT B
                           (E004 = TTY)
BD FDDF     JSR OUTCH      WRITE 59 (TAPE EOF)
86 39       LDA '9
BD FDDF     JSR OUTCH
7E F814     JMP MONITOR    RETURN I/O TO CONSOLE
```

PROGRAM LOAD

```
8E E024     LDX #PORTØB    =$E024
86 03       LDA #3
A7 84       STA ,X
86 01       LDA #1         KILLS PARITY BIT WHICH OCCASION-
                           ALLY IS DETECTED ACCIDENTLY ON TAPE
A7 84       STA ,X
BF DFE0     STX CPORT
BD FC09     JSR LOAD       NO KEYBD ENTRY, SO ENTIRE SBUG
                           LOAD ROUTINE OK
7E F814     JMP MONITOR    RETURN I/O TO CONSOLE
```

TRANSFER

```
                        NAM     TRANSFER
                        OPT     O,NOG
                        ORG     $4000

                *SUBROUTINE TO OUTPUT MSI FILE
                *IN BEGADR-ENDADR TO MODEM
                *EOT ($04) WILL TERMINATE XFER IF ENDADR TOO LARGE

    0100        MESLEN  EQU     $0100
    2800        DOS     EQU     $2800
    4600        BUFM    EQU     $4600
    E047        BAUDR   EQU     $E047
    E075        OUTCH   EQU     $E075
    E078        INCH    EQU     $E078
    E07E        PDATAI  EQU     $E07E
    E0C8        OUT4HS  EQU     $E0C8
    E0CC        OUTS    EQU     $E0CC
    E0E3        CNTRL   EQU     $E0E3
    E17D        CRLF    EQU     $E17D
    E1AC        INEEE   EQU     $E1AC
    E1D1        OUTEEE  EQU     $E1D1
    E30F        INPUT   EQU     $E30F
    F000        IOV     EQU     $F000
    F002        BEGA    EQU     $F002
    F004        ENDA    EQU     $F004
    F006        CURRA   EQU     $F006
    F016        INADD   EQU     $F016
    F018        OUTADD  EQU     $F018
    F01A        OUTSW   EQU     $F01A
    F01C        BEGADR  EQU     $F01C
    F01E        ENDADR  EQU     $F01E
    F022        MESS    EQU     $F022
    F500        ACIACC  EQU     $F500
    F528        ACIAMC  EQU     $F528

4000 7F F01A TRANSF CLR     OUTSW
4003 CE F500        LDX     #ACIACC
4006 FF F016        STX     INADD
4009 FF F018        STX     OUTADD
400C CE 4040        LDX     #PR4        'TYPE S FOR SPECTRUM XFER.'
400F BD E07E        JSR     PDATAI
4012 BD E1AC        JSR     INEEE
4015 81 53          CMP A   #$53        'S?
4017 26 09          BNE     P5          AUTOMATIC XFER
                ***DELETE NEXT 2 LINES FOR OLD TAPES***
4019 CE 0002        LDX     #$0002      ENDA+2 TO ALLOW FOR MCARED DF
401C FF 0100        STX     MESLEN
401F 7E 4080        JMP     MCREAD
4022 CE 407E P5     LDX     #P55        "INPUT BEGADR, ENDADR"
4025 BD E07E        JSR     PDATAI
4028 BD E30F        JSR     INPUT
402B CE E17D        LDX     #CRLF
402E BD E07E        JSR     PDATAI
4031 CE F528        LDX     #ACIAMC
```

TRANSFER

```
4034 FF F018          STX     OUTADD
4037 7C F01F          INC     ENDADR+1
403A FE F01C          LDX     BEGADR
403D A6 00    OUT     LDA A   0,X
403F 81 04            CMP A   #04
4041 27 09            BEQ     FINISH
4043 BD E075          JSR     OUTCH
4046 08               INX
4047 BC F01E          CPX     ENDADR
404A 26 F1            BNE     OUT
404C 39       FINISH  RTS
404D 54       PR4     FCC     *TYPE S FOR SPECTRUM AREA, RETURN FOR
4077 0D               FCB     $0D,$0A,0,0,0,0,4
4078 49       PR5     FCC     /INPUT BEGADR, ENDADR/
4092 0D               FCB     $0D,$0A,0,0,0,0,0,4

                    *PROGRAM TO UNFOLD ASCII SPECTRUM AND OUTPUT IN
                    *FORMAT(101)
                    *PATCHES FOR 6809 TAPES INCLUDED

409B CE F500  MCAREA  LDX     #ACIACC
409E FF F018          STX     OUTADD
40A1 7F F01A          CLR     OUTSW
40A4 BD E07E          JSR     PDATA1
40A7 CE 0100          LDX     #MESLEN
40AA BD E0C8          JSR     OUT4HS
40AD 8D 01            BSR     MCREAD
40AF 3F               SWI
40B0 CE F528  MCREAD  LDX     #ACIAMC
40B3 FF F018          STX     OUTADD
40B6 09       DELY    DEX
40B7 8C 0100          CPX     #MESLEN
40BA 26 F9            BNE     DELY
40BC 7A 0101          DEC     MESLEN+1 CORRECT MESLEN FOR OVERSHOOT
                    * IN MCATAPE.
40BF C6 0A            LDA B   #$0A        LF=$0A=10
40C1 F7 414C          STA B   CHAN        # CHANNELS/LINE=10
40C4 17               DBA
40C5 BD E075          JSR     OUTCH
40C8 86 0D            LDA A   #$0D
40CA BD E075          JSR     OUTCH
40CD C6 07            LDA B   #$07
40CF F7 414D          STA B   DIGIT       COUNTER=7/CHAN (INC S. SPACE)
                    ***DELETE NEXT 2 LINES FOR OLD TAPES
40D2 CE C400          LDX     #$C400      BEGA OF 6809 TAPES
40D5 20 0F            BRA     CK
40D7 CE 0102          LDX     #MESLEN+2
40DA A6 00    READM   LDA A   0,X         INPUT MESSAGE CHAR
40DC 08               INX
40DD 81 04            CMP A   #4
40DF 27 05            BEQ     CK
40E1 BD E075          JSR     OUTCH
40E4 20 F4            BRA     READM
40E6 86 0D    CK      LDA A   #$0D
```

TRANSFER

```
40EB BD E075          JSR     OUTCH
40EB 86 0A            LDA A   #$0A
40ED BD E075          JSR     OUTCH
40F0 A6 00    READ    LDA A   0,X
40F2 81 04            CMP A   #4          CHECK FOR EOT
40F4 27 41            BEQ     RETURN
40F6 7A 414D          DEC     DIGIT
40F9 27 0E            BEQ     DGRSET
40FB BD E075          JSR     OUTCH
40FE FF 414A          STX     XI
4101 08               INX
4102 BC 0100          CPX     MESLEN
4105 27 30            BEQ     RETURN      IF LAST CHANNEL SENT
4107 20 E7            BRA     READ
4109 F7 414D  DGRSET  STA B   DIGIT
410C 86 20            LDA A   #$20
410E BD E075          JSR     OUTCH
4111 7A 414C          DEC     CHAN
4114 27 02            BEQ     LINEL
4116 20 DB            BRA     READ
4118 C6 0A    LINEL   LDA B   #$0A         LINE LENGTH = 10 CHAN.
411A F7 414C          STA B   CHAN
411D C6 07            LDA B   #$07
411F 86 0D            LDA A   #$0D
4121 BD E075          JSR     OUTCH
4124 86 0A            LDA A   #$0A
4126 BD E075  LINEF   JSR     OUTCH       OUTPUT 'LF'
4129 FF F006          STX     COUNTA
412C CE 1000          LDX     #$1000      DELAY FOR MODCOMP
412F 09       DELYM   DEX
4130 26 FD            BNE     DELYM
4132 FE F006          LDX     COUNTA
4135 20 B9            BRA     READ
4137 CE F500  RETURN  LDX  @  #ACIACC
413A FF F018          STX     OUTADD
413D CE 414E          LDX     #MSG
4140 BD E07E          JSR     PDATA1
4143 FE 414A          LDX     XI
4146 BD E0C8          JSR     OUT4HS
4149 39               RTS
414A 0002     XI      RMB     2
414C 0A       CHAN    FCB     $0A
414D 07       DIGIT   FCB     $07
414E 4C       MSG     FCC     /LAST DATA LOCATION (ENDA)=/
416B 20               FCB     $20,$24,4

                      *ENTERS ASCII TEXT INTO MEMORY AT
                      *BEGA - ENDA.  TERMINATE WITH CR.

416B 0F       MTEXT   SEI
416C CE 4208          LDX     #PR1
416F BD E07E          JSR     PDATA1
4172 BD E0CC          JSR     OUTS
4175 CE 41FE          LDX     #INB
```

TRANSFER

```
417B FF F00A          STX   IOV
417E BD E047          JSR   BADDR
4181 BD E0CC          JSR   OUTS
4184 08               INX
4185 FF F004          STX   END4
4188 BD E047          JSR   BADDR
418B FF F002          STX   BEGA
418E 0E               CLI
418F BD E1AC INA      JSR   INEEE     INPUT (& ECHO) CHAR FROM TERM
 4192 81 03            CMP A  #3
4194 27 6B            BEQ   INT
4196 81 08            CMP A  #8
4198 27 06            BEQ   BS
419A 81 1B            CMP A  #$1B
419C 27 0A            BEQ   ESC
419E 20 3F            BRA   STORE
41A0 86 3C    BS      LDA A  #$3C
41A2 BD E1D1          JSR   OUTEEE
41A5 09               DEX
41A6 20 E7            BRA   INA
41A8 FF F006 ESC      STX   CURRA
41AB CE 4289          LDX   #ESCMSG
41AE BD E0[illegible]       JSR   PDATA1
41B1 FE F006          LDX   CURRA
41B4 09         ESC1  DEX
41B5 BC F002          CPX   BEGA
41B8 27 D5            BEQ   INA
41BA A6 00            LDA A  0,X
41BC 81 0A            CMP A  #$0A
41BE 26 F4            BNE   ESC1
41C0 09         ESC2  DEX
41C1 BC F002          CPX   BEGA
41C4 27 C9            BEQ   INA
41C6 A6 00            LDA A  0,X
41C8 81 0D            CMP A  #$0D
41CA 26 F4            BNE   ESC2
41CC 86 0D            LDA A  #$0D
41CE A7 00            STA A  0,X
41D0 08               INX
41D1 86 0A            LDA A  #$0A
41D3 A7 00            STA A  0,X
41D5 08               INX
41D6 20 B7            BRA   INA
41D8 FF F006 STORE    STX   CURRA
41DB A7 00            STA A  0,X
41DD 08               INX
41DE BC F004          CPX   END4
41E1 26 AC            BNE   INA
41E3 8D 03            BSR   REPMES
41E5 7E 2800          JMP   DOS
41E8 86 0D    REPMES  LDA A  #$0D
41EA BD E1D1          JSR   OUTEEE
41ED 86 0A            LDA A  #$0A
41EF BD E1D1          JSR   OUTEEE
```

```
41EF FE F002        LDX   BEGA
41F2 A6 00   OUTA   LDA A 0,X
41F4 BD E1D1        JSR   OUTEEE
41F7 08             INX
41F8 BC F004        CPX   ENDA
41FB 26 F5          BNE   OUTA
41FD 39             RTS
41FE FE F006 INQ    LDX   CURRA
4201 08             INX
4202 FF F004        STX   ENDA
4205 8D 0E          BSR   REPMES    REPEAT MESSAGE
4207 3F             SWI
4208 55        PR1  FCC   /USE INQ OR BREAK TO TERMINATE./
4221 54             FCC   /TYPE LISTER TO EXAMINE FILE/
4242 0D        CRLF1 FCB   $0D,$0A,0,0,0,0
4246 45        PR2  FCC   /ENDA LEFT IN $F004./
425B 0D        CRLF2 FCB   $0D,$0A,0,0,0,0
4261 45        PR3  FCC   /ENTER ENDA, BEGA...IN THAT ORDER!/
4282 0D        CRLF3 FCB   $0D,$0A,$0A,0,0,$3F,4
4289 2A        ESCMSG FCC  /*DELETED*/
4292 0D        CRLF4 FCB   $0D,$0A,0,0,0,0,$3F,4

429A 0F             SEI
429B CE F528        LDX   #ACIAMC  MODEM ACIA AT $F528 (CONTR
429E 86 03          LDA A #$03     MASTER RESET
42A0 A7 00          STA A 0,X
42A2 86 95          LDA A #$95     8B WORD, 0 PAR, ISR, /16, RIE
42A4 A7 00          STA A 0,X
42A6 CE 435F        LDX   #INQR    BEGINNING OF INQ ROUTINE
42A9 FF F000        STX   IOV
42AC CE 4600        LDX   #BUFA
42AF FF F002        STX   BEGA     OF BUFFER WHICH RECEIVES CYME
42B2 CE 43DA        LDX   #MSG1    BEGINNING OF MESSAGE VECTOR
                    *UPDATE IS STORED IN-$F022 (BOTTOM
                    *OF STACK AREA.
42B5 FF F022        STX   RESS
42B8 BD 43B6        JSR   LOGIN    BEGIN LOGIN PROCEDURE
42BB BD 43A1 IN1    JSR   INP      INPUT RESPONSE
42BE 81 3A          CMP A #$3A     ':
42C0 26 F9          BNE   IN1
42C2 BD 434C        JSR   REPEAT
42C5 BD 43B6        JSR   LOGIN
42C8 BD 43A1 IN2    JSR   INP
42CB 81 3F          CMP A #$3F     '?
42CD 26 F9          BNE   IN2
42CF BD 434C        JSR   REPEAT
42D2 BD 43B6        JSR   LOGIN    CR,LF
42D5 BD 43A1 IN30   JSR   INP
42D8 81 2E          CMP A #$2E     '.
42DA 26 F9          BNE   IN30
42DC BD 43A1 IN31   JSR   INP
42DF 81 0D          CMP A #$0D     'CR
42E1 26 F9          BNE   IN31
42E3 BD 43A1 IN32   JSR   INP
```

TRANSFER

```
42E6 81 0A          CMP A  #$0A      'LF
42E8 26 F9          BNE    IN32
42EA BD 434C        JSR    REPEAT
42ED BD 43B6        JSR    LOGIN
42F0 BD 43A1 IN4    JSR    INP
42F3 81 11          CMP A  #$11      'DC1
42F5 26 F9          BNE    IN4
42F7 BD 434C        JSR    REPEAT
42FA BD 43B6        JSR    LOGIN
42FD BD 43A1 IN5    JSR    INP
4300 81 11          CMP A  #$11
4302 26 F9          BNE    IN5
4304 BD 434C        JSR    REPEAT
4307 CE 4401 IN6A   LDX    #MSG6     ENTRY FOR REPEAT XMISSION (SA
 430A FF F022       STX    MESS
430D BD 43B6        JSR    LOGIN
4310 BD 43A1 IN6    JSR    INP
4313 81 11          CMP A  #$11
4315 26 F9          BNE    IN6
4317 BD 434C        JSR    REPEAT
431A 0E             CLI                ALLOW INTERRUPTS AFTER HERE
431B 20 50          BRA    DATA        XMIT DATA
431D 0F       SEND  SEI                TURN OFF IRQ'S NOW.
431E 7F F01A SEND1  CLR    OUTSW       ECHO INPUT THRU MODEM
 4321 CE F528       LDX    #ACIAMC
4324 FF F018        STX    OUTADD
4327 BD E1AC        JSR    INEEE
432A 84 7F          AND A  #$7F
432C 81 03          CMP A  #3
432E 26 09          BNE    CONT
4330 CE F504        LDX    #ACIACC
4333 FF F018        STX    OUTADD
4336 7E 2803        JMP    DOS         IF ^C DETECTED FROM KEYBD.
4339 81 0D    CONT  CMP A  #$0D        'CR
433B 26 E1          BNE    SEND1
433D 0F             SEI                HOLD IRQ FOR NORMAL RECEIVING
 433E 7C F01A       INC    OUTSW
4341 BD 43A1 RECV   JSR    INP
4344 81 11          CMP A  #$11
4346 26 F9          BNE    RECV
4348 8D 02          BSR    REPEAT
434A 20 D1          BRA    SEND
434C FF F004 REPEAT STX    ENDA
434F CE 4600        LDX    #BUF0
4352 FF F002        STX    BEGA
4355 7F F01A        CLR    OUTSW       ECHO ON FOR OUTPUT
 4358 BD 41E5       JSR    REPMES
435B 7C F01A        INC    OUTSW       PREPARE FOR INPUT
435E 39             RTS
435F 7C F01A IRQR   INC    OUTSW       ECHO OFF FOR INPUT
 4362 BD 43A1 INPCH JSR    INP
4365 81 0A          CMP A  #$0A
4367 26 F9          BNE    INPCH
4369 8D E1          BSR    REPEAT
```

TRANSFER

```
436B 3B              RTI
436C 01              NOP
436D BD 4000 DATA    JSR     TRANSFR
4370 0F              SEI                 SHUT OFF INT'S  FOR NORMAL OP
4371 BD 43B6         JSR     LOGIN
4374 BD 43A1 IN7     JSR     INP
4377 81 0A           CMP A   #$0A
4379 26 F9           BNE     IN7
437B BD 43B6         JSR     LOGIN
437E BD 43A1 IN8     JSR     INP
4381 81 11           CMP A   #$11
4383 26 F9           BNE     IN8
4385 7F F01A         CLR     OUTSW
4388 CE F500         LDX     #$F500
438B FF F018         STX     OUTADD
438E CE 4412         LDX     #MSG9
4391 BD E07E         JSR     PDATA1
4394 7E 431D         JMP     SEND
4397 CE F528 OUTT    LDX     #ACIAMC
439A FF F018         STX     OUTADD
439D BD E075         JSR     OUTCH
43A0 39              RTS
43A1 CE F528 INP     LDX     #ACIAMC
43A4 FF F016         STX     INADD
43A7 BD E078         JSR     INCH
43AA 84 7F           AND A   #$7F
43AC FE F002         LDX     BEGA
43AF A7 00           STA A   0,X
43B1 08              INX
43B2 FF F002         STX     BEGA
43B5 39              RTS
43B6 7F F01A LOGIN   CLR     OUTSW      ECHO ON FOR  OUTPUT
43B9 CE 0000          LDX     #0
43BC 08        DELAY INX
43BD 8C E000         CPX     #$E000
43C0 26 FA           BNE     DELAY
43C2 FE F022 MESG    LDX     MESS
43C5 A6 00           LDA A   0,X
43C7 08              INX
43C8 FF F022         STX     MESS
43CB 81 04           CMP A   #$04
43CD 27 07           BEQ     RESTOR
43CF 01              NOP
43D0 01              NOP
43D1 01              NOP
43D2 BD C3           BSR     OUTT
43D4 20 EC           BRA     MESG
43D6 7C F01A RESTOR  INC     OUTSW      ECHO OFF FOR INPUT
43D9 39               RTS

43DA 0D      MSG1    FCB     $0D,$0A,$04
43DD 45      MSG2    FCC
43E9 0D              FCB     $0D,$0A,4
43EC 52      MSG3    FCC     *REC*
```

TRANSFER

```
43EF 0D             FCB   $0D,$0A,4
43F2 54     MSG4    FCC   *TAPE*
43F6 0D             FCB   $0D,$0A,4
43F9 4E     MSG5    FCC   *NEW,X*
43FE 0D             FCB   $0D,$0A,4
4401 54     MSG6    FCC   *TEXT*
4405 0D             FCB   $0D,$0A,4
4408 0D     MSG7    FCB   $0D,3,4
440B 54     MSG8    FCC   *PACK*
440F 0D             FCB   $0D,$0A,4
4412 44     MSG9    FCC   *DATA TRANSFERRED INTO FILE "X".*
4431 54             FCC   *TYPE "LNN" TO VERIFY DATA.*
444B 0D             FCB   $D,$A,0,0,0,0
4451 54             FCC   *TYPE ^D TO HALT OUTPUT.*
446B 0D             FCB   $D,$A,0,0,0,0
446E 54             FCC   *THEN TYPE G 2000 TO REBOOT FDOS. *
4487 41             FCC   *AND THEN "SEND" TO SEND *
44A7 4E             FCC   *NEXT COMMAND (SAVE,X:FNAME.)*
44C3 0D             FCB   $D,$A,4
                    END
```